Proceedings of the

National Conference on
"Microplastics: Sources and Impacts"
and
The 16th Annual Conference of the
Center of Excellence on Environmental Health and Toxicology

Organized by

Center of Excellence on Environmental Health and Toxicology (CoE EHT)
(Program: Hub of Talents in Environmental Health
with Support of the National Research Council of Thailand)

June 18th, 2024

at the Convention Center, Chulabhorn Research Institute, bangkok, Thailand

ศูนย์ความเป็นเลิศด้านอนามัยสิ่งแวดล้อมและพิษวิทยา ภายใต้กรอบการดำเนินการของ
โครงการ Hub of Talents “ศูนย์ความเป็นเลิศด้านอนามัยสิ่งแวดล้อม”
การประชุมวิชาการระดับชาติ เรื่อง “ไมโครพลาสติก: ปัญหาและที่มา” และ
การประชุมวิชาการประจำปี 2567
วันอังคารที่ 18 มิถุนายน 2567
ณ ศูนย์ประชุมสถาบันวิจัยจุฬาภรณ์ กรุงเทพมหานคร

08.30 - 09.00 น. ลงทะเบียน

09.00 - 09.10 น. พิธีเปิด โดย *ศาสตราจารย์เกียรติคุณ ดร. คุณหญิงมธุรส รุจิรวัฒน์*
ผู้อำนวยการศูนย์ความเป็นเลิศด้านอนามัยสิ่งแวดล้อมและพิษวิทยา

09.10 – 09.30 น. ถ่ายภาพหมู่

09.30 - 10.10 น. สถานการณ์และการจัดการไมโครพลาสติกของประเทศไทย
โดย *ดร. ณัฐกานต์ วงศ์ฝั้น*
ผู้อำนวยการส่วนแหล่งน้ำจืด กองจัดการคุณภาพน้ำ กรมควบคุมมลพิษ

10.10 - 10.30 น. การอุบัติของไมโครพลาสติกในการผลิตน้ำประปาและน้ำดื่มบรรจุขวด
โดย *ดร.จิติมา ปรีชาวงศ์*
นักวิจัย วิทยาลัยปิโตรเลียมและปิโตรเคมี จุฬาลงกรณ์มหาวิทยาลัย

10.30 - 10.50 น. การตรวจติดตามไมโครพลาสติกในห่วงโซ่นิเวศของสัตว์ทะเล
โดย *ศาสตราจารย์ ดร. สมศักดิ์ ปัญหา*
ผู้อำนวยการศูนย์ความเป็นเลิศด้านความหลากหลายทางชีวภาพ

10.50 - 11.10 น. การตรวจวัดและปริมาณไมโครพลาสติกในอากาศในพื้นที่กรุงเทพมหานครและปริมณฑล
โดย *รองศาสตราจารย์ ดร. เอกบดินทร์ วินิจกุล*
อาจารย์ผู้เชี่ยวชาญด้านมลพิษทางอากาศ สถาบันเทคโนโลยีแห่งเอเชีย
กรรมการสนับสนุนการดำเนินงาน ศูนย์รวมผู้เชี่ยวชาญด้านมลพิษอากาศและภูมิอากาศ

11.10 - 11.30 น. การวิเคราะห์ระดับไมโครพลาสติกในอากาศและการรับสัมผัสในประชากร
โดย *รองศาสตราจารย์ ดร. พนิดา นวสัมฤทธิ์*
ผู้แทน สถาบันวิจัยจุฬาภรณ์
ศูนย์ความเป็นเลิศด้านอนามัยสิ่งแวดล้อมและพิษวิทยา

11.30 - 11.50 น. การย่อยสลายไมโครพลาสติกในดิน
โดย *ศาสตราจารย์ ดร.ประหยัด โภคฐิติยุกต์*
ผู้แทน คณะวิทยาศาสตร์ มหาวิทยาลัยมหิดล
ศูนย์ความเป็นเลิศด้านอนามัยสิ่งแวดล้อมและพิษวิทยา

11.50 - 12.00 น. กล่าวสรุปและปิดการบรรยายไมโครพลาสติก

12.00 - 13.00 น. พักรับประทานอาหารกลางวัน

13.00 - 15.00 น. ชมโปสเตอร์ (ผู้เสนอผลงานวิจัยอยู่ประจำโปสเตอร์)

15.00 - 16.30 น. นำเสนอผลงานวิจัยรูปแบบบรรยาย (Oral Presentation) ของนักศึกษาจาก 4 หน่วยวิชาการ

16.30 - 17.00 น. พิธีมอบรางวัลการประกวดโปสเตอร์ผลงานวิจัย
พิธีปิดการประชุม โดย *ศาสตราจารย์เกียรติคุณ ดร. คุณหญิงมธุรส รุจิรวัฒน์*

Center of Excellence on Environmental Health and Toxicology (EHT)

The 16th Annual Conference of the Center of Excellence on Environmental Health and Toxicology, and the National Conference on Microplastics: Sources and Impacts

Organizing Committee

Chairperson

Prof. Dr. *Khunying* Mathuros Ruchirawat	Director, EHT

Committee Members

Prof. Dr. Suchart Upatham	Advisor, EHT
Prof. Dr. Pornchai Matangkasombut	Advisor, EHT
Prof. Dr. Skorn Mongkolsuk	Advisor, EHT
Assoc. Prof. Dr. Jutamaad Satayavivad	Deputy Director, EHT
Assoc. Prof. Nardtida Tumrasvin	Assistant Management Director, EHT
Prof. Dr. Prayad Pokethitiyook	Representative, Faculty of Science, Mahidol University
Prof. Dr. Somsak Ruchirawat	Representative, Chulabhorn Graduate Institute
Assoc. Prof. Dr. Panida Navasumrit	Representative, Chulabhorn Research Institute
Assoc. Prof. Dr. Prayoon Fongsatitkul	Representative, Faculty of Public Health, Mahidol University
Asst. Prof. Dr. Bhumiphat Pachana	Representative, Faculty of Science, Burapha University

Scientific Committee

1. Assoc. Prof. Dr. Panida Navasumrit	Chulabhorn Research Institute/ Chulabhorn Graduate Institute
2. Prof. Dr. Piyarat Govitrapong	Chulabhorn Research Institute/ Chulabhorn Graduate Institute
3. Assoc. Prof. Dr. Piyajit Watcharasit	Chulabhorn Research Institute/ Chulabhorn Graduate Institute
4. Dr. Poonsakdi Ploypradith	Chulabhorn Research Institute/ Chulabhorn Graduate Institute
5. Prof. Dr. Prasat Kittakoop	Chulabhorn Research Institute/ Chulabhorn Graduate Institute
6. Assoc. Prof. Dr. Paiboon Vattanaviboon	Chulabhorn Research Institute/ Chulabhorn Graduate Institute
7. Assoc. Prof. Dr. Mayuree Fuangthong	Chulabhorn Research Institute/ Chulabhorn Graduate Institute
8. Prof. Dr. Prayad Pokethitiyook	Faculty of Science, Mahidol University
9. Asst. Prof. Dr. Puey Ounjai	Faculty of Science, Mahidol University
10. Assoc. Prof. Dr. Suphaphat Kwonpongsagoon	Faculty of Public Health, Mahidol University
11. Prof. Dr. Ubolluk Rattanasak	Faculty of Science, Burapha University
12. Assoc. Prof. Pachoenchoke Jintasaeranee	Faculty of Science, Burapha University
13. Asst. Prof. Dr. Chantima Piyapong	Faculty of Science, Burapha University

Logistics Committee

1. Mr. Preecha Sowanthip	Manager of Central Facility, Mahidol University, EHT
2. Mrs. Sasiwimol Hoontrakul	Academic Officer, EHT
3. Ms. Photjaman Nilbai	Financial Officer, EHT
4. Ms. Pusadee Nokthong	Coordinating Officer, Faculty of Science, Mahidol University
5. Ms. Thitipat La-Ongnual	Coordinating Officer, Faculty of Science, Mahidol University
6. Ms. Preeyapatra Boonma	Coordinating Officer, Faculty of Public Health, Mahidol University
7. Ms. Phunyisa Boonkunth	Coordinating Officer, Faculty of Science, Burapha University

Abbreviations

BUU	=	Environmental Science, Faculty of Science, Burapha University
CGI	=	Chulabhorn Graduate Institute
CRI	=	Chulabhorn Research Institute
PH	=	Faculty of Public Health, Mahidol University
SCBI	=	Environmental Biology / Biology, Faculty of Science, Mahidol University
SCTX	=	Toxicology, Faculty of Science, Mahidol University
EHT	=	Center of Excellence on Environmental Health and Toxicology
PERDO	=	S&T Postgraduate Education and Research Development Office

CONTENTS

Climate Change and Environmental Health

Environmental Pollution and Human Health

Environmental Pollution and Human Health (*Continued*)

Food Safety and Food Contaminants

Developmental Origins of Human Disease

Science and Technology for the Treatment and Management of Environmental Pollutants

Climate Change and Environmental Health

P-01

Development of high performance immunochromatographic methods for the detection of anti-IFN-gamma autoantibodies in adult-onset immunodeficientcy disease

Chawin Penjan[1], Akarin Intaramat[2], Mathuros Ruchirawat[2,3], and Mayuree Fuangthong[1,2,3]

[1]Applied Biological Sciences Program, Chulabhorn Graduate Institute, Bangkok, Thailand
[2]Translational Research Center, Chulabhorn Research Institute, Bangkok, Thailand
[3]Center of Excellence on Environmental Health and Toxicology (EHT), OPS, MHESI, Thailand

Abstract:

Adult-onset immunodeficiency (AOID) is a debilitating autoimmune disease characterized by the production of anti-IFN-γ autoantibodies (anti-IFN-γ AAb), resulting in susceptibility to opportunistic infections, primarily nontuberculous mycobacteria (NTM). The disease is often misdiagnosed as other systemic disorders, leading to delays in appropriate treatment while also wasting resources. The diagnosis of AOID primarily relies on detecting anti-IFN-γ AAb through methods such as ELISA, flow cytometry analysis, or western blotting. In this study, we created an AOID diagnostic test kit using two formats of immunochromatographic test (ICT). For the first format, IFN-γ gold-conjugate was used as detection probe and protein A/G was immobilized at the test zone as the capture probe. For the other format, protein A/G gold-conjugate was used as detection probe and IFN-γ was used as the capture probe. The recombinant rabbit monoclonal anti-human IFN-γ antibody (rb anti-IFN-γ) was used as the positive sample. Both ICT formats provide a similar limit of detection (LOD) at 0.625 ng/mL of rb anti-IFN-γ. When 1/500 diluted human plasma protein was mixed into the sample, the LOD was at 5 ng/mL for both formats. The test kit also demonstrated no cross-reactivity with human anti-myeloblastin antibody and human anti-myeloperoxidase antibody at a dilution of 1/100. Although more studies are needed to validate the efficiency of the ICT in clinical samples, these findings suggest a promising diagnostic test for AOID screening. This test kit has the potential to enable broader population outreach, enhance patient awareness, facilitate prompt medical intervention, and ultimately improve patient outcomes.

Keywords: Adult-onset immunodeficiency, Anti-IFN-γ autoantibodies, Nontuberculous mycobacteria (NTM), Autoimmune diseases, Immunochromatographic test

Introduction:

Adult-onset immunodeficiency (AOID) is an autoimmune disease caused by the production of anti-IFN-γ autoantibodies (anti-IFN-γ AAb) that suppress the immune function of IFN-γ. Patients with anti-IFN-γ AAb suffer from opportunistic infections, primarily nontuberculous mycobacteria (NTM), along with other pathogens. East Asia has the highest prevalence of AOID, including significant case series in Thailand and Taiwan (Wongkulab et al., 2013). Patients with AOID typically seek medical attention after opportunistic infections. Consequently, AOID is often misdiagnosed as other systemic disorders, leading to incorrect treatments and delaying the administration of appropriate care (Wu et al., 2020). The main strategy to diagnose AOID is to detect anti-IFN-γ AAb in the patient using ELISA, flow cytometry analysis, or Western blotting. These methods all take a lot of time and require both laboratories and technicians, which makes it hard to do the screening in the population. Therefore, a quick, accurate, and inexpensive test should be established to improve the prognosis of AOID.

Lateral Flow Immunoassay (LFIA), also known as immunochromatographic test (ICT), is a fast, easy, and low-cost detection method for screening diseases. LFIA can accurately detect the specific antigens of many diseases, such as hormones, proteins, bacteria, and viruses (Mainet-González, Palenzuela-Gardón, and Dayz-Argudín, 2007). The LFIA offers a promising and cost-efficient method for screening AOID within the population, initiating patient awareness, and directing doctors towards the right treatment.

Methodology:

Preparation of the test strip

The sample pads, 0903 Filter Paper (Whatman, UK) was soaked in 0.05% polyvinylpyrrolidone (PVP), 2% Triton X-100 in 50 mM Tris-HCl, pH 7.4, and dried overnight. The 8 µm pore size nitrocellulose membrane (NCM) AE99 (Whatman, UK) was immobilized with 0.5 mg/mL of protein A/G or IFN-γ at the test line and 0.5 mg/mL rabbit anti-IgY antibody at the control line. Protein A/G and IgY were immobilized by dispensing them into line shapes, while IFN-γ was immobilized by spotting. The immobilized NCM were then soaked in 1% bovine serum albumin (BSA), 0.2% trehalose in 10 mM sodium phosphate buffer, pH 7.4, and dried overnight. 3MM CHR chromatography paper (Whatman, UK) was used as absorption pad. The sample pad, NCM, and the absorption pad were assembled on plastic backing and cut into a 3 mm wide strip. The test strip was designed in two versions: one with IFN-γ as the detection probes and protein A/G as the capture probes (**Figure 1A**), and the other with protein A/G as the detection probes and IFN-γ as the capture probes (**Figure 1B**).

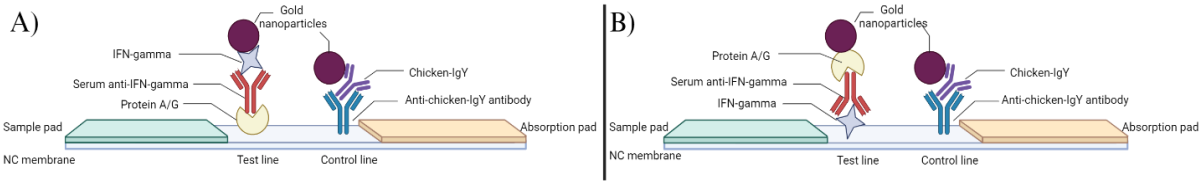

Figure 1 Test strip format with different test line system. A) IFN-γ as detection probes and protein A/G as capture probes, B) Protein A/G as detection probes and IFN-γ as capture probes.

Preparation of gold conjugate probes

40 nm colloidal gold solutions were mixed with protein A/G, IFN-γ, and IgY at pH 5.5, 11.5, and 9, respectively. The final concentration of protein A/G, IFN-γ, and IgY was 7 µg/mL, 6 µg/mL, and 6 µg/mL, respectively. After being incubated for 30 minutes, the gold solutions were blocked with 100 µL of 5% casein in 2 mM sodium borate buffer for 15 minutes. The mixtures were centrifuged at 6,000 g for 15 minutes, and the supernatant was removed. The resulting pellets were washed with washing buffer (0.5% casein in 2 mM sodium borate buffer) and centrifuged. The supernatant was discarded. Finally, the pellets were resuspended with washing buffer at 1/10 times the original volume, resulting in a 10X concentrated gold conjugate probe.

Test procedure

The recombinant rabbit anti-human IFN-γ monoclonal antibody (rb anti-IFN-γ) (Cat#MAB2853, R&D Systems, USA) was used as a positive sample. The sample for cross-reactivity testing included human anti-human proteinase 3 polyclonal antibody (anti-PR3) (Cat no.LS-C38480, LSBio, USA) and human anti-human myeloperoxidase polyclonal antibody (anti-MPO) (Cat no.LS-C16673, LSBio, USA). The pooled human plasma (Innovative Research, Canada) was applied as a mimic clinical sample to investigate the properties of the ICT system.

The gold conjugate probes (5 µL) were mixed with a 100 µL sample diluted in the running buffer, which was PBS (for the gold conjugate-IFN-γ format) and 0.5% BSA in 5 mM sodium phosphate buffer (for the gold conjugate-protein A/G format). Subsequently, the test strip was dipped into the mixture. The result was read after 30 minutes. During the reaction, the rb anti-IFN-γ in the sample binds with gold-conjugate probes and travels by capillary flow along the test strip. The gold conjugate probe-target complex is then captured by immobilized capture probes at the test line, producing a color that indicates a positive result. Additionally, the control detection probes are captured by immobilized capture probes at the control line. In the absence of rb anti-IFN-γ, the test line will not display any color. The results from the test kit were interpreted using visual observation and quantified based on a color signal. Images of the test results were captured with an 11000 Epson scanner using SilverFast scanner software. Subsequently, the color signal of the bands was analyzed using ImageQuant™ analysis software and reported as peak height.

Results and Discussion:

Detection limit and cross-reactivity

The rb anti-IFN-γ at 1 µg/mL was 2-fold diluted starting from 1/100. Both formats showed the lowest detected band at the test line, observed visually in the 1/1600 dilution sample, corresponding to 0.625 ng/mL of rb anti-IFN-γ, with no nonspecific binding observed in negative samples containing only running buffer (**Figures 2A, 2B**). We also tested the sample mixed with diluted 1/500 pooled human plasma. The sensitivity of ICT was reduced, and the LOD was at 5 ng/mL for both formats (**Figures 2C, 2D**). This reduction in sensitivity may be attributed to interferences such as salt, clotting factors, or proteins present in the plasma.

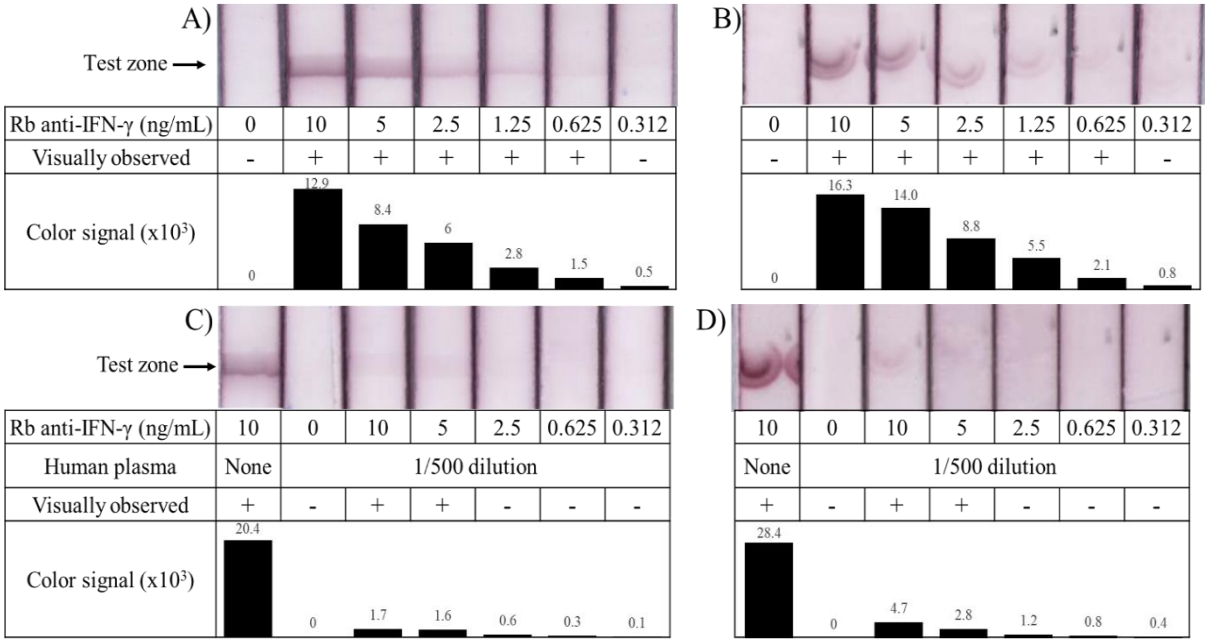

Figure 2 Detection limit of the two test kit formats. A) and C) Format with IFN-γ as detection probes. B) and D) Format with protein A/G as detection probes. In the visually observed result, "-" symbol denotes a negative result, while "+" symbol denotes a positive result.

The cross-reactivity testing was done using anti-PR3 and anti-MPO. The test system demonstrated no cross-reactivity with these two antibodies at a dilution of 1/100 (**Figure 3**).

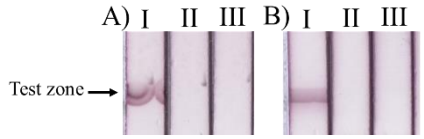

Figure 3 Cross-reactivity testing. Samples include 1/100 dilutions of Rb anti-IFN-γ (I), anti-PR3 (II), and anti-MPO (III). A) Format with IFN-γ as detection probes, B) Format with protein A/G as detection probes.

Gold conjugate-IgY as control probe

Rb anti-IFN-γ was mixed with 1 µL of gold conjugate-IgY and 5 µL of gold conjugate-IFN-γ prior to dipping the test strip. The gold conjugate-IgY binds specifically to immobilized rabbit anti-chicken IgY at the control line and shows no nonspecific binding to immobilized protein A/G at the test line, demonstrating the reliability of this control system (**Figure 4A**). In the format utilizing protein A/G as the gold-conjugate probe, the control line is visible even without the gold conjugate-IgY (**Figure 4B**). This occurs because the immobilized rabbit anti-IgY antibody, which is IgG, acts as the specific binding partner for gold conjugate-protein A/G. These two formats are promising as prototypes for a diagnostic test kit.

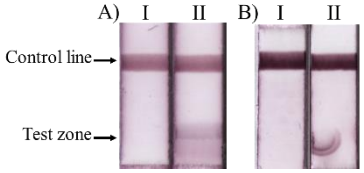

Figure 4 The test strip with both test line and control line. A) Format with IFN-γ as detection probes. B) Format with protein A/G as detection probes. Negative control (I) contains only dilution buffer. Positive sample (II) contains Rb anti-IFN-γ.

Yoshizawa et al. (2020) reported the average concentration of anti-IFN-γ antibodies in the serum of AOID patients detected with ELISA to be equivalent to 1274 ± 2682 ng/mL of mouse anti-human interferon-γ monoclonal antibody. Therefore, our test kit should be able to detect anti-IFN-γ antibodies in patients' serum even after some dilution.

Conclusion:

The optimal reagents and conditions used in preparing the test kit components significantly contributed to their promising performance. This test kit demonstrates potential as a valuable diagnostic tool for detecting anti-IFN-γ antibodies in patient serum and identifying adult-onset immunodeficiency. Nonetheless, further validation studies using clinical samples are needed to confirm its efficacy and applicability in real-world settings.

References:

Mainet-González, D., Palenzuela-Gardón, D. O., and Dayz-Argudín, T. (2007). Development of a immunochromatographic test with avidin-biotin for the detection of antibodies against antigen e of hepatitis B in human plasma. *Biotecnol. Apl., 24*, 265-275.

Wongkulab, P., Wipasa, J., Chaiwarith, R., and Supparatpinyo, K. (2013). Autoantibody to interferon-gamma associated with adult-onset immunodeficiency in non-hiv individuals in northern thailand. *PLOS ONE, 8*(9), e76371. doi:10.1371/journal.pone.0076371

Wu, U. I., Wang, J. T., Sheng, W. H., Sun, H. Y., Cheng, A., Hsu, L. Y., Chang, S. C., and Chen, Y. C. (2020). Incorrect diagnoses in patients with neutralizing anti-interferon-gamma-autoantibodies. *Clin Microbiol Infect, 26*(12), 1684.e1681-1684.e1686. doi:10.1016/j.cmi.2020.02.030

Yoshizawa, K., Aoki, A., Shima, K., Tanabe, Y., Koya, T., Hasegawa, T., Kikuchi, T., and Sakagami, T. (2020). Serum anti-interferon-γ autoantibody titer as a potential biomarker of disseminated non-tuberculous mycobacterial infection. *J. Clin. Immunol., 40*(2), 399-405. doi:10.1007/s10875-020-00762-1

P-02

Production of low-cost recombinant proteins for immunoassay to support local biologic drug development

Nonticha Ngernpisutsilp[1], Patchara Ngok-ngam[1,2], Karnpob Kanhasut[2,3], Nunthawan Thawanthalerngrit[2], Ratiphorn Sirichaichanakul[2], Mathuros Ruchirawat[2,3,4], and Mayuree Fuangthong[1,2,3,4*]

[1]Program in Applied Biological Sciences, Chulabhorn Graduate Institute, Chulabhorn Royal Academy, Bangkok 10210, Thailand
[2]Translational Research Center, Chulabhorn Research Institute, Bangkok 10210, Thailand
[3]Center for Biologics Research and Development, Chulabhorn Research Institute, Bangkok 10210, Thailand
[4]Center of Excellence on Environmental Health and Toxicology (EHT), OPS, MHESI, Thailand

Abstract:

Horseradish peroxidase (HRP) is an important enzyme in life science used as an enzyme-based signal amplification for various applications. Herein, we report the design, construction, and expression of recombinant HRP-conjugated streptavidin using the ExpiHEK293 cell expression system. HRP was purified through the Ni-NTA column. The molecular weight of HRP-streptavidin was analyzed using SDS-PAGE and Western immunoblotting. Hemin incubation was performed to activate apo-HRP. The enzymatic activity testing of hemin-activated HRP-streptavidin was tested. The activity of activated HRP-streptavidin with 2 equivalents of hemin showed the highest activity. The results provided convincing result that the production of functional HRP-streptavidin in ExpiHEK293 cells is applicable, which can be further used as a detection molecule in immunoassay to reduce the cost of commercial HRP-streptavidin in the future.

Keywords: Horseradish peroxidase, Streptavidin, ExpiHEK239, Immunoassay

Introduction:

Horseradish peroxidase (HRP) is a heme-containing enzyme, which is extensively used in various aspects because it catalyzes the oxidative reaction of several substrates, leading to visible color changes in the presence of H_2O_2. In addition, it is not prohibitively expensive (1). The demand for HRP has increased as a result of the growing HRP utilization in research and development. However, so far, commercial HRP is mostly obtained from horseradish root (*Armoracia rusticana*) but the limitations of HRP from plants are long cultivation periods, different isoenzymes, and heterogeneous glycosylation patterns of enzymes (2). Among various HRP isozymes, C1A was the most isozymes used in research (3) . Production of recombinant HRP in other organisms has been developed in bacterial system, yeast system, insect system, mammalian system, and also plant system (3, 4). However, there are still limitations in each system in terms of attribute and yield. Human embryonic kidney cell line (HEK293) is a human cell line that is commonly used in the transient production of research and pre-clinical proteins and has post-translational modifications (PTMs) machinery that can produce proteins with native PTMs (5). HEK293 cells tend to express HRP because glycan chains of recombinant mammalian HRP is already humanized, providing high-quality HRP in terms of a homogeneous isoform of HRP. Moreover, numerous market consumers prefer high-quality HRP with a small yield over high-yield but impure HRP.

In this study, we aimed to produce HRP conjugated streptavidin using ExpiHEK293 cells for utilizing in immunoassay kit used in drug development laboratory.

Material and method

Recombinant plasmid containing HRP-streptavidin design and construction

A synthetic construct of the HRP C1A gene (AB920392.1) and the synthetic streptavidin gene (KT344129.1) obtained from the National Center for Biotechnology Information (NCBI) database was inserted in pcDNA 3.1(+). The codon optimization of the nucleotide sequence of HRP-streptavidin gene was performed for the expression in ExpiHEK293 cells. Plasmid propagation was done in *E. coli* DH5α.

Transient transfection of recombinant plasmid into ExpiHEK293 cells

ExpiHEK293 cells were seeded at 3 x 10^6 cells/mL in Expi293™ expression medium at 37 ºC, 8% CO_2 at 130 rpm overnight to reach approximately 5 x 10^6 cells/mL. Then, the cells were diluted to 3 x 10^6 cells/mL in fresh expression medium and kept for at least 30 minutes in incubator. Then, transfection was performed according to ExpiFectamine™ protocol. At 18-22 hours after transfection, ExpiFectamine™ transfection Enhancer 1 and 2 were added into the culture flask. The culture was grown for an overall duration of 4 days at 37 ºC.

Enzyme purification

Expression culture was centrifuged at 3,500 g, 4 ºC for 30 minutes to collect supernatant. Supernatant was purified using Ni-NTA column (GE Healthcare). The column was pre-equilibrated with a binding buffer (20 mM sodium phosphate, 0.5 M NaCl, 5 mM imidazole, pH 7.4) followed by rinsing with 10 column volumes of binding buffer. The bound recombinant HRP-streptavidin was eluted with a 0 to 100% gradient of elution buffer (20 mM sodium phosphate, 0.5 M NaCl, 0.5 M imidazole, pH 7.4).

Sodium dodecyl sulfate-polyacrylamide gel electrophoresis (SDS-PAGE) and Western immunoblotting analysis

Samples were run through SDS-PAGE prior to Coomassie staining (InstantBlue® (ISB1L)) or Western immunoblotting. For Western immunoblotting, mouse-anti histidine, ab18184 (Abcam) and goat-anti mouse antibody (Jacksonimmunoresearch) were used. Finally, the ImageQuant LAS4000 computer (GE Healthcare, USA) was utilized to illustrate the chemiluminescent signal.

Hemin activation

HRP-streptavidin (50 µM) was mixed with 1 and 2 equivalents (eq.) of hemin in TSB solution (25 mM Tris HCl pH7.4, 150 mM NaCl) containing 2% of dimethylformaldehyde and 1 mM $CaCl_2$ and incubated at 4 °C overnight. Dialysis of activated HRP-streptavidin was performed using Slide-A-Lyzer™ MINI Dialysis Device, 3.5 kDa (Thermo Fisher Scientific). Activated HRP were characterized by UV-vis-absorption spectra on Nanodrop 1000 (Thermo Fisher Scientific) at 403 nm.

HRP Activity testing

The activity of HRP was tested by incubating the enzyme with TMB substrate (Seracare). The absorbance at 450 nm was measured and enzyme activity was calculated.

Results, Discussion, and Conclusion:

The design and construction of the recombinant plasmid pcDNA 3.1(+)-HRP-streptavidin

The recombinant plasmid pcDNA 3.1(+) containing HRP-Streptavidin was designed as shown in Figure 1. The plasmid is composed of a secretion signal sequence, secreted acid phosphatase 1 (SAP1), octahistidine for protein purification, and a tobacco etch virus protease recognition site (TEV) for removing unnecessary tags.

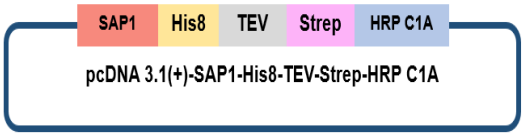

Figure 1 The figure shows pcDNA3.1(+) plasmid containing HRP-Streptavidin gene. SAP1 is secretion signal sequence. His8 is Octahistidine-tag. TEV is Tobacco etch virus protease recognition site. Strep and HRP C1A is streptavidin and horseradish peroxidase C1A, respectively.

SDS-PAGE and Western immunoblotting analysis of purified HRP-streptavidin

HRP-streptavidin was presented at molecular weight around 70 kDa demonstrated by Coomassie staining (Figure 2A.) and Western immunoblotting (Figure 2B.)

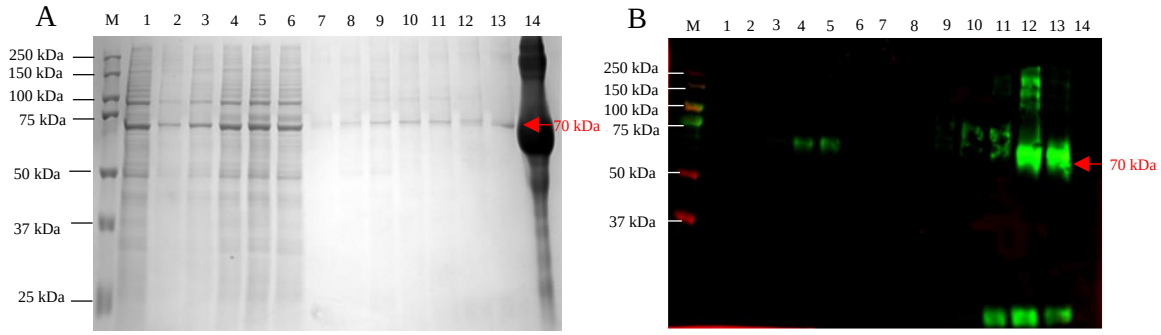

Figure 2 SDS-PAGE (A) and Western blot analysis (B) for verification of HRP-streptavidin expression. M is Marker, Lane 1 = Supernatant of non-transfected cells, Lane 2-5 = Supernatant of transfected cells day 1 to day 4, Lane 6 = Flowthrough, Lane 7-13 = Eluted fractions, Lane 14 = Commercial HRP-streptavidin.

Hemin activation

The E_{403} value of HRP-streptavidin was determined to demonstrate hemin insertion. The result showed that E_{403} value of HRP-streptavidin incubated with 2 eq. hemin (141.84 mM^{-1} mm^{-1}) was higher than 1 eq. hemin (110 mM^{-1} mm^{-1}) (Figure 3.)

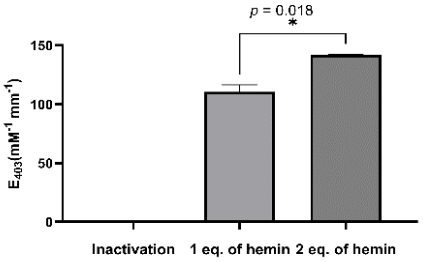

Figure 3. Molar extinction coefficient, E_{403} of inactivated, 1eq. and 2eq.of activated HRP-Streptavidin. The error bars represent standard errors, n=2. The * represented statistically significant difference using t-test with $P < 0.05$.

Preliminary enzyme activity testing

The activity of activated HRP-streptavidin was tested by incubation with substrate. The OD_{450} of activated HRP-streptavidin with 2 eq. hemin showed statistically higher than 1 eq. hemin while, there is no activity of inactivated HRP-streptavidin.

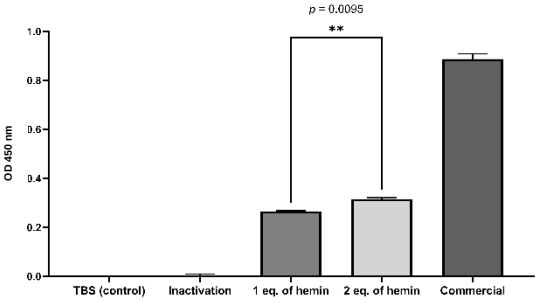

Figure 4. The absorbance at 450 nm of inactivated HRP-Streptavidin and activated by 1 eq. and 2 eq. of hemin. The commercial HRP- is used as positive control. The error bars represent standard errors, n=2. The * represented statistically significant difference using t-test with $P < 0.05$.

In conclusion, this study provides the evidence of functional HRP-Streptavidin production using ExpiHEK293 cells. The enzymes were purified and tested for its activity after activation with hemin. This information convinced that functional HRP-streptavidin can be produced in mammalian expression system, HEK cells. However, the produced HRP-streptavidin needs further immunoassay testing to confirm that the selected expression system can improve the quality and reduce the cost of the enzyme.

References

1. Porstmann B, Porstmann T, Nugel E, Evers U. Which of the commonly used marker enzymes gives the best results in colorimetric and fluorimetric enzyme immunoassays: horseradish peroxidase, alkaline phosphatase or β-galactosidase? Journal of Immunological Methods. 1985;79(1):27-37.
2. Veitch NC. Horseradish peroxidase: a modern view of a classic enzyme. Phytochemistry. 2004;65(3):249-59.
3. Krainer FW, Glieder A. An updated view on horseradish peroxidases: recombinant production and biotechnological applications. Applied Microbiology and Biotechnology. 2015;99(4):1611-25.
4. Greco O, Folkes LK, Wardman P, Tozer GM, Dachs GU. Development of a novel enzyme/prodrug combination for gene therapy of cancer: horseradish peroxidase/indole-3-acetic acid. Cancer Gene Therapy. 2000;7(11):1414-20.
5. Abaandou L, Quan D, Shiloach J. Affecting HEK293 cell growth and production performance by modifying the expression of specific genes. Cells. 2021;10(7):1667.

Environmental Pollution and Human Health

P-03

The Effects of Dibutyl Phthalate (DBP) Degrading enzyme, *EstB*, against β-lactam Susceptibility in *Pseudomonas aeruginosa*

Wirongrong Whangsuk[1], Suvit Loprasert[1], Punyawee Dulyayangkul[1*], Skorn Mongkolsuk[1,2]

[1]Laboratory of Biotechnology, Chulabhorn Research Institute, Bangkok, Thailand,
[2]Center of Excellence on Environmental Health and Toxicology (EHT), OPS, MHESI, Thailand
E-mail: punyawee@cri.or.th

Abstract:

A dual function Esterase B (EstB) from *Sphingobium* sp. SM42 had been characterized. The studies showed its ability in degrading dibutyl phthalate (DBP), the endocrine disruptor; and cleaving the side chain of antibiotic in cephalosporin family via de-arenethiolase activity. In *Sphingobium* sp. SM42, expressing EstB in periplasmic space had increased antibiotic susceptibility. Here, we used the National Center for Biotechnology Information (NCBI) public database to study the distribution of *estB* and *estB*-like genes in other organisms. Two *estB*-like genes were identified in an inserted sequence of DBP degrading *Pseudomonas aeruginosa* PS1. The two EstB-like protein are called UCM26615 and UCM26628 which are 98% and 90% identical to EstB, respectively. The finding suggested possible horizontal transfer events between microorganisms dwelling in DBP contaminated soil. To mimic multi-copies of *estB*-like genes found in PS1, we introduced plasmid encoding EstB to our surrogate *P. aeruginosa* PAO1. The effect of de-arenethiolase activity in cytoplasm and periplasmic space were studied using antibiotic susceptibility assay. Expressing EstB in the periplasmic space of PAO1 showed an increased in susceptibility to β-lactam antibiotics including carbapenems and cephalosporins suggesting that de-arenethiolase activity of EstB is not specific to *Sphingomonadaceae*. The advantages of horizontally transferred EstB-like proteins in *P. aeruginosa* PS1 is needed to be explored further.

Keywords: EstB, DBP degrading enzyme, De-arenethiolase, β-lactam, *Pseudomonas aeruginosa*

Introduction:

Esterase B (EstB) from *Sphingobium* sp. SM42 belongs to group VIII of esterase and lipase that was categorized into 19 families: I to XIX (1-3). EstB is known to degrade dibutyl phthalate (DBP) (2-4). DBP is an endocrine disruptor and one of the most abundant phthalate esters, which is used worldwide as a plasticizer. Many genera of DBP degrading bacteria have been isolated: *Pseudomonas*, *Rhodococcus*, *Gordonia*, *Achromobacter*, *Agromyces*, *Microbacterium*, *Bacillus*, *Sphingomonas*, *Comamonas*, *Curvibacter*, *Agrobacterium*, and *Providencia* (5, 6). Previously, EstB from *Sphingobium* sp. SM42 has been characterized. The studies revealed a dual activity of EstB: first degrading DBP and second de-arenethiolase activity, cleaving C-S bond at C3-side chains within the dihydrothiazine of cephalosporins, a sub-group of β-lactam antibiotics (4, 7). Interestingly, once EstB was expressed in the periplasmic space of *Sphingobium* sp. SM42, the bacteria became more susceptible to the tested cephalosporins, cefoperazone and cephazolin. The study revealed that the de-arenethiolase activity of EstB cleaves the side chain of cefoperazone and cephazolin resulting in more active β-lactam (7). In the periplasmic space, β-lactam interacts with penicillin binding proteins, halts the membrane recycling pathway and resulting in cell-death (8).

In the microorganism communities, varies species interact and genes can be transferred across genera. To investigate the distribution of interested gene, *estB,* and the possibility of the gene exchange, we searched for EstB on the National Center for Biotechnology Information (NCBI) public database. Later, the transfer of *estB*-like genes was mimicked with plasmid mediated carrying *estB* and its function was studied in the surrogate host.

Methodology:

Identifying species carrying *estB*-like genes

EstB was searched on the National Center for Biotechnology Information (NCBI) against non-redundant protein sequences using protein-protein BLAST algorithm (blastp) (9-11). Inclusion criteria was a protein with more than 90% identical to EstB whereas exclusion criteria was any protein from *Sphingomonadaceae*.

Construction of pEstB-C and pEstB-P

Cytoplasmic expressing EstB plasmid, pEstB-C was generated by ligating *estB* gene to pBBR1MCS-5, a broad host range plasmid. A periplasm expressing EstB plasmid, pEstB-P, was generated by ligating accessory and essential components i.e. *tetR* gene and *tetR* promoter that governs OmpA signal peptides fused with *estB* gene, to pBBR1MCS-5 (12).

Construction of *P. aeruginosa* carrying EstB

Plasmid encoding EstB was introduced to sucrose competent *P. aeruginosa* PAO1 cell by electroporation method (13). Transformant was selected on gentamicin (30 mg/L) and the presence of plasmids was confirmed by PCR using plasmid specific primers M13F (5'-GTAAAACGACGGCCAGT-3') and M13R (5'- GGAAACAGCTATGACCATG-3').

Antibiotic susceptibility assay

Antimicrobial susceptibility was determined and interpreted following CLSI guidelines (14). Antibiotic discs from OXIOD (United Kingdom) were placed on a lawn of bacteria on Mueller-Hinton agar. Representative of β-lactams including the carbapenems: meropenem (MEM) (10 µg) and imipenem (IPM) (10 µg); and the third-generation cephalosporins: ceftazidime (CAZ) (30 µg), (FEP) cefepime (30 µg), ceftibuten (CFT) (30 µg), cefoperazone (CFP) (75 µg), and ceftriaxone (CRO) (30 µg) were tested. In a condition were tetracycline is required to induce the expressing of EstB in periplasmic space, a sub-lethal concentration of anhydrotetracycline (2 mg/L) was introduced into Mueller-Hinton agar followed by a lawn of bacteria and antibiotic discs. Zone of inhibition (mm) was measured after 16-18 hours of incubation at 37°C. Data were reported as the mean ± SD of three independent biological replicates. t-test was used for statistical analysis, comparing with an appropriate control group.

Result and Discussion:

Identifying species carrying *estB*-like genes

NCBI blastp (9-11) of EstB (384 aa) result revealed 32 EstB-like proteins with more than 90% identical to EstB. Thirty belongs to *Sphingomonadaceae* and two belongs to a single species, *Pseudomonas sp.* PS1. This bacterium was isolated from environmental material in Guangzhou, China. This has ability to degrade DBP (1, 6). The two EstB-like proteins of PS1 are called UCM26615 (381 aa) and UCM26628 (362 aa). UCM26615 and UCM26628 are 98% and 90% identical to EstB, respectively. With the whole-genome sequence (WGS) data of *Pseudomonas sp.* PS1 (Accession number CP084484), we further confirmed that PS1 belongs to *P. aeruginosa* group using SpeciesFinder-2.0 (15). Genome comparing between *P. aeruginosa* PS1 and *P. aeruginosa* PAO1, a reference strain, revealed that the two *estB*-like genes lies within an 83 Kbp inserted sequence of PS1.

Effect of multi-copies EstB in *P.* aeruginosa PAO1

WGS of PS1 suggested that the two *estB*-like genes were integrated into the chromosome potentially from the horizontal gene transfer from other organisms dwelling in the same environment. To mimic the multi-copies of *estB*-like genes found in PS1, we introduced plasmid encoding EstB to our surrogate host, *P. aeruginosa* PAO1. The effect of de-arenethiolase activity in cytoplasm and periplasmic space were studied using antibiotic susceptibility assay, based on the assumption of EstB cleaves cephalosporins side chain generating more active β-lactam (7).

The results suggested that overexpressing EstB in cytoplasm, pEstB-C, of *P. aeruginosa* PAO1 did not change the antibiotic susceptibility (Figure 1A). pEstB-P was used for the study of EstB in periplasmic space. In pEstB-P, EstB was fused with OmpA signal peptides. OmpA is a membrane protein which was translated as pro-OmpA in cytoplasm. Pro-OmpA composed of a secretory precursor of OmpA protein so called OmpA signal peptides which will direct protein to the membrane, once the pro-OmpA translocated, the signal peptide will be cleaved generating mature OmpA protein (16). In addition, EstB fused with OmpA signal peptides was controlled under Tet-expression system where tetracycline is an inducer (17). In the absence of inducer, pEstB-P^- (control), zone of inhibition of the tested antibiotics were similar to pBBR, control, of cytoplasm expression (Figure 1A and 1B). Once the inducer was presented, pEstB-P^+, EstB fused with OmpA signal peptides will be translated and translocated to periplasmic space. *P. aeruginosa* PAO1 with EstB expressing in periplasmic space became more susceptible to all tested β-lactams. This suggesting that the proposed de-arenethiolase activity in *Sphingobium* sp. SM42 (7) is also function *P. aeruginosa* PAO1.

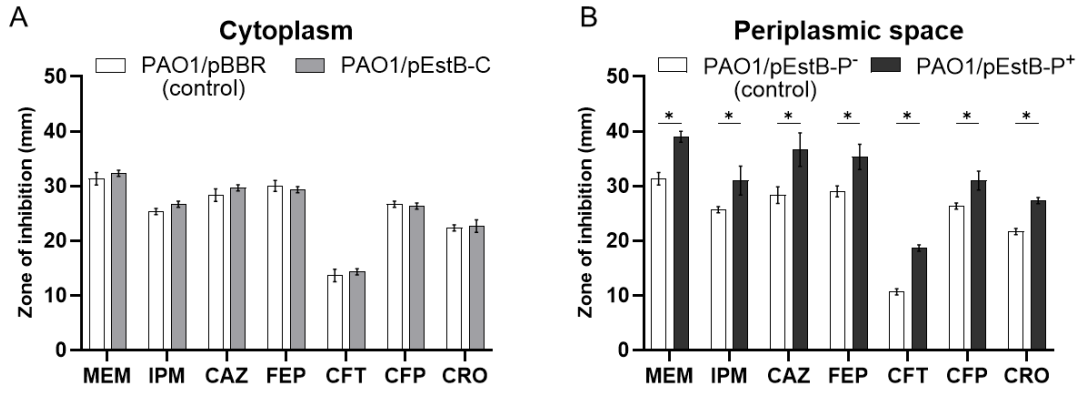

Figure 1. Localization of EstB and its effect against β-lactam susceptibility in *P. aeruginosa* PAO1. Antibiotic disc susceptibility of (A) PAO1 expressing EstB in the cytoplasm (pEstB-C) and its control (pBBR, empty plasmid); and (B) PAO1 expressing EstB in the periplasmic space (pEstB-P^+) and its control (pEstB-P^-, uninduced condition). Data representative in mean±SD of three biological replicates. *, *p*-value < 0.05 by t-test.

Conclusion:

De-arenethiolase activity of EstB in the periplasmic space of *P. aeruginosa* PAO1 increased the susceptibility of the tested β-lactam antibiotics: both carbapenems and the third-generation cephalosporins. The advantages of horizontally transferred EstB-like proteins from *Sphingobium* sp. or *Sphingomonadaceae* to *P. aeruginosa* PS1 is needed to be studied.

Acknowledgement:

We thanks to Dr. James M. Dubbs and Associate Professor Dr. Paiboon Vattanaviboon from Laboratory of Biotechnology, Chulabhorn Research Institute for valuable advice. This work is supported by Thailand Science Research and Innovation (TSRI), Chulabhorn Research Institute (Grant number 48293/4691984).

References:

1. Cheng J, Du H, Zhou MS, Ji Y, Xie YQ, Huang HB, et al. Substrate-enzyme interactions and catalytic mechanism in a novel family VI esterase with dibutyl phthalate-hydrolyzing activity. Environ Int. 2023;178:108054.
2. Ramnath L, Sithole B, Govinden R. Classification of lipolytic enzymes and their biotechnological applications in the pulping industry. Can J Microbiol. 2017;63(3):179-92.
3. Wang B, Wu S, Chang X, Chen J, Ma J, Wang P, et al. Characterization of a novel hyper-thermostable and chlorpyrifos-hydrolyzing carboxylesterase EstC: A representative of the new esterase family XIX. Pestic Biochem Physiol. 2020;170:104704.
4. Sungkeeree P, Toewiwat N, Whangsuk W, Ploypradith P, Mongkolsuk S, Loprasert S. The esterase B from *Sphingobium* sp. SM42 has the new de-arenethiolase activity against cephalosporin antibiotics. Biochem Biophys Res Commun. 2018;506(1):231-6.
5. Hu R, Zhao H, Xu X, Wang Z, Yu K, Shu L, et al. Bacteria-driven phthalic acid ester biodegradation: Current status and emerging opportunities. Environment International. 2021;154:106560.
6. Du H, Cheng J-L, Li Z-Y, Zhong H-N, Wei S, Gu Y-J, et al. Molecular insights into the catabolism of dibutyl phthalate in *Pseudomonas aeruginosa* PS1 based on biochemical and multi-omics approaches. Science of The Total Environment. 2024;926:171852.
7. Toewiwat N, Whangsuk W, Ploypradith P, Mongkolsuk S, Loprasert S. Cefoperazone induces esterase B expression by EstR and esterase B enhances cefoperazone activity at the periplasm. Int J Med Microbiol. 2020;310(2):151396.
8. Johnson JW, Fisher JF, Mobashery S. Bacterial cell-wall recycling. Ann N Y Acad Sci. 2013;1277(1):54-75.
9. Altschul SF, Madden TL, Schaffer AA, Zhang J, Zhang Z, Miller W, et al. Gapped BLAST and PSI-BLAST: a new generation of protein database search programs. Nucleic Acids Res. 1997;25(17):3389-402.
10. Camacho C, Coulouris G, Avagyan V, Ma N, Papadopoulos J, Bealer K, et al. BLAST+: architecture and applications. BMC Bioinformatics. 2009;10:421.
11. Johnson M, Zaretskaya I, Raytselis Y, Merezhuk Y, McGinnis S, Madden TL. NCBI BLAST: a better web interface. Nucleic Acids Res. 2008;36(Web Server issue):W5-9.
12. Kovach ME, Elzer PH, Hill DS, Robertson GT, Farris MA, Roop RM, 2nd, et al. Four new derivatives of the broad-host-range cloning vector pBBR1MCS, carrying different antibiotic-resistance cassettes. Gene. 1995;166(1):175-6.
13. Choi KH, Kumar A, Schweizer HP. A 10-min method for preparation of highly electrocompetent *Pseudomonas aeruginosa* cells: application for DNA fragment transfer between chromosomes and plasmid transformation. J Microbiol Methods. 2006;64(3):391-7.
14. Clinical and Laboratory Standards Institute. Performance standards for antimicrobial susceptibility testing. 33rd ed. CLSI supplement M100. USA2023.

15. Larsen MV, Cosentino S, Lukjancenko O, Saputra D, Rasmussen S, Hasman H, et al. Benchmarking of methods for genomic taxonomy. J Clin Microbiol. 2014;52(5):1529-39.

16. Movva NR, Nakamura K, Inouye M. Amino acid sequence of the signal peptide of ompA protein, a major outer membrane protein of *Escherichia coli*. J Biol Chem. 1980;255(1):27-9.

17. Skerra A. Use of the tetracycline promoter for the tightly regulated production of a murine antibody fragment in *Escherichia coli*. Gene. 1994;151(1-2):131-5.

P-04

Identification and Characterization of Small Multidrug Resistance Family Efflux Pump in *Stenotrophomonas maltophilia*

Punyawee Dulyayangkul[1]*, Wirongrong Whangsuk[1], Paiboon Vattanaviboon[1], and Skorn Mongkolsuk[1,2]

[1]Laboratory of Biotechnology, Chulabhorn Research Institute, Bangkok, Thailand.
[2]Center of Excellence on Environmental Health and Toxicology (EHT), OPS, MHESI, Bangkok, Thailand.
* E-mail: punyawee@cri.or.th

Abstract:

Quaternary Ammonium Compounds (QACs) have been used in disinfectants, sanitizers, surfactants, and preservatives. The usages had been accelerated by the COVID-19 pandemic leading to the increased exposure of QACs in microorganisms. Gram-negative bacteria acquired *qac* resistance genes via horizontal transfer mechanisms. Here, *qac* resistance gene, named *smr*, encoding Small Multidrug Resistance (SMR) efflux pump was found on genome of a QACs-resistant *Stenotrophomonas maltophilia* strain SMR. A horizontal transfer event was mimic by plasmid carrying *smr* which transferred to *S. maltophilia* strain K279a. This generating K279a/pSMR where function of *smr* against QACs resistance/tolerance was characterized. Growth kinetic of K279a/pSMR against benzalkonium chloride, benzethonium chloride, and cetylpyridinium chloride revealed that pSMR increased QACs tolerance in *S. maltophilia*.

Keywords: SMR efflux pump, QACs, disinfectant, *Stenotrophomonas maltophilia*

Introduction:

Quaternary Ammonium Compounds (QACs) are active ingredients of disinfectants and sanitizers which is widely used in households, schools, workplaces, hospitals, and industries since the outbreak of COVID-19 (1). QACs has been used as antimicrobials, preservatives, and surfactants long before the outbreak, yet the pandemic had raised the usage of QACs, significantly (2). The increased consumption during the pandemic lead to a 3-fold increase of QACs in wastewater (3). Therefore, there is an increase in QACs exposure to bacteria at the site of QACs usage and/or in the wastewater. Bacteria that can thrive antimicrobial compounds consists at least one of the resistance mechanisms: intrinsic, adaptive, and acquired resistance mechanisms (4). One of the common QACs resistance mechanisms found in Gram-negative opportunistic pathogens is the acquiring of Small Multidrug Resistance (SMR) family efflux pump by horizontal gene transfer (5, 6). In this study, a QACs-resistant *Stenotrophomonas maltophilia* strain SMR was studied aiming to understand the mechanism of QACs resistance found in this Gram-negative opportunistic pathogen.

Methodology:

Bacterial strains and growth condition

S. maltophilia K279a (7), *S. maltophilia* SMR, and *Escherichia coli* DH5α were retrieved from laboratory stock. *S. maltophilia* were grown at 35°C and *E. coli* were grown at 37°C. All bacteria were aerobically cultivated in Luria-Bertani broth (LB) with agitation at 180 rpm or on LB agar, unless specified.

Whole Genome Sequence (WGS) analysis

The genomic libraries of *S. maltophilia* SMR were sequenced on an Illumina MiSeq600 platform by PORCINOTEC (Thailand). Acquired antibiotic and antimicrobial resistance genes were identified using ResFinder (version 4.5.0) (8, 9).

Construction of pSMR1 and pSMR2

pSMR was generated by ligating *smr* amplicon to pBBR1MCS-1 (10) at SmaI site. The *smr* amplicon was amplified with high fidelity DNA polymerase using gene specific primers SMR-FW (5'- AAT TTC TCC TTC ATA CCG TAG AGG AGA TT-3') and SMR-RV (5'-GTT AGA TGC CAA CCC GGT CAA TGT-3'). pSMR and p (empty plasmid control) were introduced into *S. maltophilia* K279a by electroporation (11). The transformants were selected on LB agar plate supplemented with chloramphenicol 40 mg/L and confirmed by PCR using primers M13F (5'-GTA AAA CGA CGG CCA GT-3') and M13R (5'-GGA AAC AGC TAT GAC CAT G-3').

Determination of Minimum Inhibitory Concentration (MIC)

Benzalkonium chloride MIC was determined by broth-microdilution method. The assay was performed with Mueller-Hinton broth (12). In brief, 20 µL of OD_{600} 0.01 overnight culture were added to 180 µL of 2-fold diluted antimicrobial compounds in 96-well plates. Plates were incubated at 35°C for 18 hours and OD_{600} was measured with a microplate reader (EPOCH 2). The lowest concentration that can inhibit the growth was defined as MIC.

Growth kinetic against antimicrobial compounds

Growth kinetic against antimicrobial compounds were determined in 96-well plate. Sub-lethal concentrations of QACs were prepared by 2-fold dilution with Mueller-Hinton broth. Twenty microliters (20 µL) of OD_{600} 0.01 overnight culture were added to 180 µL of 2-fold diluted plates. The plates were incubated at 35°C with double orbital shaking and OD_{600} was measured with a microplate reader (EPOCH 2) at an interval of every 20 minutes for 20 hours. Data were plotted and growth curve of *S. maltophilia* K279a/p and K279a/pSMR in Mueller-Hinton broth, 8 mg/L of benzalkonium chloride, 16 mg/L of benzethonium chloride, and 16 mg/L of cetylpyridinium chloride were generated by GraphPad Software.

Result and Discussion:

MICs of *S. maltophilia* K279a and *S. maltophilia* SMR against benzalkonium chloride were determined as 16 mg/L and 32 mg/L, respectively. *S. maltophilia* SMR genomes were sent for sequencing, aiming to identify gene(s) responsible for the 2-fold increase of MIC benzalkonium chloride, compared to *S. maltophilia* K279a-a reference strain. Analysis *S. maltophilia* SMR genome sequence with ResFinder (8, 9) revealed that *S. maltophilia* SMR carries a *qac* resistance gene, named *smr*, encoding SMR family efflux pump. To confirm the identification, function, and mimicking the acquisition of the *qac* resistance gene; *smr* gene was cloned into a broad-host-range plasmid, pBBR1MCS-1 (10), and introduced to *S. maltophilia* K279a.

QACs resistance phenotype was studied by comparing growth kinetic of K279a/pSMR and K279a/p against various compounds at sub-lethal concentrations. K279a/pSMR represent *S. maltophilia* acquired *qac* resistant gene, *smr*, and K279a/p is a control*:* K279a with empty plasmid. K279a/p and K279a/pSMR growth curve kinetic were performed at 8 mg/L of benzalkonium chloride, 16 mg/L of benzethonium chloride, and 8 mg/L of cetylpyridinium chloride together with Mueller-Hinton broth alone as a control. The results suggested that acquiring SMR (K279a/pSMR) did not alter growth of *S. maltophilia* (Figure 1A). However, in the presence of sub-lethal concentration of QACs, K279a/pSMR grew better than K279a/p especially during log-phase state (Figure 1B-D). In addition, without pSMR, K279a growth were delayed by 2-hour, 4-hour, and 8-hour in 8 mg/L of benzalkonium chloride, 16 mg/L of benzethonium chloride, and 8 mg/L of

cetylpyridinium chloride, respectively (Figure 1B-D). These results suggested that *smr* is responsible for QACs tolerance/resistance in *S. maltophilia*.

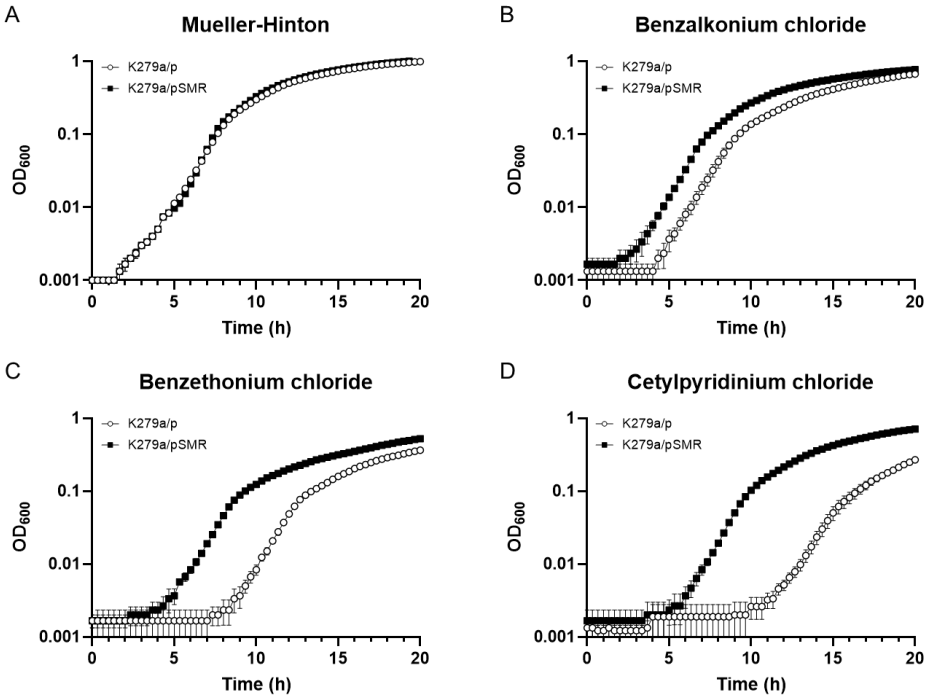

Figure 1 Growth curve of *S. maltophilia* K279a/p and *S. maltophilia* K279a/pSMR in (A) Mueller-Hinton broth, control, (B) Benzalkonium chloride at 8 mg/L, (C) Benzethonium chloride at 16 mg/L, and (D) Cetylpyridinium chloride at 16 mg/L. Data are presented in mean and SEM of three replicates.

Conclusion:

S. maltophilia SMR acquired *smr* gene which is responsible for QACs resistance. *smr* once transferred horizontally to *S. maltophilia* K279a (K279a/pSMR) increased QACs tolerance as shown in growth curve against QACs.

Acknowledgement:

This work is supported by Thailand Science Research and Innovation (TSRI), Chulabhorn Research Institute (Grant number 48293/4691984).

References:

1. Hora PI, Pati SG, McNamara PJ, Arnold WA. Increased Use of Quaternary Ammonium Compounds during the SARS-CoV-2 Pandemic and Beyond: Consideration of Environmental Implications. Environ Sci Technol Lett. 2020;7(9):622-31.
2. Arnold WA, Blum A, Branyan J, Bruton TA, Carignan CC, Cortopassi G, et al. Quaternary Ammonium Compounds: A Chemical Class of Emerging Concern. Environ Sci Technol. 2023;57(20):7645-65.
3. Mohapatra S, Yutao L, Goh SG, Ng C, Luhua Y, Tran NH, et al. Quaternary ammonium compounds of emerging concern: Classification, occurrence, fate, toxicity and antimicrobial resistance. J Hazard Mater. 2023;445:130393.

4. Pang Z, Raudonis R, Glick BR, Lin TJ, Cheng Z. Antibiotic resistance in *Pseudomonas aeruginosa*: mechanisms and alternative therapeutic strategies. Biotechnol Adv. 2019;37(1):177-92.
5. Tezel U, Pavlostathis SG. Quaternary ammonium disinfectants: microbial adaptation, degradation and ecology. Curr Opin Biotechnol. 2015;33:296-304.
6. Lu Z, Mahony AK, Arnold WA, Marshall CW, McNamara PJ. Quaternary ammonia compounds in disinfectant products: evaluating the potential for promoting antibiotic resistance and disrupting wastewater treatment plant performance. Environmental Science: Advances. 2024;3(2):208-26.
7. Crossman LC, Gould VC, Dow JM, Vernikos GS, Okazaki A, Sebaihia M, et al. The complete genome, comparative and functional analysis of *Stenotrophomonas maltophilia* reveals an organism heavily shielded by drug resistance determinants. Genome Biol. 2008;9(4):R74.
8. Camacho C, Coulouris G, Avagyan V, Ma N, Papadopoulos J, Bealer K, et al. BLAST+: architecture and applications. BMC Bioinformatics. 2009;10:421.
9. Bortolaia V, Kaas RS, Ruppe E, Roberts MC, Schwarz S, Cattoir V, et al. ResFinder 4.0 for predictions of phenotypes from genotypes. J Antimicrob Chemother. 2020;75(12):3491-500.
10. Kovach ME, Elzer PH, Hill DS, Robertson GT, Farris MA, Roop RM, 2nd, et al. Four new derivatives of the broad-host-range cloning vector pBBR1MCS, carrying different antibiotic-resistance cassettes. Gene. 1995;166(1):175-6.
11. Dower WJ, Miller JF, Ragsdale CW. High efficiency transformation of *E. coli* by high voltage electroporation. Nucleic Acids Res. 1988;16(13):6127-45.
12. Clinical and Laboratory Standards Institute. Methods for dilution antimicrobial susceptibility tests for bacteria that grow aerobically, 10th ed. M07-A10. Wayne, PA., USA. 2015.

P-05

Change in air pollutant concentration, Their associated meteorological parameters, And potential sources in Samut Prakan province

Konthon Prommachat[1,2], Suwimon Kanchanasuta[1, 2*] and Sirapong Sooktawee[3]

[1]*Mahidol University, Faculty of Public Health, Department of Environmental Health Sciences, 420/1 Rajvithi Rd., Ratchathewi District, Bangkok 10400, Thailand*
[2]*Center of Excellence on Environmental Health and Toxicology (EHT), OPS, MHESI, Thailand*
[3]*Environmental Research and Training Center, Department of Environmental Quality Promotion, Ministry of Natural Resources and Environment, Klong 5, Klongluang, Pathum Thani 12120, Thailand*
** Corresponding author: Email: suwimon.kan@mahidol.ac.th*

Abstract:

Samut Prakan province has a high air pollution in Thailand regarding many industrial factories, transportation, and open burning. This study investigated a change in air pollutant concentration associated with meteorological parameters and potential sources of air pollutant at Samut Prakan City Hall station (18t). Pollutant data (PM_{10}, $PM_{2.5}$, NO_2, O_3, SO_2, and CO) were analyzed between 2017-2021 with meteorological data (temperature, wind speed, wind direction, and relative humidity) by using time series and bivariate polar plot (BVP). The result demonstrated that high concentration of $PM_{2.5}$ related in east direction which Motorway road no. 9 or Kanchanaphisek road, National highway no. 3344-Srinakarin road, Highway no. 3 Sukhumvit-Samrong road and Phraeksa road are located. For seasonality, high pollutant concentration was found between November to February associated with low wind speed, high air pressure, poor circulation, and ventilation. For factor of land and sea breeze, the result demonstrated that wind speed at daytime (sea breeze) was higher than wind speed at nighttime (land breeze). Therefore, air pollutants concentration in daytime can be diluted rather than that in nighttime. The BVP confirmed that potential sources of PM_{10}, $PM_{2.5}$, NO_2, O_3, SO_2, and CO associated transportation and industrial area. Moreover, Samut Prakan has ecotourism areas (Bang Nam Phueng floating market, Bang Krachao, etc.) that caused VOCs emission to the air and played a role in background O_3 concentration. This study provided important potential sources of pollutants and high concentration duration that can be used by policy maker to set mitigation policy and improve environmental quality.

Keywords: Potential sources, Air pollutant, Land and sea breeze, Bivariate Polar Plot, Samut Prakan

Introduction:

Air pollution is an important issue of global public health, agriculture, economy, environment, and climate crisis. It is harmful to health, and it impacts the environment by reducing visibility and blocking sunlight, causing acid rain, and harming forests, wildlife, and agriculture [1]. Samut Prakan is a city in the metropolitan district of Bangkok. It has a coastal location, with part of the city facing onto the gulf of Thailand. It faces fluctuating levels of pollution that can differ vastly month by month, with reasons mostly related to topography, weather, and human activity [2]. The total area is 1,004 sq km (388 sq mi). Topography in the province is lowland. People in Samut Prakan use the land for agriculture and industry [3]. Samut Prakan has 6,814 factories (data on 6 July 2021). Metal products factory is the most factory in this province, following by plastic products factory and vehicle and equipment factory, respectively

[4]. The research regarding air pollution in Thailand showed that low wind speeds, low temperature, stable condition, and low sunlight radiation promote higher PM_{10} concentrations and related with diesel vehicles, particularly buses [5]. In Chiang Mai, the results showed that during the peak air pollution, the daily maximum temperature was positively correlated with the PM_{10} concentration. Relative humidity, rainfall and the number of rainy days were found to be negatively correlated with PM_{10} concentrations. The events that the concentration of PM_{10} beyond the national standard level were associated with the weak wind speed events [6]. In Sichang island, Chonburi, the result showed that the nighttime $PM_{2.5}$ concentration was higher than the daytime concentration. However, the daytime O_3 concentration is higher than the nighttime concentration [7]. The Bivariate Polar Plot (BVP) is a technique indicating the source of pollution. It can be used to identify potential sources of air pollutant in a coastal area [7] and potential sources of particulate matter (PM) from rice husk power plant in Roi Et [8].

Data and Methodology:

Data collection

Air pollutants data and meteorological parameters were obtained by Pollution Control Department **(**PCD**)**, Ministry of Natural Resources and Environment, Thailand. Surrounding area of 18t station is community area, transportation routes such as Motorway road no. 9 or Kanchanaphisek road, National highway no. 3344-Srinakarin road, Highway no. 3 Sukhumvit-Samrong road and Phraeksa road, industrial plants, and agricultural area (Figure 1). The analysis parameters consisted of particulate matter diameter less than 10 micron (PM_{10}), particulate matter diameter less than 2.5 micron ($PM_{2.5}$), nitrogen dioxide (NO_2), ozone (O_3), sulfur dioxide (SO_2), carbon monoxide (CO), temperature, relative humidity, wind speed, and wind direction. The data of air pollutant and meteorological parameters were collected between 1 January 2017-31 December 2021.

Figure 1 Study area and air quality monitoring station.

Data analysis method

The OpenAir and other packages in the R program were used to analyze data. The result demonstrates time variation of air pollutant and meteorological parameters. The Bivariate Polar Plot **(**BVP**)** function of OpenAir packages in the R program can plot mean concentrations on polar coordinates that associate with wind speed and wind direction. The output of BVP provides a graphical result in spatial concentration-wind speed dependencies. The concept of BVP is based on the relation in resultant existing pollutant concentration and wind. First, concentration data were partitioned in bins associated with each wind direction and wind speed range. Wind direction interval is of 10 degree and wind speed range is divided in 30 intervals. Concentrations in each bin were calculated to gain the relevant statistical metrics such as mean. Each bin (a cell) consisted of wind direction, wind speed, and mean concentration. To provide smooth concentration surface, the Generalized Additive Model with the isotropic smooth function was used, and expressed as $\sqrt{Ci} = s(u, v) + e_i$. Where, $c_i$is the i^{th} pollutant

concentration, s is the smooth function, e_i is the i^{th} residual, $u = ws.sin(2\pi/wd)$, and $v = ws.cos(2\pi/wd)$. Wind direction (wd) and wind speed (ws) corresponded to θ and r in polar coordinates, respectively. Thus, each mean concentration could be plotted using polar coordinates. Shading surface of concentrations on the polar coordinate could highlight the potential source areas of pollutants [9, 10].

Results and Discussion:

Air Pollutant Concentration and Potential Sources Area

The analysis of air quality monitoring station at Samut Prakan City Hall (18t) demonstrated that concentration of carbon monoxide (CO), nitrogen dioxide (NO_2), sulfur dioxide (SO_2), particulate matter diameter less than 2.5 micron ($PM_{2.5}$), and particulate matter diameter less than 10 micron (PM_{10}) were high during in the morning (06:00-08:00) and in the evening (18:00-23:00). It can be explained that at 06:00-08:00 and 18:00-23:00 is a duration that people spent their time in transportation. The concentration in weekends is lower than weekdays. This result related with a previous study; Tong et al. revealed $PM_{2.5}$ emission levels of motor vehicle on normal weekdays were overall higher than on weekends. Total $PM_{2.5}$ emission were closely associated with road traffic condition [11]. Meanwhile, concentration of ozone (O_3) was high during the daytime due to sunlight acting as a catalyst. The O_3 concentration on weekdays and weekends were not different.

An announcement of the National Environmental Commission of Thailand on standard definition of particulate matter diameter less than 2.5 micron ($PM_{2.5}$) in general ambient air determined a $PM_{2.5}$ concentration 24 hours average less than 37.5 μg/m³. The concentration of $PM_{2.5}$ was high over the Thailand's standard in the east direction of air quality monitoring station (Figure 2) where Motorway road no. 9 or Kanchanaphisek road, National highway no. 3344-Srinakarin road, Highway no. 3 Sukhumvit-Samrong road and Phraeksa road are located. The result demonstrated that transportation is a main source of particulate matter in this area. Lozhkina et al. revealed $PM_{2.5}$ concentration become higher when the road is covered with huge dust deposits accumulated through the winter and vehicle related PM air pollution especially diesel passenger fleet [12]. Wind rose analysis showed that wind direction come from southwest direction (Figure 3) which is gulf of Thailand. It diluted the intensity of pollutants into the land.

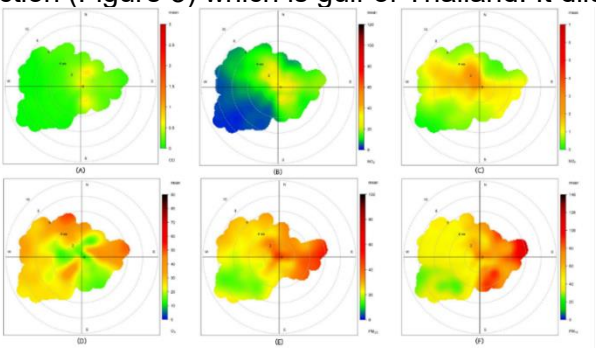

Figure 2 Pollutants concentration of 18t station. (A) CO, (B) NO_2, (C) SO_2, (D) O_3, (E) $PM_{2.5}$, (F) PM_{10}

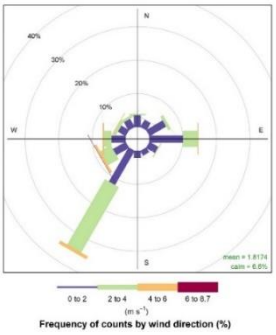

Figure 3 Wind rose of 18t station.

Influence of Land and Sea Breezes

Samut Prakan has a coastal location, with part of the city facing onto the gulf of Thailand. It faces fluctuating levels of pollution that can differ vastly month by month, with reasons mostly relate to topography, weather, and human activity. Air pollutants data of 18t station is divided to 3 seasons (winter, summer, and rainy season) with 2 periods (06:00-18:00 and 18:00-06:00). $PM_{2.5}$ was different in each season and period (Figure 4). Thailand was influenced from

southwest monsoon in summer and rainy season (Figure 5). The boundary of concentration was extended in daytime due to sea breeze. Kanchanasuta et al. revealed the nighttime $PM_{2.5}$ concentration was higher than the daytime concentration [7].

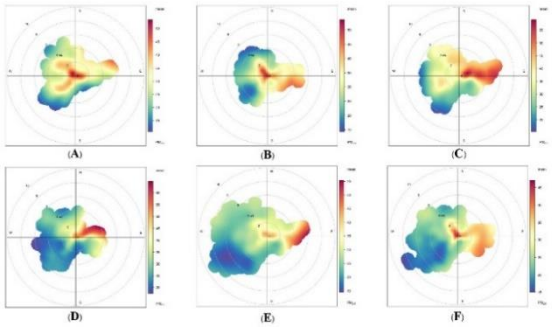

Figure 4 $PM_{2.5}$ concentration at 18t station
(A) Winter season (06:00-18:00)
(B) Winter season (18:00-06:00)
(C) Summer season (06:00-18:00)
(D) Summer season (18:00-06:00)
(E) Rainy season (06:00-18:00)
(F) Rainy season (18:00-06:00)

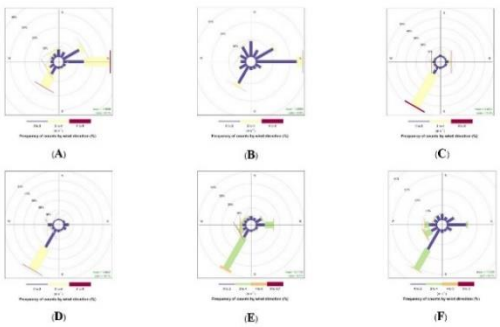

Figure 5 Wind rose analysis at 18t station
(A) Winter season (06:00-18:00)
(B) Winter season (18:00-06:00)
(C) Summer season (06:00-18:00)
(D) Summer season (18:00-06:00)
(E) Rainy season (06:00-18:00)
(F) Rainy season (18:00-06:00)

Conclusion:

The result of this study could be used to troubleshoot air pollution problem in Samut Prakan and neighboring areas. The results demonstrated that air pollutants related with meteorological parameters and land use around air monitoring station. The concentration of CO, NO_2, SO_2, $PM_{2.5}$, and PM_{10} were high during in the morning (06:00-08:00) and in the evening (18:00-23:00) regarding people spent this duration in transportation. The concentration in weekends is lower than weekdays. Meanwhile, the concentration of O_3 was high during the daytime. Land-sea breeze influenced the dispersion of air pollutants. Wind speed at daytime (sea breeze) was higher than wind speed at nighttime (land breeze). The Bivariate Polar Plots (BVP) showed that the potential sources areas of PM_{10}, $PM_{2.5}$, NO_2, O_3, SO_2, and CO were in transportation and industrial area.

References:

1. UCAR Center for science education. Effect of air pollution. UCAR Center for science education. [Cited 2023 May 15]. Available from: https://scied.ucar.edu/learning-zone/air-quality/effects-air-pollution
2. IQAir. Air quality in Samut Prakan. [Cited 2023 May 15]. Available from: https://www.iqair.com/th-en/thailand/samut-prakan
3. The Samut Prakan provincial office of comptroller general. Topography and climate in Samut Prakan Province, Thailand. [Cited 2023 May 16]. Available from: https://www.samutprakan.go.th/
4. Department of Industrial Works. Industrial factory statistics. [Cited 2023 May 16]. Available from: https://www.diw.go.th/webdiw/static-fac/
5. Kanchanasuta S, Sooktawee S, Patpai A, Vatanasomboon P. Temporal variations and potential source areas of fine particulate matter in Bangkok, Thailand. Air, Soil and Water Research. 2020;13.
6. Chotamonsak C, Lapyai D. Meteorological factors related to air pollution in Chiang Mai province. JSTEL. 2018;9(2):1-13.

7. Kanchanasuta S, Sooktawee S, Bunplod N, Patpai A, Piemyai N, Ketwang R. Analysis of short-term air quality monitoring data in a coastal area. AIMS Environmental Science. 2021;8(6):517-31.
8. Sooktawee S, Kanchanasuta S, Boonyapitak S, Patpai A, Piemyai N. Distinguish potential source areas of $PM_{2.5}$ and PM_{10} by statistical data analysis. IOP Conf. Ser.: Earth Environ. Sci. 2020;489(1):012024.
9. Carslaw D.C, Ropkins K. openair — An R package for air quality data analysis. Environmental Modelling & Software. 2012;27–28:52-61.
10. Carslaw D.C, Beevers S.D. Characterising and understanding emission sources using bivariate polar plots and k-means clustering. Environmental Modelling & Software. 2013;40:325-29.
11. Tong R, Liu J, Wang W, Fang Y. Health effects of $PM_{2.5}$ emissions from on-road vehicles during weekdays and weekends in Beijing, China. Atmospheric Environment. 2020;223:117258.
12. Lozhkina O, Lozhkin V, Nevmerzhitsky N, Tarkhov D, Vasilyev A. Motor transport related harmful $PM_{2.5}$ and PM_{10}: from on-road measurements to the modelling of air pollution by neural network approach on street and urban level. IOP Science. 2016;772:012031.

P-06

Effects of short-term exposure to $PM_{2.5}$ on outpatient department visits for anxiety and stress-related disorders in Mae Hong Son, Thailand

Suwat Worratanakit[1,2*], Arthit Phosri[1,2], Tanasri Sihabut[1,2] , Tawach Prechthai[1,2]

[1]Department of Environmental Health Sciences, Faculty of Public Health, Mahidol University 420/1 Rajvithi Rd., Rajchathawee, Bangkok, Thailand
[2]Center of Excellence on Environmental Health and Toxicology (EHT), OPS, MHESI, Thailand
** Corresponding author E-mail address: suwat.wor@student.mahidol.ac.th*

Abstract:

Mae Hong Son is a province situated in the northern region of Thailand, which suffers from air pollution originated mainly from forest fires, biomass open burning, and transboundary haze. However, the scientific evidence showing health effects associated with air pollution is limited. Therefore, this study aims to examine the effect of short-term exposure to $PM_{2.5}$ on outpatient department (OPD) visits for anxiety and stress-related disorders. Daily concentration of air pollution was obtained from air quality monitoring stations and daily meteorological data were obtained from weather monitoring stations between January 2017 and December 2022. Daily number of OPD visits for anxiety and stress-related disorders (ICD-10 code: F40– F48) during the same period was obtained from the database of the National Health Security Office (NHSO) according to the Universal Health Coverage (UHC) system. A time-stratified case-crossover design with the conditional quasi-Poisson regression model was applied to estimate the effects of $PM_{2.5}$ on OPD visits for anxiety and stress-related disorders, adjusting for temperature and relative humidity. We found that the relative risk (RR) of OPD visits for anxiety and stress-related disorders was 1.0257 (95% Confidence Interval (CI): 1.0042, 1.0476) per each 10 $\mu g/m^3$ increase in $PM_{2.5}$ at lag 0-1 days. Findings of this study can be used as scientific evidence for improving air pollution control policies to reduce the concentration of $PM_{2.5}$ and for protecting population health in Mae Hong Son, Thailand.

Keywords: $PM_{2.5}$, Short-term exposure, Outpatient department visit, Anxiety and stress

Introduction:

Ambient air pollution is considered one of the major causes of public health burdens worldwide caused by rapid industrialization and urbanization (1). Recent study found that the population across the globe is exposed to air pollution that exceeded the recommended limits of the World Health Organization (WHO) and there are approximately seven million premature deaths each year attributable to both short- and long-term exposure to ambient air pollution (2). Particulate matter (PM) is currently the most important air pollution problem, causing environmental and public health issues worldwide depending on its size (3). Short- and long-term exposures to $PM_{2.5}$ have been associated with spectrums of negative human health outcomes and there are increasing trends of epidemiological study showing the association of $PM_{2.5}$ with mental and behavioral disorders such as anxiety, depression, and even suicide (4). Thailand is encountering $PM_{2.5}$ as a major environmental problem, especially in upper northern region, due mainly to intensive burning of agricultural residues (5), but there is limited epidemiological study on the relationship between $PM_{2.5}$ and mental and behavioral disorders. Therefore, this study aims to investigate the short-term effect of $PM_{2.5}$ exposure and OPD visits for mental and behavioral disorders, which is anxiety and stress-related disorders in Mae Hong Son, Thailand.

Materials and Methods:

This study was conducted in Mae Hong Son, Thailand. Hourly concentrations of $PM_{2.5}$, PM_{10}, CO, O_3, NO_2, and SO_2 in Mae Hong Son were obtained from air quality monitoring stations operated by the Pollution Control Department (PCD) from January 2017 to December 2022, and 24-hr average concentrations of $PM_{2.5}$, PM_{10}, CO, NO_2, SO_2 and maximum 8-hr rolling average concentrations of O_3 was then calculated, where the days that had hourly air pollution data available less than 18 hours (75%) was defined as the missing value and missing data was imputed using the random forest approach with meteorological normalization technique. Daily meteorological data in the same period of $PM_{2.5}$ data were obtained from weather monitoring stations operated by the Thai Meteorological Department (TMD). Daily number of OPD visits for anxiety and stress-related disorders (ICD-10 code: F40-F48) during the same periods as air pollution and meteorological data were obtained from the database of the NHSO according to the UHC scheme, and the effect of short-term exposure to $PM_{2.5}$ on OPD visits for anxiety and stress-related disorders was analyzed using the time-stratified case-crossover design with the conditional quasi-Poisson model (Eq. 1), adjusting for temperature and relative humidity using the natural cubic spline function. In particular, case-crossover design generally considers only case and the case day was selected from every single day of OPD visits for anxiety and stress-related disorders, where each case serves as his or her own control but on different days that are the same day of the week within the same month of the same year before and after the case days, where this case and its control is considered as a stratum. This design is thus automatically controlled many internal confounding factors, such as sex, age, socio-economic status, the pre-existing health conditions, day of the week, and long-term trend and seasonality. The sensitivity analysis was also performed by changing degree of freedom of the natural cubic spline function for temperature and relative humidity and bi-pollutant model was also examined to test the robustness of the effect estimates by incorporated other air pollutants into model one at a time. The results were reported as the relative risk (RR) and 95% confidence interval (CI) of OPD visits for anxiety and stress-related disorders associated with a 10 $\mu g/m^3$ increases of $PM_{2.5}$.

$$Log(E(Y_t)) = \alpha + \beta_1 Z_t + ns(Temp_t, df = 3) + ns(RH_t, df = 3) + stratum_t \quad (1)$$

Where $Log(E(Y_t))$ is logarithmic scale for the expected numbers of anxiety and stress-related disorders at time *t* ($E(Y_t)$); α is the model intercept; β_1 is the regression coefficient associated with a unit increase in Z; Z_t is the concentration of $PM_{2.5}$ at time *t*; ns(●) is the natural cubic spline function with 3 degrees of freedom (df) guided by minimizing quasi Akaike Information Criterion (QAIC); $Temp_t$ and RH_t is temperature and relative humidity at time *t*, respectively; $stratum_t$ defines case and control days within the same stratum.

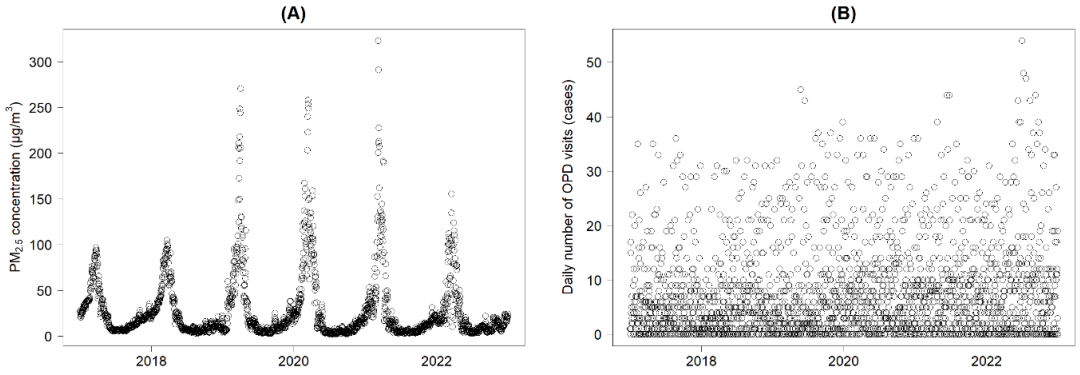

Figure 1 Daily average $PM_{2.5}$ concentration (A) and daily number of OPD visits for anxiety and stress-related disorders (B) overtime.

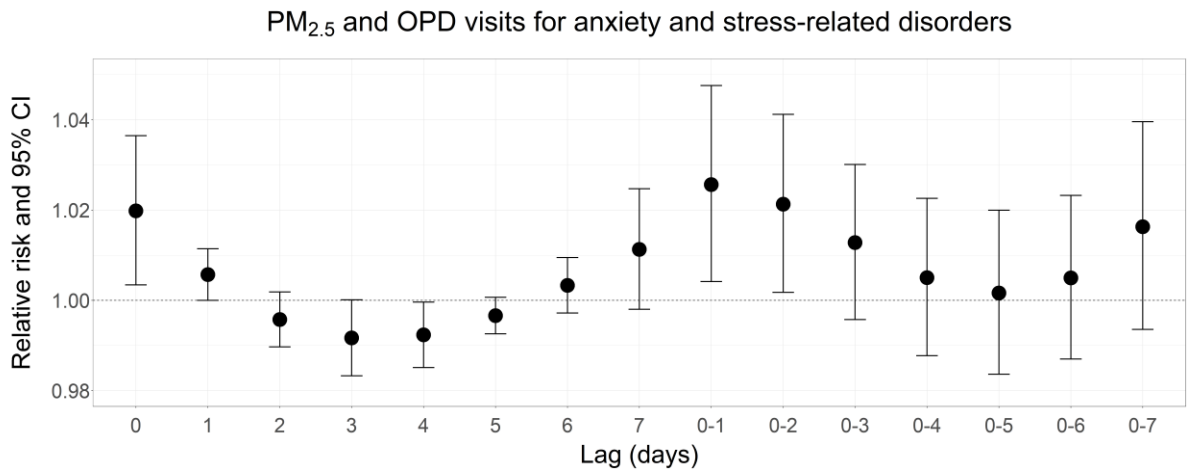

Figure 2 The RR of OPD visits for anxiety and stress-related disorders associated with a 10 μg/m^3 increases of $PM_{2.5}$ at difference lag days

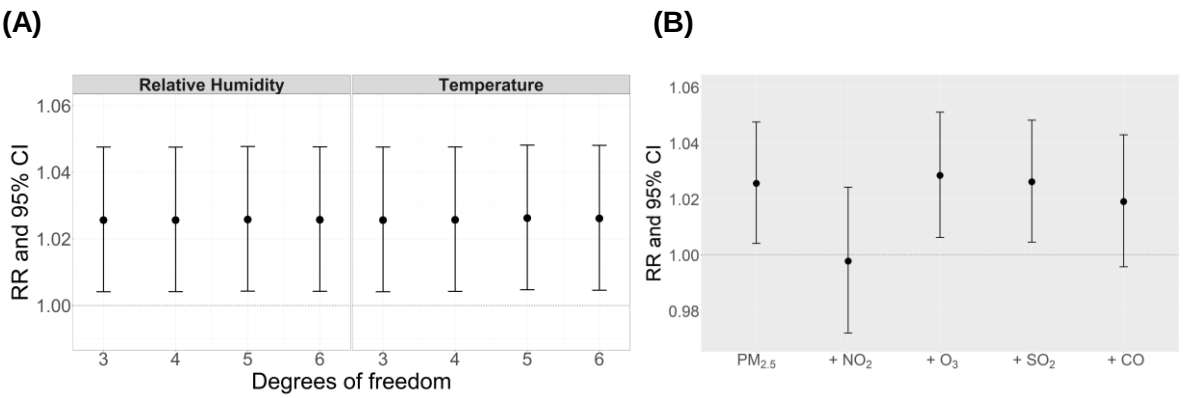

Figure 3 The RR of OPD visits for anxiety and stress-related disorders associated with a 10 μg/m^3 increases in $PM_{2.5}$ varying degrees of freedom of the natural splines function for temperature and relative humidity (A) and bi-pollutant model (B) at lag 0-1 days

Results and Discussion:

During the study period (from January 1, 2017 to December 31, 2022), a total number of OPD visits for anxiety and stress-related disorders in Mae Hong Son was 16,438, ranged from 0 to 54 cases per day. Daily concentrations (± standard deviation) of $PM_{2.5}$, PM_{10}, NO_2, SO_2, O_3, and CO were 27.25 (± 35.91) μg/m^3, 36.15 (± 41.99) μg/m^3, 4.59 (± 3.16) ppb, 1.21 (± 0.37) ppb, 29.47 (± 19.56) ppb, and 0.63 (± 0.34) ppm, respectively. Daily average temperature and relative humidity was 26.31 ^oC and 75.77%, respectively. The daily concentration of $PM_{2.5}$ and number of OPD visits for anxiety and stress-related disorders overtime is illustrated in Fig.1, showing that $PM_{2.5}$ has seasonal variation, while OPD visits was not. We observed significant association between $PM_{2.5}$ and OPD visits for anxiety and stress-related disorders in Mae Hong Son at current day (lag 0) and one day before visits (lag 1), and the highest estimate was found at the cumulative

lag 0-1 days at attenuated over the lag period (Fig. 2), implying that exposure to $PM_{2.5}$ has transient effect on anxiety and stress-related disorders in Mae Hong Son, Thailand, where the RR of OPD visits for anxiety and stress-related disorders associated with a 10 $\mu g/m^3$ increase in $PM_{2.5}$ concentration was 1.0257 (95% CI: 1.0042, 1.0476), The effect estimate was remained significant even after changing the degrees of freedom for temperature and relative humidity (Fig. 3A). In the bi-pollutant model, the effect of $PM_{2.5}$ on OPD visits for anxiety and stress-related disorders was attenuated after incorporating NO_2 into the model, indicating that the effect of $PM_{2.5}$ might not be independent to that of NO_2, therefore NO_2 may be taken into consideration when estimating the effect of $PM_{2.5}$, and vice versa. Finding from this study is in agreement with many previous studies, indicating that exposure to $PM_{2.5}$ was associated with increased risks of hospital visits for mental and behavioral disorders in Korea, China, and the U.S. (6,7,8). The plausible explanation for this result has been supported by previous studies that exposure to $PM_{2.5}$ is able to impair brain functions and the central nervous system (9,10), resulting to the cognitive impairment, decision-making, personality, and social behavior (11).

Conclusion:

Finding from this study indicated that short-term exposure to $PM_{2.5}$ was significantly associated with increased risk of anxiety and stress-related disorders in Mae Hong Son, Thailand that can be applied as evidence-based information for improving the related environmental regulations and policies to reduce $PM_{2.5}$ concentration for protecting population health.

References:

1. Song J, Song TM. Social Big-Data Analysis of Particulate Matter, Health, and Society. Int J Environ Res Public Health 2019;16(19):3607.
2. Orru H, Ebi KL, Forsberg B. The Interplay of Climate Change and Air Pollution on Health. Curr Environ Health Rep 2017;4(4):504-513.
3. Rasmussen N, Knudsen H. Particulate Matter: Sources, Emission Rates, and Health Effects. New York: Nova Science Publishers, Inc.; 2012.
4. Thangavel P, Park D, Lee YC. Recent Insights into Particulate Matter ($PM_{2.5}$)-Mediated Toxicity in Humans: An Overview. Int J Environ Res Public Health 2022;19(12):7511.
5. Mueller W, Vardoulakis S, Steinle S, Loh M, Johnston HJ, Precha N, et al. A health impact assessment of long-term exposure to particulate air pollution in Thailand. Environ Res Lett 2021;16(5):055018
6. Lee S, Lee W, Kim D, et al. Short-term $PM_{2.5}$ exposure and emergency hospital admissions for mental disease. Environ Res 2019;171:313-320.
7. Liu H, Zhao H, Huang J, He M. Air pollution associated with hospital visits for mental and behavioral disorders in Northeast China. Front Epidemiol 2023;3:1090313.
8. Yoo EH, Roberts JE, Eum Y, Li X, Chu L, Wang P, et al. Short-term exposure to air pollution and mental disorders: a case- crossover study in New York City. Environ Res Health 2022;1:015001
9. Liu XQ, Huang J, Song C, Zhang TL, Liu YP, Yu L. Neurodevelopmental toxicity induced by PM2.5 Exposure and its possible role in Neurodegenerative and mental disorders. Hum Exp Toxicol 2023;42:9603271231191436.
10. Zundel CG, Ryan P, Brokamp C, Heeter A, Huang Y, Strawn JR, Marusak HA. Air pollution, depressive and anxiety disorders, and brain effects: A systematic review. Neurotoxicol 2022;93:272-300.
11. Lee S, Lee W, Kim D, et al. Short-term $PM_{2.5}$ exposure and emergency hospital admissions for mental disease. Environ Res 2019;171:313-320.

P-07

Estimation of surface $PM_{2.5}$ concentration in Thailand using satellite remote sensing and machine learning algorithm

Thunyachote Khempunjakul[1,2*], Arthit Phosri[1,2], Withida Patthanaissaranukool[1,2], and Suwimon Kanchanasuta[1,2]

[1]Department of Environmental Health Sciences, Faculty of Public Health, Mahidol University 420/1 Rajvithi Rd., Rajchathawee, Bangkok, Thailand
[2] Center of Excellence on Environmental Health and Toxicology (EHT), OPS, MHESI, Thailand
** Corresponding author E-mail address: thunyachote.khe@student.mahidol.ac.th*

Abstract:

Particulate matter with aerodynamic diameter less than or equal to 2.5 microns ($PM_{2.5}$) is one of the most serious air pollutants, causing detrimental effects on human health in Thailand to date. The monitoring network operated by the Pollution Control Department (PCD) has been used to measure real-time concentration of $PM_{2.5}$ and other criteria air pollutants throughout Thailand, but the number of monitoring stations remains limited, where $PM_{2.5}$ concentration in unmonitored areas could not be reported. Therefore, satellite remote sensing data might be applied to monitor the concentration of $PM_{2.5}$ in such locations. This study aimed to estimate ground-level $PM_{2.5}$ concentration across Thailand using the Multi-Angle Implementation of Atmospheric Correction Aerosol Optical Depth (MAIAC AOD) and other meteorological and land-use data with the 2-stage random forest model using the data from January to December 2022. In the first stage model, the missing MAIAC AOD was imputed by 500 decision trees of random forest model, and the imputed MAIAC AOD was then applied with other predictor variables to estimate ground-level concentration of $PM_{2.5}$ in the second stage model via 500 decision trees of random forest model. The model was then validated using holdout approach by splitting 80% of the data for training and the remaining 20% was used for testing. Results indicated that the coefficient of determination (R-square: R^2) and the root mean square error (RMSE) in estimating MAIAC AOD in the first stage model in training dataset were 0.94 and 0.03, respectively, and those in validating dataset were respectively 0.42 and 0.06. Moreover, R^2 and RMSE in estimating surface $PM_{2.5}$ concentration in the second stage model in training dataset were 0.94 and 4.03, respectively, and those in validating dataset were 0.51 and 9.43, respectively. Finding of this study can be used as a tool to monitor daily $PM_{2.5}$ concentration throughout Thailand, even in the areas without monitoring station.

Keywords: $PM_{2.5}$, Aerosol Optical Depth, Random Forest, Machine Learning

Introduction:

$PM_{2.5}$ is an important air pollutant impacting public health worldwide, and the World Health Organization (WHO) has established a guideline for air quality, including $PM_{2.5}$ levels, with the aim of safeguarding public health (1). In Thailand, $PM_{2.5}$ originates from many emission sources, especially vehicle emissions and biomass open burning. Therefore, monitoring $PM_{2.5}$ concentration is a crucial measure in preventing and controlling $PM_{2.5}$ in Thailand. However, the fixed-site air quality monitoring stations remains limited, which is currently covered by 56 out of 77 provinces, leading to a lack of information for monitoring $PM_{2.5}$ concentration. Moreover, monitoring air quality is deemed essential as it yields valuable data and enhances our comprehension of the situation that used to improve the relevant strategies for reducing $PM_{2.5}$ concentration. To address the problem of insufficient fixed-site air quality monitoring station, satellite data have been applied to estimate ground-level $PM_{2.5}$ concentration through statistical

model or machine learning algorithm (2). For example, numerous previous studies have applied mathematical models and machine learning techniques to estimate ground-level $PM_{2.5}$ levels in various countries such as in China, South Africa, and Japan (3,4,5). However, the method used to estimate surface concentration of $PM_{2.5}$ in Thailand is limited to Bangkok and to the Northern Region (6,7). Therefore, a study that focused broadly on $PM_{2.5}$ prediction throughout Thailand would be able to address insufficient fixed-site air quality monitoring in measuring the concentration of $PM_{2.5}$.

Materials and Methods:

This study conducted the analysis across Thailand during the period spanned from January to December 2022. Specifically, data product for Aerosol Optical Depth (AOD) was acquired from the Moderate Resolution Imaging Spectroradiometer (MODIS) on board the Terra and Aqua satellites. This data has been preprocessed into 1 km spatial resolution using the Multi-Angle Implementation of Atmospheric Correction (MAIAC) algorithms, known as MAIAC AOD. The meteorological variables, including temperature, wind speed and wind direction, relative humidity, and the planetary boundary layer height (PBLH), were downloaded from the Modern-Era Retrospective analysis for Research and Applications version 2 (MERRA-2) data product. The normalized difference vegetation index (NDVI) was applied as a proxy for green vegetation and was extracted from the MODIS instrument on board the Terra satellite. This data has a spatial resolution of 0.1° × 0.1° and a temporal resolution of 16 days, and it is provided by NASA Earth Observation. The road length was also used as one of the predictor variables in this study and was acquired from OpenStreetMap. The acquired road length was then summed by 1 km pixel. Hourly $PM_{2.5}$ concentration data was obtained from all fixed-site air quality monitoring stations operated by the PCD throughout Thailand, and daily average concentration from 10:00 to 14:00 local time (LT) was computed to make it coincide with retrieval AOD data.

The 2-stage random forest model was used in this study. In the first stage model, the missing MAIAC AOD was imputed via 500 decision trees of random forest model using temperature, wind speeds and wind directions, relative humidity, PBLH, and NDVI as predictor variables. The algebraic equation for the first stage random forest model is shown in Eq. 1.

$$AOD_{it} = RF(PBLH_{it}, TS_{it}, T2M_{it}, T10M_{it}, U2M_{it}, U10M_{it}, V2M_{it}, V10M_{it}, NDVI_{it}, RH_{it}) \quad (1)$$

Where AOD_{it} is MAIAC AOD at station i on day t; $PBLH_{it}$ is PBLH at station i on day t; TS_{it} is the surface skin temperature at station i on day t; $T2M_{it}$ is 2-meter air temperature at station i on day t; $T10M_{it}$ is 10-meter air temperature at station i on day t; $U2M_{it}$ is 2-meter eastward wind speed at station i on day t; $U10M_{it}$ is 10-meter eastward wind speed at station i on day t; $V2M_{it}$ is the 2-meter northward wind speed at station i on day t; $V10M_{it}$ is 10-meter northward wind speed at station i on day t; RH_{it} is relative humidity at station i on day t, and $NDVI_{it}$ is NDVI value at station i on day t.

The predicted AOD was then integrated to the original dataset to form the completed AOD, and it was subsequently used as predictor variable along with other meteorological variables to estimate ground-level $PM_{2.5}$ concentration in the second stage using 500 decision trees of the random forest model, and the accuracy of the model performance was justified using the coefficient of determination (R^2) and the root mean square error (RMSE). The algebraic equation for the second stage model is shown below.

$$PM_{2.5it} = RF(C\_AOD_{it}, PBLH_{it}, TS_{it}, T2M_{it}, U2M_{it}, V2M_{it}, T10M_{it}, U10M_{it}, V10M_{it}, NDVI_{it}, RH_{it}, Road\ length_{it}) \quad (2)$$

Where $PM_{2.5it}$ is $PM_{2.5}$ concentration at station *i* on day *t*; C_AOD_{it} is the completed MAIAC AOD values obtained from the first stage random forest at station *i* on day *t*; $Road\ length_{it}$ is the road length buffered at 1 km of station *i* on day *t*. The model was validated using holdout validation method by splitting 80% of the data for training and the remaining 20% was used for testing to evaluate how accurate of the developed model is in the terms of estimating the concentration of $PM_{2.5}$.

Results and Discussion:

Table 1 indicates the actual and predicted values for MAIAC AOD (from the first stage) and for $PM_{2.5}$ (from the second stage). The actual and predicted values were similar to each other, indicating that the developed model could be accurately used to estimate ground-level $PM_{2.5}$ concentration, to some extent.

Table 1 Summary statistics of the 2-stage random forest model

Stage	Model	R^2	RMSE	Mean ± Standard Deviation*	
				Actual	Predicted
Stage 1 Imputing AOD	Training (80%)	0.94	0.03	0.18 ± 0.08	0.18 ± 0.06
	Testing (20%)	0.42	0.06	0.18 ± 0.08	0.18 ± 0.05
Stage 2 Estimating $PM_{2.5}$	Training (80%)	0.94	4.03	18.72 ± 18.76	18.77 ± 18.94
	Testing (20%)	0.51	9.43	18.76 ± 13.02	18.94 ± 8.35

*The unit for AOD is unitless, and that for $PM_{2.5}$ is $\mu g/m^3$

The coefficient of determination (R^2) and the root mean square error (RMSE) in estimating MAIAC AOD in the first stage model in training dataset were 0.94 and 0.03, respectively (Table 1), and those in validating dataset were respectively 0.42 and 0.06. Moreover, the R^2 and RMSE in estimating ground-level concentration of $PM_{2.5}$ in the second stage model in the training dataset were respectively 0.94 and 4.03, and those in validating dataset were 0.51 and 9.43, respectively (Fig. 1), indicating that this model is accurate in estimating $PM_{2.5}$ by 51%.

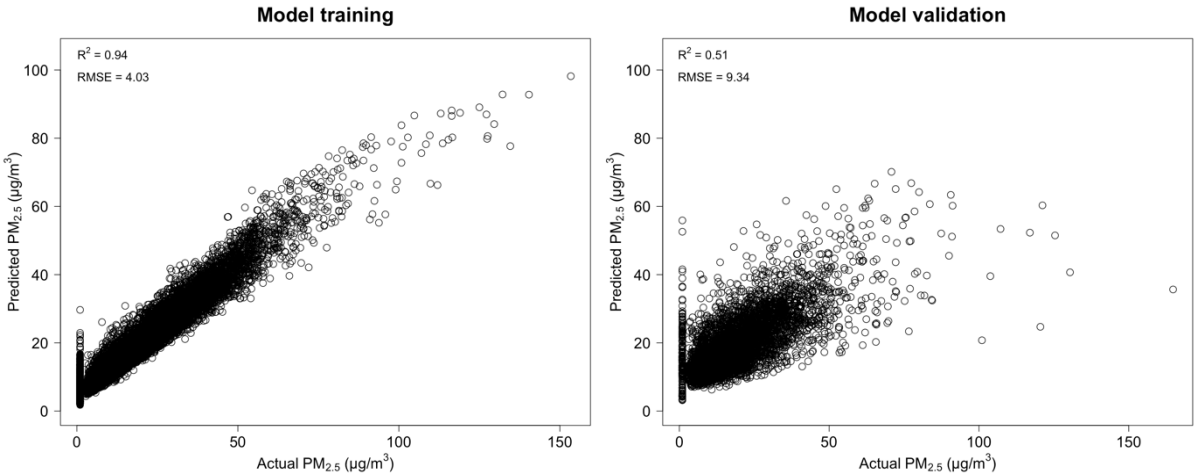

Figure 1 The relationship between the actual $PM_{2.5}$ and predicted $PM_{2.5}$ concentrations obtained from model training and model validation

Conclusion:

This study demonstrates the feasibility of using satellite remote sensing data and a machine learning algorithm to estimate surface $PM_{2.5}$ concentrations across Thailand. The developed 2-stage random forest model, incorporating MAIAC AOD data, meteorological variables, and land-use data, showed high performance results during training, but there was a decrease in performance during holdout validation. This overfitting may occur when the model training process accurately estimates the data used to train the model, but when it used to estimate in other datasets, the accuracy was declined, suggesting that the model used in this study may need to adjust a certain relevant variable to reduce the occurrence of overfitting and improve accuracy. This study was developed to handle the challenges in data deficiency in managing $PM_{2.5}$ in Thailand that can serve as analytical instruments supporting policy decisions related to public health, contributing to ongoing efforts to safeguard public health in the future.

References:

1. WHO ambient air quality database 2021 update [Internet]. World Health Organization; 2021 [cited 2024 April 30]. Available from: https://cdn.who.int/media/docs/default-source/air-pollution-documents/air-quality-and-health.
2. Tiwari A, Aljoufie M. Modeling spatial distribution and determinant of $PM_{2.5}$ at micro-level using geographically weighted regression (GWR) to inform sustainable mobility policies in campus based on evidence from King Abdulaziz University, Jeddah, Saudi Arabia. Sustainability 2021; 13(21): 12043.
3. You X, Cao X, Guo Y, Wang D, Qiu W, Zhou C, et al. Associations between short-term $PM_{2.5}$ exposure and daily hospital admissions for circulatory system diseases in Ganzhou, China: A time series study. Front Public Health 2023; 11: 1134516.
4. Zhang D, Du L, Wang W, Zhu Q, Bi J, Scovronick N, et al. A machine learning model to estimate ambient PM2.5 concentrations in industrialized highveld region of South Africa. Remote Sens Environ 2021; 266: 112713.
5. Jung CR, Chen WT, Nakayama SF. A national-scale 1-km resolution $PM_{2.5}$ estimation model over Japan using MAIAC AOD and a two-stage random forest model. Remote Sens 2021; 13(18):3657.
6. Peng-in B, Sanitluea P, Monjatturat P, Boonkerd P, Phosri A. Estimating ground-level PM2.5 over Bangkok Metropolitan Region in Thailand using Aerosol Optical Depth retrieved by MODIS. Air Qual Atmos Health 2022; 15(11): 2091–102.
7. Wongnakae P, Chitchum P, Sripramong R, Phosri A. Application of satellite remote sensing data and random forest approach to estimate ground-level $PM_{2.5}$ concentration in Northern region of Thailand. Environ Sci Pollut Res 2023; 30(38): 88905-88917.

P-08

In utero exposure to polycyclic aromatic hydrocarbons (PAHs): DNA damage in maternal urine and placental tissue

Injleen[1], Panida Navasumrit[1,2,3], Preeyanut Rattanayut[2], Samroeng Chanjamsai[2] , Jeerawan Promvijit[2] and Mathuros Ruchirawat[1,2,3]

[1]Applied Biological Sciences and Environmental Health, Chulabhorn Graduate Institute, Bangkok, Thailand, 10210
[2]Environmental Toxicology Laboratory, Chulabhorn Research Institute, Bangkok, Thailand, 10210
[3]Center of Excellence on Environmental Health and Toxicology (EHT), OPS, MHESI, Thailand, 10210
Email: injleen@cgi.ac.th

Abstract:

Polycyclic aromatic hydrocarbons (PAHs) are ubiquitous carcinogenic pollutants produced from natural and anthropogenic sources, i.e., traffic emissions from fuel combustion. Exposure to particulate PAHs is associated with respiratory diseases and lung cancer in humans. Cytochrome P450 enzymes metabolize PAHs into benzo[a]pyrene diol epoxide (BPDE) resulting in the formation of BPDE-DNA adducts. In addition, PAH metabolism induces oxidative stress, leading to oxidative DNA damage and lipid peroxidation. Pregnant women are particularly susceptible to PAH exposure because they can easily penetrate the placental barrier and potentially cause developmental abnormalities in the fetus. This study aimed to assess the effects of PAH exposure during pregnancy on DNA damage in pregnant women and newborns.

The study was conducted in high- and low-traffic congested areas as the exposed and control sites. A total of 100 pregnant women were recruited from the study sites consisting of 50 exposed and 50 control subjects. Analysis of particulate PAHs by gas chromatography-tandem mass spectrometry (GC-MS/MS) showed that the traffic-congested area had a significantly higher ($p<0.01$) concentration of PAHs bound to $PM_{2.5}$ (PAHs-$PM_{2.5}$) and ultrafine particles (PAHs-UFPs) than those in the low-traffic area by 1.9- and 1.3-fold, respectively. PAH exposure in pregnant women assessed by urinary 1-hydroxypyrene (1-OHP), a metabolite of PAHs, was significantly higher ($p<0.05$) in exposed subjects than in control subjects. Liquid chromatography-tandem mass spectrometry (LC-MS/MS) analysis of DNA damage and lipid peroxidation in urine revealed that exposed pregnant subjects had higher levels of BPDE-DNA adducts (2.1-fold), 8-hydroxydeoxyguanosine (8-OHdG; 1.1-fold) and malondialdehyde (MDA; 1.9-fold). In agreement with maternal exposure to PAHs, BPDE-DNA adducts and 8-OHdG were detected in placental tissues indicating DNA damage in newborns, potentially influenced by exposure to particulate PAHs during pregnancy.

In conclusion, this study demonstrates that exposure to traffic-related particulate PAHs *in utero* can result in transplacental transfer, leading to fetal exposure to PAHs. Exposure to PAHs during pregnancy has the potential to increase DNA damage in pregnant women and placental tissue which may affect fetal development. Therefore, this study highlights the importance of being aware of *in utero* exposure to particulate PAHs which may lead to an increased health risk of disease development in newborns.

Keywords: Polycyclic aromatic hydrocarbons, Particulate matter, *in utero* exposure, 1-hydroxypyrene, DNA damage, PAH-DNA adducts, oxidative DNA damage.

Introduction:

Air pollution is a global issue that profoundly impacts human health and is among the leading causes of mortality. According to the World Health Organization (WHO), about 90% of the world's population resides in areas with extremely polluted air. Several air pollutants increase the risk of morbidity and mortality in humans such as particulate matter (PM), nitrogen oxides (NO_x), sulfur dioxide (SO_2), and volatile organic compounds (VOCs). PM is listed as a criteria pollutant for determining air quality indexes of various organizations and countries such as WHO, the United States, and the European Union. The toxicity of PM depends on the size and chemical composition of the particles, for instance, $PM_{2.5}$ are smaller particles and can effectively deposit in the alveoli and enter the bloodstream. In addition, the genotoxicity and cytotoxicity of PM are associated with its organic components polycyclic aromatic hydrocarbons (PAHs) that exhibit carcinogenic and mutagenic activity (1, 2). PAHs are produced from natural and anthropogenic sources such as automobile exhaust, biomass burning, tobacco smoke, industrial activities, food cooking, and domestic heating.

There are more than 100 structurally different PAHs in the environment, of which 16 are categorized as priority PAHs by the US Environmental Protection Agency (EPA) due to their carcinogenic, teratogenic, and genotoxic capabilities. The International Agency for Research on Cancer (IARC) has classified PAHs as carcinogenic and mutagenic for humans (3). Humans are exposed to PAHs via all routes of exposure. The atmospheric PAHs exist as a complex mixture, they are bound to particulate matter (PM). However, PAH mixtures are represented by a single compound named Benzo[a]pyrene (B[a]P) in scientific research and environmental guidelines. B[a]P is one of the priority PAHs and is classified as a class 1 carcinogen by the International Agency for Research on Cancer (IARC).

In humans, PAHs are metabolized by cytochrome P450 enzymes, leading to DNA damage, lipid peroxidation, protein modification, and antioxidant depletion. Fetuses and children are extremely sensitive to PAH exposure *in utero* due to lower immune competence, higher cell proliferation rates, a decreased capability to detoxify carcinogens, and a delay in DNA repair processes. A previous study reported that PAHs are developmental toxicants; *in utero* exposure to PAHs in the ambient air elevated PAH-DNA adducts in the umbilical cords of the fetus and significantly reduced the weight, length, and head circumferences of neonates at birth. (4). Additionally, *in utero* exposure to PAHs has been related to asthma low birth weight, preterm delivery, congenital abnormalities, and nervous system complications (3).

Objective:

To assess the effects of PAH exposure during pregnancy on DNA damage in pregnant women and newborns.

Methodology:

Study locations and study subjects

The study locations were selected based on traffic density. The high-traffic site is located at Somdej Chaophrya Road, Klomgsan District. It has a high traffic density i.e. more than 2000 vehicles per day. The selected low-traffic site is Buddhamontol 3 Road located in Peri-Bangkok with less vehicle density.

A total of 100 pregnant women were recruited from residents living in the study sites consisting of 50 exposed and 50 control subjects. The health status of both control and exposed subjects was assessed before sample collection. Inclusion criteria for the study included the individual aged 20-40 years old, who had been resident in the study area for at least one year. Pregnant women with a history of pregnancy complications such as miscarriage, hypertension, and HIV-positive were excluded from the study.

Analysis of PAHs in the ambient air

Air samples were collected at the roadside of the selected study locations using polytetrafluoroethylene (PTFE) membrane filters. The air samples were collected for 8 hours on (PTFE) membrane filters. Segregated impactors were attached to battery-powered sampling pumps and operated at a flow rate of 2 liter/minute. After sample collection, PTFE filters were dried and stored in a desiccator for 24 hours. Next, PTFE filters were weighed and analyzed by GC-MS/MS.

Assessment of PAH exposure in pregnant women

The urinary 1-hydroxypyrene (1-OHP), a specific metabolite of PAHs, was determined as a biomarker of PAH exposure. Briefly, urine samples (50 mL) were collected from pregnant women and were stored at -20ºC until analysis. A fraction of urine samples (400 µL), 100 µL acetate buffer (0.5 M, pH 5) and 5 µL B-glucuronidase were mixed and vortexed for 10 seconds. Subsequently, the samples were incubated at 37ºC for 16 hours. After incubation, 700 µL acetonitrile was added and vortexed for 10 seconds. The samples were centrifuged at 10,000 g and incubated at 20° C for 10 minutes. Then the supernatant was analyzed for 1-OHP by Ultra high-performance liquid chromatography equipped with Fluorescence detector (UHPLC-FLD).

Analysis of DNA damage and lipid peroxidation in maternal urine

A fraction of the urine sample (1 mL) was mixed with 100 µL DNTP and vortexed for 10 seconds. The sample was diluted with 9 mL mili Q water and vortexed well. Then, the sample was incubated at room temperature for 30 minutes. After that, the extraction column was pre-conditioned with 1 mL methanol and 1 mL mili Q water. Then the sample was loaded into the column, washed with 1 mL 5% methanol, and eluted with 1 mL100% HPLC-grade methanol. The eluate was evaporated at 4ºC in the evaporator until dry. The dried sample was redissolved in 200 µL of 5% methanol and subjected to LC-MS/MS analysis of DNA damage (BPDE-DNA adducts and 8-OHdG) and lipid peroxidation (MDA).

Analysis of PAHs exposure and DNA damage in placenta

BPDE-DNA adducts in placental tissue can be used as a biomarker of PAH exposure and early biological effects, while 8-OHdG can be used as a biomarker of oxidative DNA damage. To investigate *in utero* exposure to PAHs, placental tissues were collected after the delivery of a lived-born baby. Then the samples were stored at -80ºC until further analysis. Placental DNA was isolated and analysis of DNA damage (BPDE-DNA adducts and 8-OHdG) in placental DNA by LC-MS/MS.

Statistical evaluation

Statistical analysis was performed using Mann-Whitney U test to compare the difference between groups. A difference with a p-value < 0.05 was considered statistically significant.

Results, Discussion, and Conclusion:

1. Analysis of PAHs in the ambient air

The levels of PAHs in the ambient air analyzed by GC-MS/MS showed that the high-traffic area had significantly increased concentrations of PAHs-$PM_{2.5}$ (19.9±2.89) and PAHs-UFPs (10.21±0.49), compared to those in the low-traffic area. These results indicate that fuel combustion in traffic-congested areas is one of the major sources of particulate PAH air pollution.

2. Assessment of PAH exposure in pregnant women

Urinary 1-hydroxy pyrene (1-OHP), which is a urinary metabolite of PAHs can be used as a biomarker of PAH exposure. In this study, PAH exposure in pregnant subjects assessed by measurement of 1-OHP showed that urinary 1-OHP in maternal urine was significantly higher ($p<0.05$) in exposed subjects (0.15 µmol/mol creatinine), compared to that of control subjects (0.12 µmol/mol creatinine).

3. Assessment of DNA damage in pregnant women

The assessment of DNA damage and lipid peroxidation in pregnant women was analyzed in urine samples using LC-MS/MS. Three biomarkers were investigated in maternal urine samples including BPDE-N2-dG for PAH-DNA adduct, 8-OHdG for oxidative DNA damage and MDA for lipid peroxidation. The results showed that the urinary concentrations of BPDE-N2-dG, 8-OHdG, and MDA were increased in exposed pregnant subjects by 1.1-, 2.7-and 1.9-fold, respectively, compared to those of the controls. These results suggested that increased levels of DNA damage and lipid peroxidation were in line with increased PAHs exposure in pregnant subjects who live in high-traffic congested area.

4. Assessment of PAHs exposure and DNA damage in placenta

BPDE-DNA adducts in placental tissue indicating transplacental PAH exposure can be used as a potential biomarker of PAH exposure and PAH-specific genetic damage in the fetus. Some of the placental tissues were obtained after baby delivery from exposed pregnant subjects. The BPDE-DNA adducts were detected in the placental tissues suggesting fetal exposure to PAHs *in utero*. Apart from BPDE-DNA adducts, 8-OHdG was also detected in the placental tissue. BPDE-DNA adducts and 8-OHdG are mutagenic DNA damage that has been associated with an increased risk of adverse birth outcomes and development of childhood diseases.

Conclusion

Taken together, this study showed that the high-traffic location had higher ambient levels of particulate PAHs compared to the low-traffic location. Pregnant subjects who resided in the traffic-congested area had higher levels of urinary PAH metabolite (1-OHP), DNA damage (PAH-DNA adduct and 8-OHdG) and lipid peroxidation (MDA), compared to those of the control subjects who resided in the low-traffic areas. Moreover, PAHs exposure during pregnancy can eventually lead to fetal exposure via the placenta resulting in increased DNA damage. Therefore, *in utero* exposure to ambient particulate PAHs has the potential to cause DNA damage in pregnant women and eventually in newborns.

References:

1. Zhang L, Tokuda T, Yang L, Zhou Q, Zhang X, Xing W, et al. Characteristics and Health Risks of Particulate Polycyclic Aromatic Hydrocarbons and Nitro-polycyclic Aromatic Hydrocarbons at Urban and Suburban Elementary Schools in Shanghai, China. Asian Journal of Atmospheric Environment. 2019;13(4):266-75.
2. Masih J, Dyavarchetty S, Nair A, Taneja A, Singhvi R. Concentration and sources of fine particulate associated polycyclic aromatic hydrocarbons at two locations in the western coast of India. Environ Technol Innov. 2019;13:179-88.
3. Wanying L, Okromelidze MT, Ramírez-Coronel AA, Zekiy AO, Obaid RF, Jawhar ZH, et al. The association of in-utero exposure to polycyclic aromatic hydrocarbons and umbilical liver enzymes. Science of The Total Environment. 2023;889:164220.
4. Bozinovic G, Shea D, Feng Z, Hinton D, Sit T, Oleksiak MF. PAH-pollution effects on sensitive and resistant embryos: Integrating structure and function with gene expression. PLoS One. 2021;16(4):e0249432.

P-09

Potential source areas of air pollution in Bangkok, Thailand : a case study in north Thonburi zone

Asadavudh Buachum[1], Suwimon Kanchanasuta*[1,2], Sirapong Sooktawee[3]

[1] Department of Environmental Health Sciences, Faculty of Public Health, Mahidol University, Bangkok, Thailand.
[2]Center of Excellence on Environmental Health and Toxicology (EHT), OPS, MHESI, Thailand.
[3] Environmental Research and Training Center, Department of Climate Change and Environment, Ministry of Natural Resources and Environment, Pathum Thani, Thailand.
Corresponding author: Email: Suwimon.kan@mahidol.ac.th

Abstract:

Air pollution is a major issue in Southeast Asia, especially in Bangkok. The primary sources of air pollution are road traffic, industrial plants, and open burning. This study aims to identify potential source areas and air pollution situation in Bangkok. Air pollutant data (PM_{10}, $PM_{2.5}$, O_3, NO_2, CO, and SO_2) and meteorological data (wind direction and speed) were collected from air quality monitoring stations in Bangkok between January 2017 and December 2021. Time series analysis and the Bivariate Polar Plot technique were used for analysis. Results showed PM_{10}, $PM_{2.5}$, NO_2, CO, and SO_2 pollutants are found in the highest concentrations in the morning (08.00-09.00 a.m.) and at night (08.00-10.00 p.m.). Additionally, the highest concentrations of O_3 were observed in the afternoon (02.00-03.00 p.m.), which can be attributed to photochemical reactions. Bivariate polar plots were used to identify the potential source areas at Station 02T. These areas serve as potential sources of air pollution due to traffic activities, leading to increased concentration values in the surrounding areas. Additionally, the potential source areas contributing to the increase in PM_{10} concentration in the afternoon is attributed to construction activities along Charoen Nakhon Road and Charoen Krung Road. This result can support the policymaker in the area for the management and reduction of air pollutants.

Keywords: Air pollution, Bangkok, Bivariate polar plot, Potential source areas

Introduction:

Air pollution is a major environmental health issue that affects the health of people around the world and caused the premature deaths of over 4.2 million people per year due to stroke, heart disease, lung cancer and chronic respiratory diseases. 91% of those premature deaths (estimated 3.8 million people) occurred in the Southeast Asia (SEA) and Western Pacific regions (1). Economic development in SEA has led to notable social and environmental changes. Among the various environmental risks to health, air pollution presents a significant challenge to the inhabitants of large cities in SEA countries. Bangkok, the capital of Thailand, is a major economic, cultural, and political hub of the country. In recent years, it has experienced rapid economic growth, but this has come at the cost of increased air pollution, which is a serious concern in the city. Air pollutant monitoring data were provided by the Pollution Control Department (PCD), Ministry of Natural Resources and Environment, Thailand. It shows that the situation of air pollution in Bangkok in 2021 has a few exceedance days 89 days, with the levels of O_3, $PM_{2.5}$ and PM_{10} above the Thailand's national standards, whereas other gaseous pollutants such as CO, NO_2 and SO_2 were well below that standard (2). The sources of air pollution in the Bangkok area are road traffic, industrial plants, and open burning. Most of the pollution generated from traffic consists of $PM_{2.5}$ caused by the combustion of fuel, from pick-up trucks and trucks that use diesel as fuel (3). Road traffic is also a major source of NO_x and volatile organic compounds in the

atmosphere, which are the precursors to secondary emissions of particulate matter. These various air pollution problems are causing impacts on the health of people in the area both in the short and long term. To solve the problem of air pollution in Bangkok, it is necessary to know the source of air pollution in each area. To make it easier to manage and control the situation in time, receptor modeling, the bivariate polar plot (BVP) is one of the techniques used to identify the source of air pollution (4). The concept of BVP represents the variation of air pollutant concentration versus the wind direction and wind speed for calculate statistical values and show results in the polar coordinate system (4,5). In recent research in Thailand, BVP has been used as a Potential source of PM in each area but it is not cover other air pollutants such as O_3, NO_2, and SO_2. Therefore, this study aimed to study the air pollutants situation in Bangkok and potential source areas of a criteria air pollutants ($PM_{2.5}$, PM_{10}, O_3, NO_2, CO and SO_2) in Bangkok: a case study in Thonburi zone to identify by using Bivariate polar plot technique.

Data and Methodology

Air pollution and meteorological data

Hourly concentrations of air pollutants data ($PM_{2.5}$, PM_{10}, O_3, NO_2, CO, SO_2) and hourly meteorological data (wind direction, wind speed) were measured by 13 air quality monitoring stations in Bangkok from January 2017 to December 2021 (5 years). 12 air quality monitoring stations belong to the Pollution Control Department (PCD) and 1 air quality monitoring station belongs to the Bangkok Metropolitan Administration (BMA).

Data analysis method

In this study, using an analysis of data by the Openair package function embedded with the R program, reveal time series, and detect the potential source areas of air pollution. Bivariate Polar Plot (BVP) is one of the techniques used to determine the source of air pollution (6). The concept of BVP represents the variation of air pollutant concentration versus the wind direction and wind speed (7). First, wind speed, wind direct and air pollutant concentration calculated for each bin. The wind direct interval is 10 degree and wind speed is divided in 30 intervals. The wind components, u and v are calculated i.e. $u = \bar{u}\,sin(2\pi/\theta),\ v = \bar{u}\,cos(2\pi/\theta)$ When, $\bar{u}$ is the mean hourly wind speed and θ is the mean wind direction in degrees with 90 degrees as being from the east. Air pollutant concentrations in each bin were calculated to gain the relevant statistical metrics such as mean, maximum, minimum. In each bin include wind speed, wind direction and mean air pollutant concentrations. The Generalized Additive Model (GAM), with the isotropic smooth function, is used to provide smooth air pollutant concentration surface. In the following equation $\sqrt{C_i} = s(u,v) + e_i$ When, C_i is the pollutant concentrations, $s(u_i,v_i)$ is the smooth function and e_i is residual. However, each mean air pollutant concertation could be potted using polar coordinates. Air pollution concentrations are shaded on polar coordinates and show the potential source area of air pollution (8,9).

Results and Discussion:

Temporal variation

The air quality monitoring station at Bansomdejchaopraya Rajabhat University, Thonburi District (Station 02T), has shown that the concentrations of PM_{10}, $PM_{2.5}$, NO_2, CO, and SO_2 changed over time during the morning and night with similar characteristics. The peak concentrations occur in the morning from 8.00-9.00 a.m. and at night from 8.00-10.00 p.m. It indicates that these air pollutants may be influenced by the same source. The peak times also corresponded to high traffic activity in the area, which release pollutants through vehicle exhaust pipes during combustion processes. During the afternoon, the concentration of PM_{10} was higher compared to the decreasing $PM_{2.5}$ concentration. However, it was discovered that coarse particles ($PM_{2.5\text{-}10}$) had the highest values during this time. This indicates that the primary cause of the

increased concentration was dust generated by mechanical activities such as construction dust. As O_3 is a secondary pollutant, its concentration exhibited distinct characteristics from other air pollutants. One characteristic that sets O_3 apart from other pollutants is the pattern of increasing concentration. Unlike other pollutants, O_3 concentration is related to sunlight, with the highest peak occurring in the afternoon between 2.00-3.00 p.m. When comparing the changes in O_3 and NO_2 over time, we can see that O_3 concentrations increase during the day. While the concentration of NO_2 tends to decrease. The increase of O_3 during the daytime is caused by a reaction between NO_2 and light, generating NO + O and oxygen radicals (O), which then react with O_2 in the atmosphere to form O_3 through a photochemical reaction.

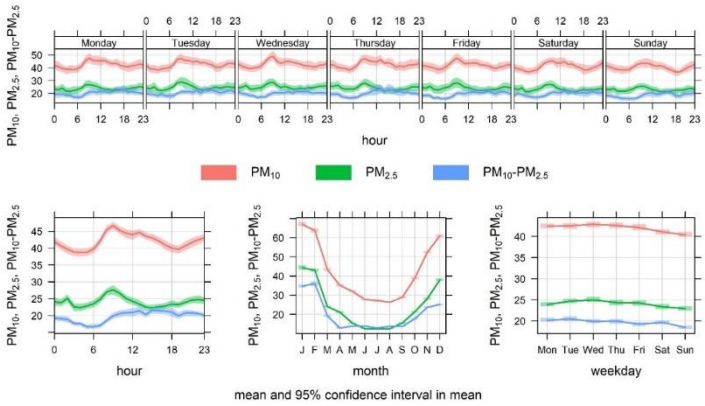

Figure 1 Time variation of PM_{10}, $PM_{2.5}$, and $PM_{2.5\text{-}10}$ at Station 02T

Potential source areas

The Bivariate Polar Plots (BVPs) analysis has discovered that the areas along Charoen Nakhon Road to Taksin Bridge and Charoen Krung Road from Taksin Bridge to Chan Road are potential sources of PM_{10}. The concentration of PM_{10} significantly increased in the afternoon due to construction activities in the area, including the construction of large residential buildings along the Chao Phraya River, shopping centers, and the Gold Line Skytrain station on Charoen Nakhon Road. As a result of construction activities in the area mentioned, PM_{10} concentration significantly increased in the afternoon. In addition, some factors also caused the concentrations of PM_{10}, $PM_{2.5}$, NO_2, CO, and SO_2 to increase in the morning and at night. However, O_3 concentrations increased only during the daytime due to photochemical reactions. These factors associated with the traffic activities in the vicinity of the air quality station (02T Station). The potential sources of air pollutants are along roads and intersections with heavy vehicle traffic. The BVPs analysis showed that the main source area covered Prajadhipok Road, particularly around the Ban Khaek intersection where Prajadhipok Road meets Itsaraphap Road, Arun Amarin Road runs parallel to Itsaraphap Road, Somdet Chao Phraya Road, Lat Ya Road, Charoen Nakhon Road, Charoen Krung Road, and Sanam Chai Road parallel to Rachini Road. Other affected areas include Ratchadamnoen Nok Road, Nakhon Sawan Road, Lan Luang Road, and Phitsanulok Road. This location is also host to schools, hospitals, government offices, popular tourist destinations, and large shopping centers.

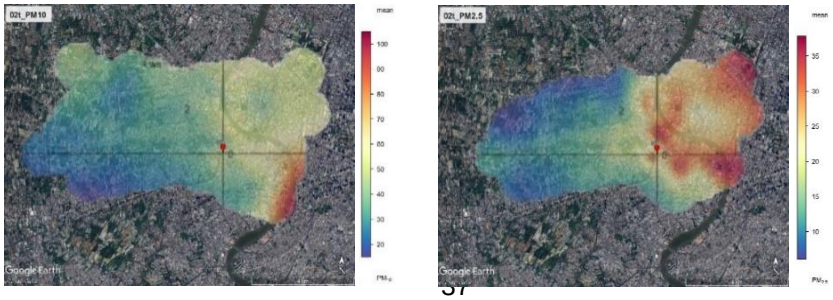

Figure 2 Potential source areas of PM_{10} and $PM_{2.5}$ at Station 02T

Conclusion:

This study found the peak concentrations of PM_{10}, $PM_{2.5}$, NO_2, CO, and SO_2 pollutants occured twice daily, with the highest concentrations in the morning between 08.00-09.00 a.m. and in the evening from 08.00-10.00 p.m. These high concentrations are primarily attributed to heavy traffic on nearby roads, particularly at the 02T Station located at the Ban Khaek intersection (Prajadhipok Road and Itsaraphap Road) and the Khlong San intersection (connecting Somdet Chao Phraya Road, Lat Ya Road, and Charoen Nakhon Road). The study also found that increased $PM_{2.5-10}$ concentrations in the afternoon, along with decreased $PM_{2.5}$ concentrations, resulted from coarse particles generated by construction activities along Charoen Nakhon Road. This area is witnessing the development of large shopping centers, residential buildings, and the Gold Line Skytrain. Finally, identifying potential source areas allows policymakers to determine various measures to reduce emissions and protect the health of residents in affected areas.

References:

1. World Health Organization [Internet]. Ambient (outdoor) air pollution. [cited 2023 Dec 20]. Available form: https://www.who.int/news-room/fact-sheets /detail/ ambient-(outdoor)-air-quality-and-health
2. Pollution Control Department [Internet]. The State of Air and Noise Pollution in Thailand 2021. 2022 [cited 2023 Dec 28]. Available form: http://air4thai.pcd.go.th
3. Narita D, Oanh N.T.K, Sato K, Huo M, Permadi D.A., et al. Pollution Characteristics and Policy Actions on Fine Particulate Matter in a Growing Asian Economy: The Case of Bangkok Metropolitan Region. Atmosphere, 2019; 10,227
4. Sooktawee S, Ketwang R, Patpai A, Piemyai N. A Study on Determining the Potential Source Area of PM2.5 Using Bivariate Polar Plot Technique on Short-Term Monitoring Data in Bhan Phi District, Khonkhen Province, Thailand. Journal of Applied Research on Science and Technology (JARST), 2022; 21(2): 66-78.
5. Kanchanasuta S, Sooktawee S, Bunplod N, Patpai A, Piemyai N, Ketwang R. Analysis of short-term air quality monitoring data in a coastal area. AIMS Environmental Science, 2021; 8(6): 517-531.
6. Sooktawee S, Kanabkaew T, Boonyapitak S, Patpai A, Piemyai N. Characterising particulate matter source contributions in the pollution control zone of mining and related industries using bivariate statistical techniques. Sci Rep 10, 2020; 21372
7. Moufarrej L, Courcot D, Ledoux F. Assessment of the PM2. 5 oxidative potential in a coastal industrial city in Northern France: Relationships with chemical composition, local emissions and long range sources. Science of The Total Environment, 2020; 748, 141448.
8. Carslaw DC, Ropkins K. Openair an R package for air quality data analysis. Environmental Modelling & Software, 2012; 27, 52-61.
9. Ropkins K, Carslaw DC. openair-Data Analysis Tools for the Air Quality Community. R Journal, 2012; 4(1).

P-10

Assessment of *in utero* exposure to micro-nanoplastics and potential health effects in mother and newborns

Wanrada Jiranantawut[1], Panida Navasumrit[1,2,3], Amporn Kuntinuguntanon[1], Chaida Chompoobutr[2] and Mathuros Ruchirawat[1,2,3]

[1]Environmental Toxicology Program, Chulabhorn Graduate Institute, Bangkok, Thailand, 10210; [2]Environmental Toxicology Laboratory, Chulabhorn Research Institute, Bangkok, Thailand, 10210; [3]Center of Excellence on Environmental Health and Toxicology (EHT), OPS, MHESI, Thailand, 10210

E-mail: wanrada@cgi.ac.th

Abstract:

Microplastics (MPs) have become a major emerging threat to the environment worldwide, due to the widespread use of plastics. Airborne microplastics are contributors to microplastic pollution which can be directly inhaled and pose health risks to humans due to their potential adverse effects. Growing evidence suggests that maternal exposure to toxic substances during pregnancy can have profound impacts on fetal development and childhood disorders. This study aimed to assess the prenatal exposure of airborne MPs and their potential health effects in pregnant women and newborns.

This study was conducted in high- and low- traffic density locations. The study included 50 exposed pregnant subjects living in high traffic and 50 control pregnant subjects recruited from low-traffic areas. MPs in ambient air samples and urine samples were analyzed and identified using Pyrolysis GC-MS/MS. Various polymers of MPs were detected in ambient air including polyvinyl chloride (PVC), polyethylene (PE), polyethylene terephthalate (PET), nylon (N66), styrene-butadiene rubber (SBR), polymethyl methacrylate (PMMA) and polystyrene (PS). The total concentrations of MPs in ambient air from high-traffic location were approximately 1.5-fold significantly higher than those of low-traffic location (4.32 vs 2.88 μg/m^3, $p<0.05$). Total MPs in maternal urine were also higher in the exposed group than the control group with the detected MPs including N6, N66, PE, PS, PVC and SBR. Urinary biomarker of oxidative DNA damage (8-hydroxydeoxyguanosine, 8-OHdG) and lipid peroxidation (8-iso-prostaglandin F2α; 8-isoPGF2 and malondialdehyde; MDA) were analyzed using LC-MS/MS. The concentrations of 8-OHdG, 8-isoPGF2 and MDA were higher in the exposed-group with a significant 2-fold increase in MDA (7.17 vs 3.59 μg/ml, $p<0.05$). Consistent with the presence of MPs in maternal urine, MPs were detected in placental tissue suggesting transplacental transferred and fetal exposure. In addition, mutagenic DNA adducts including 8-OHdG and ethenodeoxy adenosine (1N^6εdA), a lipid peroxidation-derived DNA adduct, were detected in placental tissue.

Taken together, the results obtained suggest that traffic emissions contribute to air pollution of MPs. Exposure to MPs during pregnancy can increase DNA damage in pregnant women. The detection of MPs and mutagenic DNA damage in placental tissue indicates fetal exposure to MPs which may increase the health risk of adverse birth outcomes and disease development in newborns

Keywords: Microplastics, Air pollution, *In utero* exposure, Oxidative DNA damage, Lipid peroxidation

Introduction:

Microplastics (MPs) have emerged as a significant global environmental concern due to the widespread use of plastics, with an estimated 170 trillion plastic particles currently floating in the world's oceans. These particles, totaling about 2 million metric tons, have the alarming potential to triple by 2040 if urgent actions are not taken (1). MPs are categorized as either primary, intentionally added to consumer products, or secondary, formed unintentionally through the breakdown of larger plastics, including those used in cosmetics, personal care items, pharmaceuticals, and detergents (2). Microplastics, defined as plastic particles generally less than 5 millimeters in size, pose challenges in detection and removal from the environment due to their small dimensions, allowing them to be ingested by various organisms and potentially causing ecological and health concerns (3). Exposure to plastic particles poses potential health hazards to humans, including the risk of cancer, immunotoxicity, cardiovascular diseases, inflammation, and adverse effects on pregnancy with maternal exposure to offspring (2). Atmospheric MPs can enter the human body through inhalation and ingestion, potentially traversing biological barriers and accumulating in various tissues. A recent study reported the presence of MPs in the human placenta, indicating exposure during pregnancy (4). Understanding the implications of in utero exposures to MPs is crucial for designing effective strategies to mitigate risks and safeguard the health of pregnant women and newborns. The potential health impacts and long-term consequences of such exposure are areas of active research, highlighting the importance of ongoing investigation into the health impact of in utero exposure to MPs in pregnant women and newborns, including the determination of MPs concentrations in biological samples and the assessment of oxidative damage in maternal urine and placenta tissues.

Objectives:

The objectives of this study aimed to assess in utero exposure to microplastics and potential health effects in pregnant women and newborns.

Methodology:

Study locations

The study was conducted in high- and low-traffic congested areas in Bangkok, Thailand. The initial criteria for selecting the study sites involve assessing traffic density. The study area in the high-traffic site was Klongsan District along Somdej Chaophraya Road and in low-traffic site is located in peri-Bangkok at Buddhamontol 3 Road.

Sample collection

A total of 100 pregnant women were recruited at the first semester of pregnancy from healthy pregnant women from high- and low-traffic exposed sites. The ambient air samples were collected using an air sample pump connected to a cascade impactor with aluminium foil filters to trap the ambient air. Ambient air sample consisted of 16 samples of low traffic areas and 8 samples of high traffic areas. The urine samples from pregnant subjects were collected and stored at -20ºC and placental tissue was collected after the delivery of lived-born baby and stored at -80ºC.

Determination of MPs in ambient air samples

The collected filters were cut into small pieces and then placed into the eco cup. The samples were analyzed and identified using Pyrolysis GC-MS/MS. Using the F-search MPs 2.0 software to quantitative of MPs in ambient air samples.

Determination of MPs in maternal urine samples

A fraction of maternal urine samples (5 ml) were filtered using filter membranes (0.6 µm pore-size) and dried at 45ºC for 4 hours. Subsequently, the dried filtered was cut into the sample cup and analyzed using Pyrolysis GC-MS/MS.

Determination of MPs in placenta tissues

Placental tissues were cut into small pieces and dried at 100ºC. The samples were grinded and analyzed using Pyrolysis GC-MS/MS.

Measurement of DNA damage and lipid peroxidation

Maternal urine samples (1 ml) were extracted by solid-phase extraction (SPE) and subjected to analyze oxidative damage by LC-MS/MS. The concentration of 8-hydroxydeoxyguanine (8-OHdG), biomarker of oxidative DNA damage and 8-iso-prostaglandin F2α (8-isoPGF2) and malondialdehyde (MDA), biomarkers of lipid peroxidation, were determined.

Statistical evaluation

Mann-Whitney U test was performed to compare the statistically difference between groups. A p-value < 0.05 was considered the difference with a statistical significance.

Results and Discussion:

1. Microplastics (MPs) in the ambient air

The concentration of MPs in ambient air from high-traffic areas was significantly higher ($p<0.05$) than that in the low-traffic sites by approximately 1.5-fold (4.32 vs 2.88 µg/m^3). When stratified by particle size, the MPs concentrations in the particle size 2.5-1 µm, 1-0.5 µm and 0.5-0.25 µm were significantly higher than those in the low-traffic areas by approximately 1.28-, 1.57- and 1.82-fold, respectively. The profile of MPs polymers found in ambient air both in high- and low-traffic sites was PVC, PE, SBR, PET, N66, PS, and PMMA. The concentrations of PVC, SBR and PS from high-traffic site were significantly higher than those in ambient air from low-traffic site by approximately 1.8-fold, 2-fold and 4.6-fold, respectively.

2. Maternal exposure to microplastics (MPs) and health risk of oxidative damage

The concentration of MPs in maternal urine samples from high-traffic sites was higher than that in maternal urine samples from low-traffic sites. The major MPs polymer found in the maternal urine were PE, N6, PVC, N66, SBR and PS. The increased urinary concentration of MPs in exposed pregnant subjects indicating maternal exposure to MPs, was in agreement with the increased levels of airborne MPs in high-traffic areas.

Health risk of oxidative damage in study subjects was determined by measurement of 8-OHdG, 8-isoPGF$_2$ and MDA. The urinary concentrations of 8-OHdG in exposed pregnant subjects were higher than that control subjects by approximately 1.18-fold (0.47 vs 0.39 µg/mL). The concentration of MDA was significantly higher ($p<0.01$) in exposed pregnant subjects than that in control pregnant subjects by approximately 2-fold (7.17 vs 3.59 µg/mL), while the concentration of 8-isoPGF2 was higher in exposed pregnant subjects, but not statistical significant.

3. Microplastics (MPs) in placental tissues

Consistent with the presence of MPs in maternal urine, MPs were detected in placental tissue suggesting transplacental transferred and fetal exposure. The detected MPs polymers in placental tissues included PE, ABS, PET, N6, N66, PVC, SBR, and PS.

In addition, mutagenic DNA adduct including 8-OHdG and ethenodeoxy adenosine (1N6εdA), a lipid peroxidation-derived DNA adduct, were detected in placental tissue.

Conclusions:

The results obtained suggest that traffic emissions contribute to MPs air pollution. Exposure to MPs during pregnancy can increase DNA damage in pregnant women. The detection of MPs and mutagenic DNA damage in placental tissue indicates fetal exposure to MPs which may increase the health risk of adverse birth outcomes and disease development in newborns. Thus, the national policy for exposure to MPs should be established for improving the ambient air quality and reducing human health risk of exposure to MPs, particularly in pregnant women and newborns.

References:

1. Eriksen M, Cowger W, Erdle LM, Coffin S, Villarrubia-Gómez P, Moore CJ, et al. A growing plastic smog, now estimated to be over 170 trillion plastic particles afloat in the world's oceans—Urgent solutions required. PLOS ONE. 2023;18(3):e0281596.
2. Osman AI, Hosny M, Eltaweil AS, Omar S, Elgarahy AM, Farghali M, et al. Microplastic sources, formation, toxicity and remediation: a review. Environmental Chemistry Letters. 2023;21(4):2129-69.
3. Sarkar S, Diab H, Thompson J. Microplastic Pollution: Chemical Characterization and Impact on Wildlife. Int J Environ Res Public Health. 2023;20(3).
4. Ragusa A, Svelato A, Santacroce C, Catalano P, Notarstefano V, Carnevali O, et al. Plasticenta: First evidence of microplastics in human placenta. Environment International. 2021;146:106274.

P-11

Human exposure of microplastic by consumption of canned sardines in tomato sauce

Thitiwat Mataroepayotorn[1], Thanomsak Boonphakdee[2,4*] and Supranee Kaewpirom[3,4]

[1]Graduate Program in Environmental Science, Faculty of Science, Burapha University, Chonburi 20131, Thailand

[2]Department of Aquatic Science, Faculty of Science, Burapha University, Chonburi province. 20131 Thailand

[3]Department of Chemistry, Faculty of Science, Burapha University, Chonburi 20131, Thailand

[4]Center of Excellence on Environmental Health and Toxicology (EHT), OPS, MHESI, Thailand

[*]Corresponding author: nuiosk@gmail.com

Abstract:

Study of small-sized microplastics (1-20 µm) in canned sardines produced from four different countries. Microplastics were found in canned sardines from Thailand (0.42±0.05 mg/can), Malaysia (1.28±0.15 mg/can), Vietnam (0.33±0.05 mg/can), and the Philippines (0.29±0.13 mg/can), with the majority coming from sardine meat. The risk assessment of consumers' exposure and accumulation of microplastics in the body from consuming canned sardines per day (Thailand - FDA = 0.73 mg_{MPs}/day, IFOSY = 0.01 mg_{MPs}/day, and Maximum case = 1.25 mg_{MPs}/day) suggests that excessive accumulation of microplastics in the body may pose health risks to consumers. This underscores the importance of establishing food standards for microplastic contamination (ISO22004).

Keywords: Small-sized microplastics, Canned sardines, Exposure assessment

Introduction:

Microplastics are a global environmental concern impacting soil, air, and water supplies, among other ecosystems. Microplastics in the environment are typically less than 20 µm in size, with marine environments being the most significant accumulators of plastics in the world [1]. The accumulation of those small microplastics in aquatic ecosystems affects organisms in the food chain, which can be transferred to top consumers through the consumption of seafood [2]. There is an increasing presence of small-sized microplastics (<20 µm) detected in processed seafood products such as smoked salmon, canned tuna, canned mackerel [3], and canned sardines [4].

Microplastics, particularly those smaller than 20 µm, can accumulate in the human body by consuming microplastic-contaminated products [2]. These small microplastics remain in the human body and can be toxic to human cells, affecting the functioning of the nervous, respiratory, reproductive, and digestive systems [5]. Microplastics are carriers of chemicals and pathogenic microorganisms and are also one of the causes of drug resistance in microorganisms [5]. There is no current research indicating the health risks associated with the number of microplastics humans ingest, and there are no food standards for microplastic contamination from the International Standardization Organization (ISO 22004) [6]. This study can assist in identifying the sources of microplastics in products and guide consumers in choosing seafood with the lowest levels of microplastic contamination. It can also lead to the establishment of seafood standards for microplastic contamination to ensure seafood safety, particularly canned sardines, in the future.

Materials and Methods:

Sardines canned products were purchased from Thailand, Malaysia, Vietnam, and the Philippines during January 2024. Three replicates per sample were analysed (n=3).

Extraction of microplastics

The microplastics were extracted from the sample according to the method modified from Duman et al. (2023) [3]. NaOH, proteinase, 30% H_2O_2, and 20% SLS were used with 50°C incubation. The solution was filtered through a sieve with a pore size of 20 µm and put into sedimentation cones with NaI solution. The supernatant was filtered through 1 µm Polycarbonate (PCTE) Membrane Filters (Sterlitech) and stained with a few drops of Nile-Red solution. Microplastics were counted under a Fluorescence stereo microscope at 4 0 x magnification (Model camera KÖnigsalle optronic, Germany).

Morphology and elemental composition of microplastics

The surface morphology, structure, chemical composition, and qualitative and quantitative analysis of microplastics were studied using Scanning Electron Microscope-Energy Dispersive X-Ray Analysis (SEM-EDX) [3]. This technique was employed to analyse the polymer's carbon (C) and oxygen (O) components ratio. Additionally, a portion of the polymers was randomly selected for analysis of chemical functional groups using micro-Fourier Transform Infrared Spectroscopy (µ-FTIR) [7].

The results from the SEM-EDX analysis revealed that the main components of the identified microplastics are carbon (C) and oxygen (O). This indicates that the microplastics found were polymers, accounting for more than 94% (**Fig.1a**). Furthermore, analysis of a portion of the polymers using the µ-FTIR technique showed similarities to Polyethylene terephthalate (PET) at 92.95% (**Fig.1b**) [7].

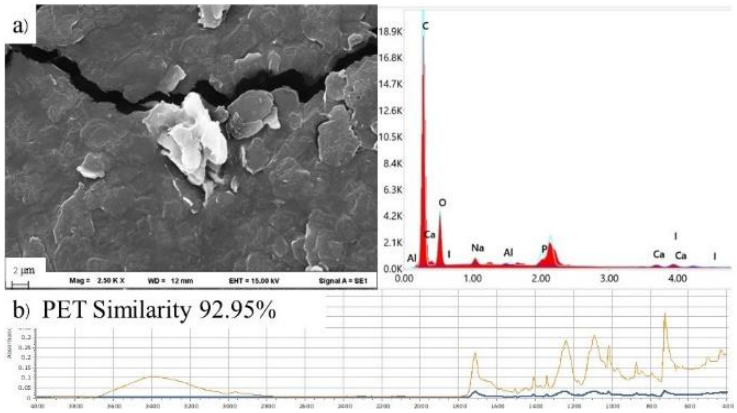

Figure 1 Example of microplastic analysis using a) SEM-EDX and b) µ-FTIR.

Quality control and quality assurance

All water and solutions used in the analysis undergo filtration through a 0.45 µm Cellulose nitrate filter (Whatman), and control sets are prepared using distilled water to check for potential contamination that may occur during the analysis in the laboratory [5]. After completing the counting of microplastic samples, the quantity of microplastics counted from the control sets is subtracted from the amount of microplastics counted from the actual samples to obtain the proper quantity of microplastics [3].

Microplastic extraction and separation efficiency from the samples is assessed by processing microplastic pieces sized between 20-300 µm using the same extraction and separation procedures as the samples. %Recovery of the microplastic extraction process is calculated based on the counted microplastic quantity. The %Recovery is 93.00±4.36%, which falls within an acceptable range. This indicates that the microplastic extraction method used in this study efficiently separates microplastics from the samples, similar to the microplastic extraction methods in the research of Duman et al. (2023) [3].

Weight of microplastics

The mass of microplastics can be calculated from equation (1) [8].

$$\sum W = \sum 4/3\ \rho\pi r^3 \quad (1)$$

$\sum W$ = Total weight of microplastics (g_{MPs}), ρ = Density of microplastics (g_{MPs}/cm^3) and r = Average size of microplastics (cm)

From the test results using microplastics of each size, weighed and processed through the extraction and separation process, it was found that the calculated weights, when compared, had a deviation of no more than 10%. Subsequently, the Simple two sources mixing model was used to compare and analyse the quantities and sources of microplastics in canned sardines.

Exposure assessment

This study evaluates Human intake of microplastics by calculating The quantity of food consumed per serving according to the Food and Drug Administration (FDA): 85 g (1 serving) for adults [9]; the annual statistical report from the Iranian Fisheries Organization Statistical Yearbook (IFOSY) regarding the consumption rate of canned fish per capita among Thailand people (3.14 g/person/day) for adults [10], and Assessment of consuming canned fish three times a day (3 canned/person/day).

Human intake of microplastics can be calculated using the equation [11]:

$$HIM = IR \times C \quad (2)$$

HIM = Average quantity of microplastics received per day (g_{MPs}/day), IR = Consumption rate of canned fish per day (g_{fish}/day, canned/day) and C = Total weight of microplastics (g_{MPs}/g_{fish}, g_{MPs} /canned)

Results and Discussion:

Quantity of microplastics in canned sardines in tomato sauce.

Canned sardines from all countries were contaminated with microplastics in the sauce and the fish meat in varying quantities. Interestingly, the highest amount of microplastics was found in the fish meat. This indicates that fish meat is a significant source of microplastic contamination in canned sardines.

Canned sardines from Malaysia were found to have the highest level of microplastic contamination, with over 441% more microplastics compared to canned sardines from the Philippines, which had the lowest contamination levels (**Fig.2**). Additionally, the fish meat from Malaysia was found to have the highest level of contamination (**Fig.3**), contributing to the overall high quantity of microplastics found in the canned sardines.

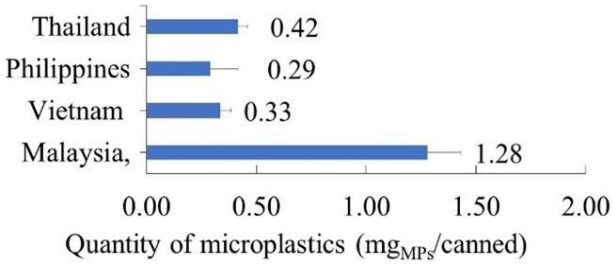

Figure 2 The quantities of MPs sized 1-20 µm found in canned fish (mg_{MPs}/canned)

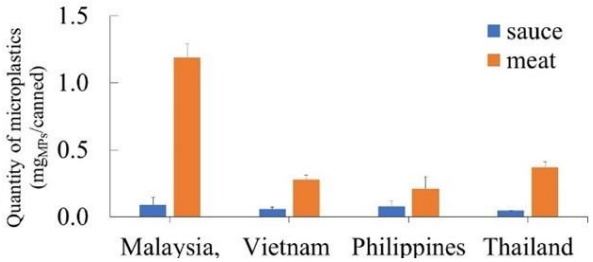

Figure 3 The quantities of MPs sized 1-20 µm found in meat and sauce of canned fish (mg_{MPs}/canned).

Human intake of microplastics

Assessment of the intake and accumulation of microplastics in consumers' bodies from consuming canned sardines in each country, which is eaten consecutively on week, month and year. **(Table 1)**

Table 1 shows that the maximum amount of microplastics that consumers can intake per day is 3.83 mg_{MPs} from eating canned sardines from Malaysia. If consumers want to reduce the risk of accumulating microplastics from consuming canned sardines, they should choose canned sardines from the Philippines, which can reduce the daily accumulation to 2.96 mg_{MPs}.

Table 1 Average quantities of microplastics consumed by consumers through canned sardines. (mg_{MPS})

Country	Factor	Day	Week	Month	Year	Country	Factor	Day	Week	Month	Year
Malaysia	FDA	1.52	10.64	45	553	Philippines	FDA	0.49	3.43	15	178
	IFOSY	0.02	0.14	0.56	7		IFOSY	0.01	0.07	0.18	2
	Limit	3.83	26.81	115	1,399		Limit	0.87	6.09	26	318
Vietnam	FDA	0.68	4.76	20	249	Thailand	FDA	0.73	5.11	22	267
	IFOSY	0.01	0.07	0.25	3		IFOSY	0.01	0.07	0.27	3
	Limit	1.00	7	30	366		Limit	1.25	8.75	37	455

*day = 1, week = 7, mount = 30 and year = 365

Conclusion:

Summary of microplastic testing results in canned sardine products from each country revealed that microplastics sized 1-20 µm were most prevalent in canned sardines from Malaysia and least prevalent in those from the Philippines. The canned sardines' meat is a significant source of microplastics that humans may ingest into their bodies.

Acknowledgements:

This research was granted by NRCT. Researchers express their gratitude to the Department of Aquatic Science, Department of Chemistry, and the Environmental Science program, Faculty of Science, Burapha University, for providing analytical tools and equipment for sample analysis.

References:

1. Gomes, T., Bour, A., Coutris, C., Almeida, A. C., Bråte, I. L., Wolf, R., Bank, M. S., & Lusher, A. L. 2022. Ecotoxicological Impacts of Micro- and Nanoplastics in Terrestrial and Aquatic Environments*. In Microplastic in the Environment: Pattern and Process* (pp. 199-260)
2. Wang, W., Do, A. T. N., & Kwon, J. H. 2022. Ecotoxicological effects of micro- and nanoplastics on terrestrial food web from plants to human beings. *Sci Total Environ*, 834, 155333.
3. Duman, S., Doyen, P., Merveillie, P., Andersson, N., Bayeuil, R., Grard, T., Dehaut, A., & Duflos, G. 2023. Optimization of a method designed to extract and characterize microplastics in different packaged fish products. *Food Control*, 154.
4. Hussien, N. A., Mohammadein, A., Tantawy, E. M., Khattab, Y., & Al Malki, J. S. (2021). Investigating microplastics and potentially toxic elements contamination in canned Tuna, Salmon, and Sardine fishes from Taif markets, KSA. *Open Life Sci*, 16(1), 827-837.
5. Fournier, E., Etienne-Mesmin, L., Grootaert, C., Jelsbak, L., Syberg, K., Blanquet-Diot, S., & Mercier-Bonin, M. 2021. Microplastics in the human digestive environment: A focus on the potential and challenges facing in vitro gut model development. *Journal of Hazardous Materials*, 415.
6. Chen, H., Liu, S., Chen, Y., Chen, C., Yang, H., & Chen, Y. 2020. Food safety management systems based on ISO 22000: 2018 methodology of hazard analysis compared to ISO 22000: 2005. *Accreditation and Quality Assurance*, 25, 23-37.
7. Tagg, A.S., Sapp, M., Harrison, J.P. and Ojeda, J.J. 2015. Identification and Quantification of Microplastics in Wastewater Using Focal Plane Array-Based Reflectance Micro-FT-IR Imaging, *Analytical Chemistry*, vol. 87, May 2015, pp. 6032-6040.
8. Torosian, G. T., & Ashley Mac Millan, P. E. (2016). 6 - Physical properties, behavior, and testing of geotextiles. In R. M. Koerner (Ed.), *Geotextiles* (pp. 105-113). Woodhead Publishing.
9. ACFS. (2015). FOOD CONSUMPTION DATA OF THAILAND. from https://www.acfs.go.th /files/files/attach-files/867_20190606145951_625162.pdf.
10. FDA, U. (2016). Food labeling: serving sizes of foods that can reasonably be consumed at one eating occasion; dual-column labeling; updating, modifying, and establishing certain reference amounts customarily consumed; serving size for breath mints; and technical amendments. Final rule. Federal register, 81(103), 34000-34047.
11. Akhbarizadeh, R., Dobaradaran, S., Nabipour, I., Tajbakhsh, S., Darabi, A. H., & Spitz, J. 2020. Abundance, composition, and potential intake of microplastics in canned fish. *Marine Pollution Bulletin*, 160, 111633.

P-12

Risk assessment of exposure to small microplastics (1-60 µm) from green mussel consumption

Tanyaporn Buatang[1], Thanomsak Boonphakdee[1,2,5*], Supranee Kaewpirom[3,5], and Chuta Boonphakdee[4,5]

[1]Graduate Program in Environmental Science, Faculty of Science, Burapha University, Chonburi 20131, Thailand
[2]Department of Aquatic Science, Faculty of Science Burapha University, Chonburi province. 20131 Thailand
[3]Department of Chemistry, Faculty of Science Burapha University, Chonburi province. 20131 Thailand
[4]Department of Biology, Faculty of Science, Burapha University, Chonburi 20131, Thailand
[5]Center of Excellence on Environmental Health and Toxicology (EHT), OPS, MHESI, Thailand
** Corresponding author: nuiosk@yahoo.com*

Abstract:

The purpose of this work was to investigate the accumulation and risk assessment of microplastics in an urban populated area (Sriracha) and a rural pristine area (Chang Island). The microplastics in mussels accumulated in the digestive tract were 322.68 ± 195.67 and 193.12. ± 85.90 ng/g (wet weight), and accumulated in tissues were 212.40 ± 105.55 and 49.66 ± 15.38 ng/g (wet weight), respectively. The accumulation of microplastics in mussels may be caused by exposure to different humans. In addition, the microplastics found in mussels can be identified using µ-FTIR techniques and are 72% similar to PP plastics. Risk assessment calculations show that humans consume more microplastics from mussels in urban than rural areas. Therefore, it may be beneficial to develop practical solutions to environmental problems.

Keywords: microplastic, mussel, µ-FTIR, risk assessment

Introduction:

Increased plastic production has resulted in more plastic waste entering the environment. There are concerns about the degradation of plastics and the movement of plastic debris from inland waterways to coastal waters. Plastic debris exposed to sunlight (radiation energy), oxygen, and mechanical abrasions is broken into small particles (<5 mm), forming microplastics. Classified as secondary plastic, primary microplastics (e.g., nurdles) are produced specifically for producing plastic products. Microplastic contamination in the marine environment poses a risk to humans [1]. Consuming seafood causes microplastics contaminated with water to enter the food chain through ingestion by aquatic animals. This causes the accumulation of microplastics within the bodies of aquatic animals, such as bivalves, which can cause severe tissue inflammation. Microplastics in bivalves may enter humans through consumption [2], and most of the accumulated microplastics are small. Moreover, it may be less excreted by the body. This is because studies in rats have found that microplastics accumulate in organs in the body, such as the gastrointestinal tract, gallbladder, liver, and kidneys [3].

This study aims to investigate the abundance of small microplastics in the digestive tract and tissue and risk assessment of green mussel (*Perna viridis*) samples collected from a cultured mussel along the coast of Siracha and the reference site located on Chang Island, Trat Province. These two locations are affected by different anthropological activities and pollution levels. Our study will be expected to provide the baseline data for human sub-health early warning and human pathology research.

Methodology:

Sample preparation and identification

Samples of green mussel (*Perna viridis*) were collected from mussel farms along the coast of Sriracha (Sr) and Chang Island (Ch) in Chonburi and Trat Provinces (Figure 1), respectively, in August 2019 and January 2020. The latter area is classified as the reference site. The Sriracha (Sr) coast receives municipal wastewater from densely populated communities before emptying into the coast [4]. The reference site (Ch) in Chang Island was expected to contain a very low abundance of microplastics among the sites [5].

In the laboratory, the shell length of green mussel samples was measured using a Vernier caliper. The tissue was removed from the shell and weighed (wet weight) with a microbalance, and the dissected organs were separated into two parts: the digestive tract and tissues. The methods of digestion, separation, and collection of microplastics were modified from [6]. The soft tissues were finely chopped and placed into a glass bottle before adding distilled water, 50 mM NaOH, and sodium dodecyl sulfate (SDS) solution. The chemical digestion was further performed using 30% hydrogen peroxide (H_2O_2). After digestion, 4M NaI solution was added to the bottle to keep the microplastics suspended for 24 hours. The overlying water was filtered through a sieve with a pore size of 1000–5000, 300–1000, and 60–300 µm. In order to remove large microplastics, it was filtered through a polycarbonate membrane (1 µm, diameter 47 mm) and dried at 60 ˚C for 24 h, adding a few drops of Nile Red.

We observed microplastic particles under a fluorescence stereoscopic microscope (Zeiss, stemi 305). The identification of microplastics was conducted with a µ-FTIR microscope. All the spectra were directly compared with a database of standards for polymers. The spectra matching a quality index ≥70 were accepted. No transformation or postprocessing of the spectra was carried out.

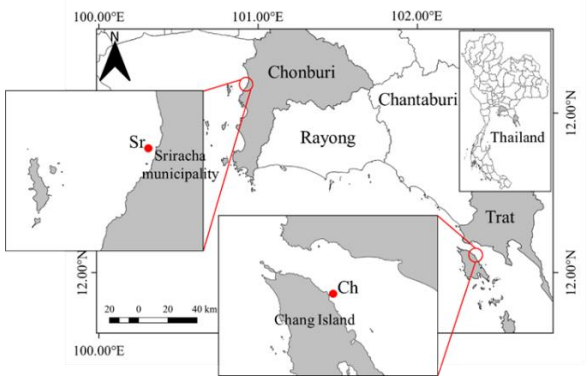

Figure 1 Map of the study areas and sampling stations along the eastern seaboard of the Gulf of Thailand. Red dots (●) indicate green mussel sampling sites from an urban populated area at Sriracha (Sr) coast, and a rural pristine coast at Chang Island (Ch)

Risk assessment

The Estimated Annual Intake (EAI) of microplastics by Thai consumers of mussels from the Gulf of Thailand was calculated using the following equation [7].

$$EAI = C \times AIR$$

C: Average number of microplastics per gram detected in mussel tissue (ng/g ww.) AIR is a Thai consumer's Annual Ingestion Rate of mussel soft tissues. AIR was calculated by dividing the Thai annual production of *P. viridis* mussels (51,310.8 tons per year) by the Thai population, 60,052,615 people [8]. The calculated AIR of the mussel soft tissues of a Thai consumer was found at 7.77×10^{11} ng/person/year.

Results and Discussion:

Abundance of microplastics

Small microplastics (1–60 µm) were detected in the digestive tract and tissue of green mussels from Sr and the reference site (Ch). The abundance of microplastics was 322.68 ± 195.67 ng/g (wet weight) in the digestive tract, and 212.40 ± 105.55 ng/g (wet weight) in the tissue of green mussels from Sr. Microplastics accumulation from Sr compared to Ch is a reference in that mussels contained a low concentration of microplastics in the digestive tract 193.12 ± 85.90 ng/g (wet weight). Tissue was 49.66 ± 15.38 ng/g (wet weight). The amount of microplastics was significantly different ($p<0.05$) (Figure 2). This is consistent with studies by [9] that found that small microplastics (<200 µm) accumulated in mussels. The amount of these microplastics detected indicates that mussels filter-feed particles smaller than 200 µm, indicating that the size of microplastics is similar to the natural diet of mussels [10].

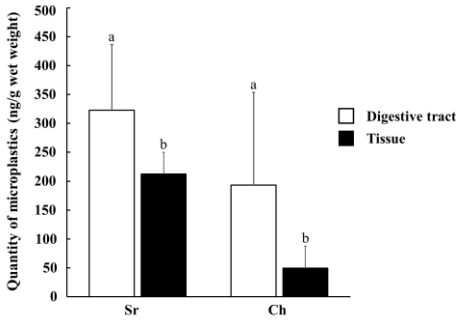

Figure 2 The amount of microplastics found in the digestive tract and tissue of mussels (*P. viridis*). Different English letters indicate that there were statistically significant differences among stations. ($p<0.05$)

Microplastic identification

The microplastic samples were analysed with µ-FTIR and confirmed to be plastic polymers. Microplastics found in mussels can identify types of plastic similar to polypropylene (PP) plastics by up to 72%. The type of polymer PP was detected in this study. There is a high detection rate for mussels, including invertebrates, seawater, and sediment [9], which has been recorded as PP plastic floating in surface waters. Because they have a lower density than water [11], microplastics may contaminate the municipal wastewater released into the sea [6].

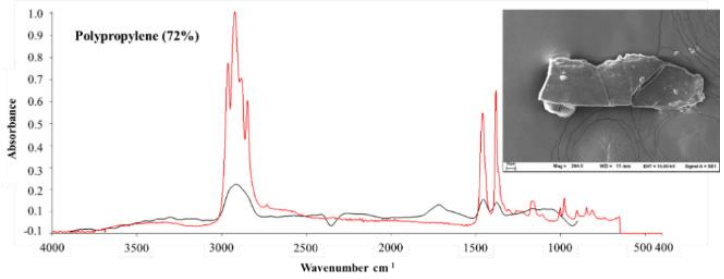

Figure 3 µ-FTIR spectra and match degrees of selected microplastics. Black curves are the µ-FTIR spectra of microplastic samples, and the red curves are the µ- FTIR spectra of standard polymers in spectral libraries, polypropylene (PP).

Risk assessment

From the results, it was found that the risk assessment resulted in the mean microplastic intensity in the tissues of *P. viridis* was determined as 4.16×10^{14} and 1.89×10^{14} ng/capita/year for green mussels in urban and rural areas, respectively (Table 1). Therefore, it can be said that urban areas are at higher risk than rural areas. MPs taken up by mussels may transfer to humans via the food chain, posing severe dangers to human health and biota [2]. Although microplastics can accumulate in the human body, most are eliminated by the liver or spleen and excreted in the faeces [12]. However, further studies on the ecological risks of MPs contamination are critical.

Table 1 The potential for contamination by microplastics.

		Quantity of microplastics (ng/capita/year)	Percentage of remove microplastics
Sr	Whole body	4.16×10^{14}	0
	No digestive tract	1.65×10^{14}	60.31
Ch	Whole body	1.89×10^{14}	0
	No digestive tract	3.86×10^{13}	79.54

Conclusion:

This work has revealed the accumulation of microplastics in the human body and the risks associated with consuming green mussels. Most microplastics accumulate in mussels closer to urban areas than in rural areas. This is because the former area receives much wastewater from the community. In addition, mussels accumulated significantly more microplastics in their digestive tracts than in their tissues. Furthermore, the microplastics found can be identified as polypropylene (PP) (72%). Mussels can be used as good bioindicators of plastic pollution in aquatic environments. However, it can also be used as a bioremediation tool to decontaminate water contaminated by microplastics. Although the microplastics in mussels are in high concentrations, Thai people can consume mussels generally by removing the digestive system of the mussels before consumption. This is because microplastics accumulate more in the digestive tract than in tissues. Therefore, further studies are needed to know the potential effects of microplastics on aquatic organisms and humans.

References:

1. Burns, E. E, Boxall, A. B. A. Microplastics in the aquatic environment: evidence for or against adverse impacts and major knowledge gaps. Environ. Toxicol. Chem. 2018;37:2776–2796.
2. Bråte, I.L.N., Hurley, R., Iversen, K., Beyer, J., Thomas, K.V., Steindal, C.C., Green, N.W., Olsen, M., Lusher, A. Mytilus spp. as sentinels for monitoring microplastic pollution in Norwegian coastal waters: a qualitative and quantitative study. Environ. Pollut. 2018;243:383–393.
3. Keinänen, O., Dayts, E. J., Rodriguez, C., Sarrett, S. M., Brennan, J. M., Sarparanta, M., Zeglis, B. M. Harnessing PET to track micro- and nanoplastics in vivo. Scientific Reports. 2021;11:11463.

4. Boonkwang, N., Boonphakdee, T. Sources and Distribution of Organic Matter in Coastal Area of Muang Chonburi District, Eastern Thailand: Using Carbon and Nitrogen Stable Isotopes. Environment and Natural Resources Journal. 2022;20(4):348-358.
5. Ocharoen, Y., Boonphakdee, C., Boonphakdee, T., Shinn, A. P., Moonmangmee, S. High levels of the endocrine disruptors bisphenol-A and 17β-estradiol detected in populations of green mussel, Perna viridis, cultured in the Gulf of Thailand. Aquaculture. 2018;497:348-356
6. Li, J., Green, C., Reynolds, A., Shi, H., Rotchell, J.M. Microplastics in mussels sampled from coastal waters and supermarkets in the United Kingdom. Environmental Pollution. 2018;241:35-44.
7. Wakkaf, T., El Zrelli, R., Kedzierski, M., Balti, R., Shaiek, M., Mansour, L., Tlig-Zouari, S., Bruzaud, S., Rabaoui, L. Microplastics in edible mussels from a southern mediterranean lagoon: preliminary results on seawater-mussel transfer and implications for environmental protection and seafood safety. Mar. Pollut. Bull. 2020;158:111355.
8. The Bureau of Registration Administration. Official statistics registration systems. 2023. https://stat.bora.dopa.go.th/stat/pk/pk_66.pdf, Accessed date: 20 April 2024.
9. Jeong, J., Shim. W. J., Cho, Y., Han, G. M., Jang, M., Hong, S. H. Intra-annual variation in microplastics in mussels (Mytilus galloprovincialis) inhabiting an urbanized bay of South Korea. Marine Pollution Bulletin. 2023;196:115673.
10. Patterson, J., Jeyasanta, K.I., Sathish, N., Booth, A.M., Edward, J.K.P. Profiling microplastics in the Indian edible oyster, Magallana Bilineata collected from the Tuticorin coast, Gulf of Mannar, Southeastern India. Science of the Total Environment. 2019;691:727-735.
11. Maddah, H. A. Polypropylene as a Promising Plastic: A Review. American Journal of Polymer Science. 2016;6(1):1-11
12. Prata, J.C. Microplastics and human health: Integrating pharmacokinetics. Critical Reviews in Environmental Science and Technology. 2023;53(16):1489–1511.

P-13

Toxicity of polyethylene microplastics on human THP-1 monocyte-derived macrophage cells

Ariya Sithalon[1], Jantamas Kanitwithayanun[1,2,3], Nedsai Uddin Babar[2], Noppawan Rittapai[2], Jutamaad Satayavivad[1,2,3]

[1]Environmental Toxicology Program, Chulabhorn Graduate Institute, Bangkok 10210, Thailand
[2]Laboratory of Pharmacology, Chulabhorn Research Institute, Bangkok 10210, Thailand
[3]Center of Excellence on Environmental Health and Toxicology (EHT), OPS, MHESI, Thailand

Abstract:

Polyethylene microplastics (PE-MPs) are one of the most commonly found microplastics in the environment. Due to their small size, they can widely distribute in various ecosystems and could get exposed by humans which may result in adverse effects. Macrophages play a key role in innate immunity and regulate the inflammatory response. However, the possible mechanism underlying the toxicity of PE-MPs to macrophage cells has remained rather unclear. This study aimed to assess the PE-MPs' effects on cytotoxicity, reactive oxygen species (ROS production), inflammatory response, and macrophage cell surface expression by using human THP-1 monocyte-derived macrophage cells. MTT assay showed a significant decrease in cell viability at high PE-MPs concentrations (500-2000 µg/mL) after 48-hour exposure, while lower PE-MPs concentrations (0.1-250 µg/mL) did not exhibit cytotoxicity compared to control. Flow cytometry assay demonstrated a significant increase ($p < 0.05$) in ROS production in THP-1 macrophages following 24 hours treatment of PE-MPs (25 µg/mL) by 1.19-fold compared to control but no change was seen after 48 hours. Macrophage functions were assessed by determining the level of pro-inflammatory cytokine production and CD86 which is a pro-inflammatory (M1) phenotype marker via ELISA and flow cytometry assays, respectively. The result showed that 50 pg/mL LPS and IFN-γ 20 ng/mL treatment increased the IL-6 level indicated macrophage activation, whereas PE-MPs themselves did not affect the level of IL-6. Notably, PE-MPs (25 µg/mL) significantly increased ($p < 0.05$) IL-6 production in the LPS and IFN-γ-activated macrophage cells. Moreover, the activated macrophages exposed to PE-MPs (0.1-25 µg/mL) exhibited slightly increased in $CD86^+$ M1 macrophage cells after 48 hours treatment when compared to the LPS and IFN-γ treatment alone. These findings suggest that PE-MPs exerted effects on macrophages partly through induced ROS production, up-regulation of pro-inflammatory phenotype marker and increased pro-inflammatory cytokines production.

Keywords: Polyethylene microplastics, THP-1 cells, macrophage cells, reactive oxygen species, pro-inflammatory cytokine, cell surface expression

Introduction:

Microplastics (MPs) are plastic particles less than 5 mm in diameter which can either be intentionally manufactured or derived from decompose of larger plastics. Polyethylene (PE) is plastic polymer that commonly used in various products including packaging materials, toiletry bottles, shopping bags, and containers (1). PE-MPs are prevalent in various environments as its use has increased tremendously. Microplastic pollutants are major health of concern due to their ability to enter organisms and potentially translocating into the circulatory system. Previous study reported that MPs were detected in human biological specimens including feces, sputum, saliva, blood, bronchoalveolar lavage fluid, placenta, and other organs suggesting systemic distribution (2). Despite growing concerns about MPs' adverse effects on human health, their impact on the immune system remains unclear. Since macrophages play a role as modulator

and effector cells of the innate immune system that gives prompt immune response. Therefore, this study aimed to investigate the potential effects of PE-MPs on human THP-1 monocyte-derived macrophage cells. The toxicities related to cell viability, ROS production, and inflammation and pro-inflammatory phenotype expression will be studied to evaluate whether PE-MPs could induce toxicity on the function and inflammatory response of macrophage cells.

Materials and methods:

Cell maintenance and culture: THP-1 cells were cultured in RPMI 1640 Medium supplemented with 1% L-glutamine, 1% penicillin/streptomycin, 1% Sodium pyruvate solution, 10% Fetal Bovin Serum (FBS), 0.5% D-(+)-Glucose Solution, 0.05 mM β-mercaptoethanol at 37°C with 5% CO_2.

Cell differentiation and polarization: THP-1 monocytes were differentiated into macrophages using 20 ng/mL phorbol 12-myristate 13-acetate (PMA) for 72 hours, followed by 48 hours in complete RPMI 1640 Medium. Macrophages were either used for experiments or polarized into M1 phenotype by incubating with 50 pg/mL *E. coli* lipopolysaccharide (LPS) and 20 ng/mL interferon gamma (IFN-γ) at 37 °C and 5% CO_2.

Cell viability determination: cells were treated with PE-MPs diameter sizes 740-4990 nm (0.1 to 2000 µg/mL) in RPMI 1640 Medium for 48 hours. After treatment, MTT solution was added for 4 hours , and absorbance was measured at 570 nm using microplate reader.

Intracellular ROS determination: cells were treated with PE-MPs (0.01 to 25 µg/mL) for 24 and 48 hours. Positive control cells were treated with 100 mM H_2O_2 for 15 minutes. DCFH-DA was added 30 minutes before the end of treatment, and fluorescence intensity was measured using flow cytometry.

Cytokine production determination: cells were differentiated and induced into M1 phenotype then treated with PE-MPs (0.01 to 25 µg/mL) for 48 hours. Levels of IL-6 in cell supernatants were quantified using ELISA kit according to the manufacturer's protocol.

Macrophage cell surface marker determination: cells were differentiated and induced into M1 phenotype then treated with PE-MPs (0.01 to 25 µg/mL) for 48 hours. After exposure, cells were washed and stained with PE anti-human CD86 antibody. CD86 expression was measured using flow cytometry.

Statistical analysis: The results were expressed as mean ± SEM. Statistical significance was determined using GraphPad Prism version 8.0.1 software, with a significance level less than 0.05 considered significant.

Results and discussion:

The results from MTT assay revealed that treatment with 500, 1000, and 2000 µg/mL PE-MPs significantly decreased cell viability to 90.75%. ($p < 0.05$), 88.52% ($p < 0.01$), and 86.52% ($p < 0.001$) relative to control, respectively. Conversely, no significant cytotoxicity was observed at PE-MPs concentrations ranging from 0.1 to 250 µg/mL. The non-cytotoxic concentrations (0.1-25 µg/mL) that cover the PE-MPs level found in human blood (7.1 µg/mL) and PE levels from drinking water treatment (10-40 µg/mL) (3,4) were chosen for further study.

The level of intracellular ROS production in THP-1 macrophage cells was quantified using the DCFH-DA assay after PE-MPs (0.1-25 µg/mL) treatment for 24 and 48 hours. The result showed that PE-MPs treatment slightly increased ROS production after 24-hours of exposure when compared to the control (Figure 1). A significant increase in ROS production was observed at 25 µg/mL treatment by 1.19-fold ($p < 0.05$) relative to the control, suggesting PE-MPs effected on intracellular ROS production. No effect on ROS level was observed after 48 hours of exposure to PE-MPs, indicated that ROS stayed increase during 24 hour-exposure time frame.

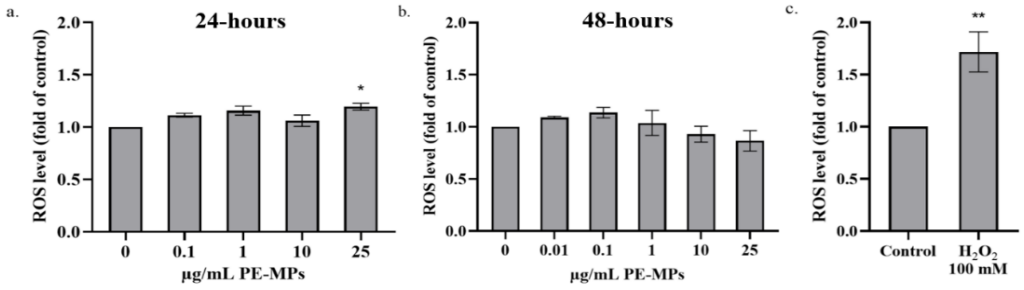

Figure 1 The effects of PE-MPs on the ROS level in THP-1 macrophage cells. Cells were treated with different concentrations of PE-MPs (0.1, 1, 10, and 25 µg/mL) for 24 hours (a) or PE-MPs (0.01, 0.1, 1, 10, and 25 µg/mL for 48 hours (b). Cells treated with 100 µM H_2O_2 for 48 hours served as the positive control (c). The data are expressed as mean ± SEM; *p < 0.05 and **p < 0.01, represent statistically significant differences compared to the control group at the respective treatment times, n = 4-5.

To assess whether PE-MPs affect pro-inflammatory cytokine (IL-6) production, THP-1 macrophages were activated into M1 phenotype by treating with 50 pg/mL LPS and IFN-γ 20 ng/mL. Immediately after activation, cells were exposed to various concentrations of the PE-MPs (0.01-25 µg/mL) for 48 hours.

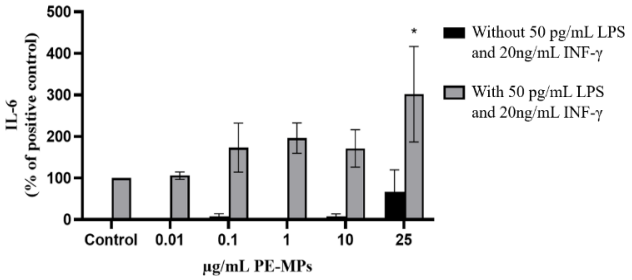

Figure 2: The effect of PE-MPs on the IL-6 levels in THP-1 macrophage cells. Cells were activated with 50 pg/mL LPS and 20 ng/mL IFN-γ with or without PE-MPs (0.01, 0.1, 1, 10, and 25 µg/mL) co-treatment for 48 hours. Cells treated only 50 pg/mL LPS and 20 ng/mL IFN-γ served as positive control. The data are expressed as mean ± SEM; *p < 0.05 represent significant differences compared to control, n = 3.

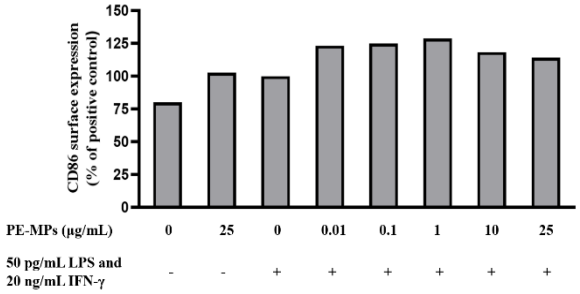

Figure 3: The effect of PE-MPs on $CD86^+$ cell surface marker expression in THP-1 macrophage cells. Cells were activated with 50 pg/mL LPS and 20 ng/mL IFN-γ and co-treated with PE-MPs (0.01, 0.1, 1, 10, and 25 µg/mL) for 48 hours. Cells treated with only 50 pg/mL LPS and 20 ng/mL IFN-γ for 48 hours served as positive control, n = 2.

The level of IL-6 was determined by an ELISA assay. The results showed that PE-MPs treatment alone (0.01-25 µg/mL) did not affect IL-6 level similar to the unstimulated cells (Figure 2). Conversely, in the positive group, LPS and IFN-γ treatment increased the IL-6 level when compared to the control group, indicating macrophage cell activation. The result showed that

PE-MPs treatment at 25 µg/mL significantly increased ($p < 0.05$) IL-6 production from the activated macrophage cells compared to the positive control that treated only LPS and IFN-γ. These results suggested that PE-MPs could induce inflammatory response in THP-1 macrophage-activated cells. PE-MPs by themselves did not affect cytokine production.

It has been known that M1 macrophages are highly express CD86 (5). To assess whether PE-MPs affected cell surface marker expression, the THP-1 macrophages were activated with 50 pg/mL LPS and IFN-γ 20 ng/mL and simultaneously treated with PE-MPs (0.1-25 µg/mL) for 48-hour. Cells were stained with PE anti-human CD86 surface expression. The results showed that PE-MPs (0.1-25 µg/mL) could slightly increase $CD86^+$ M1 macrophage cells when compared to the positive control cells (Figure 3), indicating PE-MPs could induce M1 macrophage polarization in THP-1 macrophage-activated cells.

Conclusion:

Exposure to PE-MPs could alter the inflammatory response and macrophage functions as evidenced by inducing ROS production, increasing pro-inflammatory cytokine (IL-6) consistent with increasing M1 macrophage polarization in THP-1 macrophage-activated cells. Therefore, the overproduction of these inflammatory responses and functions following PE-MPs exposure may increase the risk of exacerbating the immune-related effects of macrophage cells.

References:

1. Horton, A. A., Walton, A., Spurgeon, D. J., Lahive, E., and Svendsen, C. Microplastics in freshwater and terrestrial environments: Evaluating the current understanding to identify the knowledge gaps and future research priorities. Sci Total Environ. 2017;586:127-141.
2. Osman, A. I., Hosny, M., Eltaweil, A. S., Omar, S., Elgarahy, A. M., Farghali, M., Yap, P. S., Wu, Y. S., Nagandran, S., Batumalaie, K., Gopinath, S. C. B., John, O. D., Sekar, M., Saikia, T., Karunanithi, P., Hatta, M. H. M., and Akinyede, K. A. Microplastic sources, formation, toxicity and remediation: a review. Environ Chem Lett. 2023;1-41.
3. Leslie HA, van Velzen MJM, Brandsma SH, Vethaak AD, Garcia-Vallejo JJ, Lamoree MH. Discovery and quantification of plastic particle pollution in human blood. Environ Int. 2022;163:107199.
4. Mao Y, Hu Z, Li H, Zheng H, Yang S, Yu W, Tang B, Yang H, He R, Guo W, Ye K, Yang A, Zhang S. Recent advances in microplastic removal from drinking water by coagulation: Removal mechanisms and influencing factors. Environ Pollut. 2024;349:123863.
5. Bertani FR, Mozetic P, Fioramonti M, Iuliani M, Ribelli G, Pantano F, Santini D, Tonini G, Trombetta M, Businaro L, Selci S, Rainer A. Classification of M1/M2-polarized human macrophages by label-free hyperspectral reflectance confocal microscopy and multivariate analysis. Sci Rep. 2017;7(1):8965.

P-14

Arsenic reduced insulin expression in differentiated neuroblastoma SH-SY5Y cells

Thitirat Luangwong[1,2], Napada Leelarprachakul[1,2], Piyajit Watcharasit[1,2,3] and Jutamaad Satayavivad[1,2,3]

[1]Laboratory of Pharmacology, Chulabhorn Research Institute, Bangkok, Thailand
[2]Environmental Toxicology program, Chulabhorn Graduate Institute, Chulabhorn Royal Academy, Bangkok, Thailand
[3] Center of Excellence on Environmental Health and Toxicology (EHT), OPS, MHESI, Thailand

Abstract:

Arsenic contamination in ground water is a well-known issue. Previously, we reported that prolonged arsenic exposure caused insulin signaling impairment in neurons. As neurons have been reported to be able to synthesize insulin similar to pancreatic β cells, thus we questioned whether arsenic altered insulin expression in neurons. Here, we examined the levels of insulin in differentiated human neuroblastoma SH-SY5Y cells by ELISA, immunofluorescent staining, and immunodot blot analysis. We found that arsenic dramatically decreased intracellular insulin levels. Additionally, level of insulin in the medium was reduced by arsenic treatment. In conclusion, arsenic may reduce production and secretion of insulin in neurons.

Keywords: Arsenic, Insulin, Neurons

Introduction:

Arsenic (As) is a metalloid toxicant widely found in natural environmental compartments. Due to its ubiquitous presence at high level, World Health Organization (WHO) estimated over 200 million people are exposed to arsenic through the consumption of contaminated water exceeding the safety standards set by WHO (1). Arsenic can interfere with insulin signaling pathways, impair glucose uptake by cells, and contribute to inflammation and oxidative stress, all of which can lead to insulin resistance (2). Previously, we reported that prolonged exposure to arsenic led to insulin signaling impairment in neurons (3, 4). Interestingly, insulin synthesis has been observed in neurons (5). Because alteration of insulin expression was found associated with insulin resistance condition (6). Recently, our laboratory demonstrated that arsenic disrupted neuronal insulin signaling without altering levels of insulin receptor (3). Therefore, we hypothesized that arsenic may induce insulin signaling impairment in neurons by alteration of insulin expression.

Methodology:

Cell culture and treatment: Human neuroblastoma SHSY5Y cells were cultured in a complete medium composed of mixture of 1:1 minimum essential medium (MEM) and Ham's F-12 medium, 10% fetal bovine serum (FBS), 100 U/mL penicillin, 100 U/mL streptomycin, and 2 mM L-glutamine. Cells were maintained at 37ºC in 5% CO_2 humidified incubator. For differentiation, cells were cultured with differentiation medium containing of 1:1 MEM and Ham's F-12 medium, 1% FBS, 100 U/mL penicillin, 100 U/mL streptomycin, 2 mM L-glutamine, and 10 µM retinoic acid for 3 days before treatment. For treatment, cells were treated with 1, 5, and 10 µM $NaAsO_2$ for indicated time. Cells were fed with fresh differentiation medium with or without $NaAsO_2$ every other day.

Insulin Enzyme Linked Immunosorbent Assay (ELISA): At the end of treatment, whole cell lysates, representing intracellular level of insulin, was harvested. quantity of insulin was measured using the insulin human ELISA kit (ab100578, Abcam, UK) as instructed by the manufacturer.

Immunofluorescent staining: At the end of treatment, cells were fixed with 4% paraformaldehyde. Following fixation, cells were permeabilized with 0.1% Triton X 100 and subsequently blocked with 5% bovine serum albumin. Thereafter, cells were incubated with insulin and N-cadherin antibodies (both at 1:100), followed by incubation secondary antibodies, and Hoechst. Finally, cells were photographed using confocal fluorescent microscope.

Immunodot blot analysis: At the end of the experiment, cultured medium was collected. Subsequently, 200 µL of cultured medium was dotted onto a nitrocellulose membrane. The membrane was immunoblotted with insulin antibody (CST #4590, Cell signaling technology, USA) as primary antibody, followed by rabbit antibody as secondary antibody. Visualization of the blotted membrane was achieved using ECL and the Chemidoc™ Touch Image System with Lab™ Touch Software (Bio-Rad, USA).

Results and Discussion:

Arsenic decreased insulin levels in differentiated SH-SY5Y cells

To investigate effect of arsenic on levels of insulin, differentiated SH-SY5Y cells were treated with $NaAsO_2$ at 1, 5 or 10 µM for 3 days, or at 5 µM for 1, 3, or 5 days, and insulin level was determined by ELISA kit. The results showed that after 3 days of 1, 5, or 10 µM $NaAsO_2$ treatment, levels of insulin decreased with increasing arsenic concentration (Fig. 1A). This result indicated that arsenic dose dependently decreased insulin levels in whole cell lysate. Additionally, the result showed that insulin level equally decreased at both 1 and 3 days, and dramatically decreased at 5 days after treatment with 5 µM $NaAsO_2$ (Fig. 1B), indicating that arsenic decreased insulin levels in whole cell lysate, with a notable decrease after 5 days of treatment. Because insulin can be synthesized by neurons (5), and arsenic has been shown to cause insulin signaling impairment (3) therefore, it is reasonable to conclude that arsenic exposure may decrease insulin production in neuronal cells.

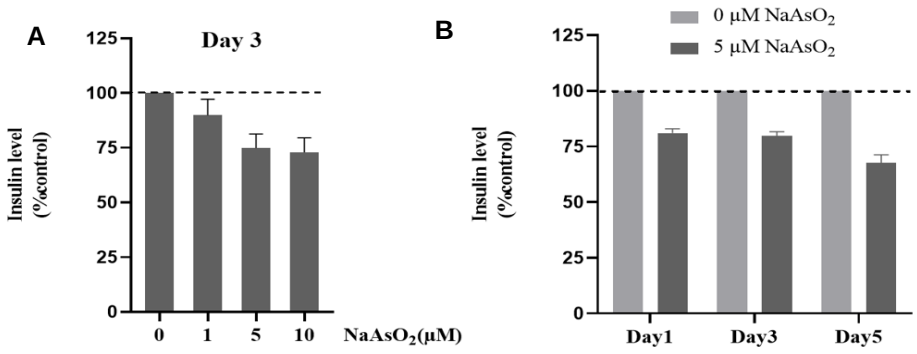

Figure 1 Arsenic decreased insulin levels in differentiated SH-SY5Y cells.

Differentiated SH-SY5Y cells were treated with $NaAsO_2$ at 1, 5 or 10 µM for 3 days (A) or at 5 µM for 1, 3 or 5 days (B). Insulin level in whole cell lysate was measured using insulin ELISA kit. The results were calculated as % control.

Arsenic decreased insulin expression

To confirm the decrease in intracellular insulin level by arsenic, we examined insulin expression after arsenic treatment in differentiated SH-SY5Y cells using immunofluorescent staining. The cells were treated with or without 5 µM $NaAsO_2$ for 3 days, and stained with insulin (green), N-cadherin (red, a membrane marker) and, Hoechst (blue). The results from immunofluorescent staining support the findings of the ELISA assay, confirming a reduction in insulin levels following treatment with 5 µM $NaAsO_2$ (Fig. 2).

Arsenic decrease insulin secretion

We next investigated whether arsenic affected insulin secretion in differentiated SH-SY5Y cells. The cells were treated with or without 1, 5 or 10 µM $NaAsO_2$ for 3 days, and medium was collected for insulin determination using immunodot blot analysis. The result showed that the levels of insulin in the medium slightly decreased at 1 µM $NaAsO_2$ and dramatically decreased at 5 and 10 µM $NaAsO_2$ (Fig. 3). These results showed that arsenic reduced levels of insulin the medium in a concentration-dependently manner. Therefore, it is possible that arsenic reduces insulin secretion. However, the mechanisms underlying this reduction remains unclear.

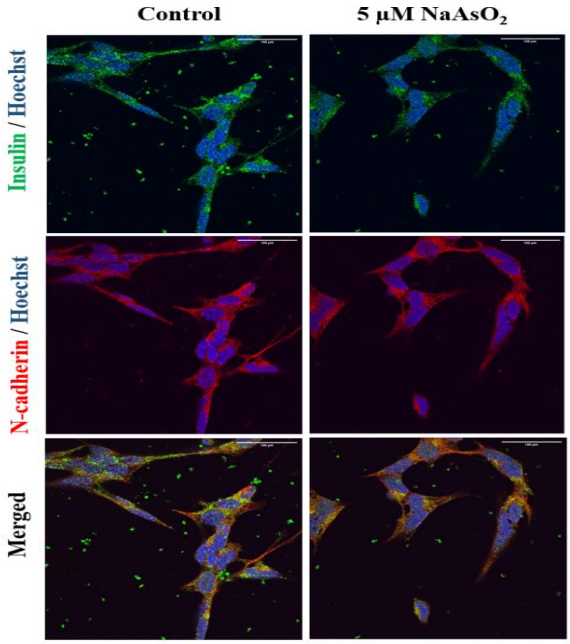

Figure 2 Arsenic decreased insulin expression.
Differentiated SH-SY5Y were treated with or without 5 µM $NaAsO_2$ for 3 days. Cells were stained with insulin (green) and N-cadherin (red) antibodies, and counterstained with Hoechst (blue). Images were taken by confocal microscope at 100x magnification.

Conclusion:

Collectively, this study demonstrates that arsenic exposure may lead to reductions of insulin production and secretion in neuronal cells.

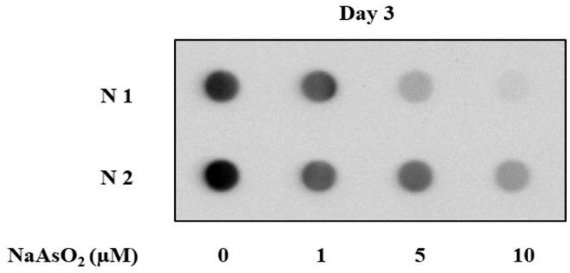

Figure 3 Arsenic decreased insulin secretion.

Differentiated SH-SY5Y cells were treated with NaAsO2 at 1, 5 or 10 µM for 3 days. Level of insulin in the medium was determined by immunodot blot analysis.

References:

1. Naujokas Marisa F, Anderson B, Ahsan H, Aposhian HV, Graziano Joseph H, Thompson C, et al. The Broad Scope of Health Effects from Chronic Arsenic Exposure: Update on a Worldwide Public Health Problem. Environmental Health Perspectives. 2013;121(3):295-302.
2. Javaid A, Akbar I, Javed H, Khan U, Iftikhar H, Zahra D, et al. Role of Heavy Metals in Diabetes: Mechanisms and Treatment Strategies. Critical Reviews in Eukaryotic Gene Expression. 2021;31(3):65-80.
3. Wisessaowapak C, Watcharasit P, Satayavivad J. Arsenic disrupts neuronal insulin signaling through increasing free PI3K-p85 and decreasing PI3K activity. Toxicology Letters. 2021;349:40-50.
4. Niyomchan A, Visitnonthachai D, Suntararuks S, Ngamsiri P, Watcharasit P, Satayavivad J. Arsenic impairs insulin signaling in differentiated neuroblastoma SH-SY5Y cells. Neurotoxicology. 2018;66:22-31.
5. Kuwabara T, Kagalwala MN, Onuma Y, Ito Y, Warashina M, Terashima K, et al. Insulin biosynthesis in neuronal progenitors derived from adult hippocampus and the olfactory bulb. EMBO Molecular Medicine. 2011;3(12):742-54.
6. Samuel VT, Shulman GI. The pathogenesis of insulin resistance: integrating signaling pathways and substrate flux. Journal of Clinical Investigation. 2016;126(1):12-22.

P-15

Effect of arsenic on stem cell aging and its impact on the differentiation to hematopoietic stem cells

Tanasub Sakultanasub[1], Thitirat Ngaotepprutaram[2], Panida Navasumrit[2,3] and Mathuros Ruchirawat[2,3]

[1]Environmental Toxicology Program, Chulabhorn Graduate Institute, Bangkok, Thailand 10210
[2]Environmental Toxicology Laboratory, Chulabhorn Research Institute, Bangkok, Thailand, 10210
[3]Center of Excellence on Environmental Health and Toxicology (EHT), OPS, MHESI,Thailand, 10210

Abstract:

Arsenic contamination in groundwater poses a significant public health concern, with over 300 million individuals exposed to levels exceeding the WHO recommendations of 10 µg/L. Arsenic can readily cross the placental barrier resulting in not only the adverse pregnancy outcomes, but also increasing the risk of disease development in both childhood (higher risk of acute respiratory infections in children) and adult life (higher risk of developing cardiovascular and metabolic diseases) in populations exposed to arsenic since *in utero*. Apart from induction of oxidative stress as a main mechanism involved in arsenic toxicity, accumulating evidences revealed that arsenic exposure can promote cellular senescence in various cell types including stem cells with potential disrupting stem cell function and organ development. Furthermore, several studies underscore the impact of early–life insults on the development of fetal immune system, which can permanently alter the immune function of the offsprings leading to long–term unfavorable health outcomes. This study aimed to explore whether chronic exposure to arsenic induces cellular senescence and its effects on the development of human hematopoiesis using an *in vitro* differentiation model. Treatment with 1 µM $NaAsO_2$ resulted in an increased activity of β–galactosidase, a commonly used biomarker of cellular senescence, in human iPSCs and an impairment of their hematopoietic differentiation potential as evidenced by decreasing the number of hematopoietic stem cells (HSCs). In summary, this study provides more understanding on the potential detrimental effects of arsenic exposure on stem cell function, which may permanently alter the immune function of the offspring.

Keywords: Arsenic, Cellular senescence, Human induced pluripotent stem cells, Hematopoietic differentiation, Hematopoietic stem cells.

Introduction:

Arsenic is one of environmental contaminants known as a transplacental toxicant which can penetrate the placental barrier, potentially targeting fetal stem cells during gestation (1). Exposure to arsenic during this critical organogenesis period with rapid proliferative growth and cell differentiation may increase the risk of developing several diseases later in life (2). Prenatal exposure to arsenic has been linked to the development of various diseases through multiple mechanisms such as oxidative stress, inflammation–induced DNA damage, and alterations in gene expression. Recent evidence suggests that arsenic exposure induces cellular senescence in various cell types including stem cells (3). Thus, prolonged *in utero* exposure to arsenic may disrupt the function of stem cells, which play pivotal roles in embryonic development.

Hematopoiesis refers to a process for generating all blood cell types, both erythrocytes and leukocytes, which were derived from the progenitor cells known as hematopoietic stem cells (HSCs). The immune system relies on the proper function of leukocytes. Thus, disruptions in the generation and/or function of HSCs would compromise the proper function of the immune system, potentially leading to the increased risk of both infectious and non-communicable diseases (4).

In addition, several studies has been demonstrated that arsenic inhibits stem cell differentiation into several essential organs such as neurons, skeletal myotubes, cardiomyocytes, and hepatocytes (5-8). However, there hasn't been as much exploration of its effect on the generation of HSCs and their lineages. Here, we aimed to investigate the effect of chronic exposure to arsenic on the induction of premature stem cell aging and its effects on the development of human hematopoiesis using human iPSCs as a surrogate of fetal stem cells.

Objectives:

1. To evaluate whether arsenic exposure induces premature cellular aging of human iPSCs
2. To assess the HSCs differentiation potential of the senescent human iPSCs induced by arsenic exposure

Methodology:

1. Cell culture and treatment

Human iPSCs (ACS, 1030) were obtained from ATCC, USA. Cells were maintained in pre-coated cell culture vessels as indicated with a 1:50 dilution of Matrigel® (Corning®, USA). Cells were cultured as colonies in mTeSR™ medium (STEMCELL Technologies, Canada) at 37°C with 5% CO_2. The medium was changed daily. Cell passaging was performed when iPSC colonies reached approximately 80% confluence or a diameter larger than 300 µm using an enzyme–free dissociation reagent (ReLeSR™, STEMCELL Technologies) by seeding of small aggregates (50–100 µm) in pre–coated cell culture vessels as indicated. For experimental treatments, iPSCs were treated with various concentrations of $NaAsO_2$ (0.1, 0.5, and 1 µM) as indicated.

2. HSCs population identification by flow cytometry

The expression of specific HSCs markers was assessed by flow cytometry to enumerate the number of HSCs. At day 12 of hematopoietic differentiation, cells were harvested and stained with LIVE/DEAD™ Fixable Near-IR Dead Cell Stain Kit (Thermo Fisher Scientific, USA), anti–human CD34 FITC–conjugated antibody (Immunotools, Germany), anti–human CD43 APC–conjugated antibody (Immunotools), and anti– human CD45 PE– conjugated antibody (Immunotools) according to the manufacturer's protocol. The stained cells were subsequently analyzed using a CytoFLEX flow cytometer from Beckman Coulter, USA.

3. β–galactosidase analysis by flow cytometry

The senescence–associated β–galactosidase activity was determined by using the CellEvent™ Senescence Green Detection Kit (Invitrogen, USA) according to the manufacturer's protocol. The stained cells were subsequently analyzed using an automated microscope (LionHeart, BioTek, USA).

4. Real–Time Quantitative Reverse Transcription PCR (qRT–PCR)

A total of 1000 ng of RNA was subjected to reverse transcription to generate cDNA using the High–Capacity cDNA Reverse Transcription kit from Applied Biosystems, USA. qRT–PCR was performed utilizing the KAPA SYBR® FAST qPCR Master Mix (2X) Kit on a QuantStudio3 Real–Time PCR System. The relative expression level of pluripotency genes (*OCT4*, *SOX2* and *NANOG*), senescence–associated genes (*p16INK4A*, *p21CIP1*, and *GLB1*) and senescence associated secretory phenotype (SASP)–related genes (*CCL2* and *IL-8*) to the expression level of reference gene (*PPIA*) was calculated using the $2^{-\Delta\Delta Ct}$ method.

Results and Discussion:

1. Effect of $NaAsO_2$ treatment on the induction of cellular senescence in human iPSCs

Human iPSCs were treated with different concentration of $NaAsO_2$ (0.1, 0.5, and 1 µM) at various time points. In comparison to the control (untreated group), time–course treatment with 1 µM $NaAsO_2$ showed growth inhibition as observed by less number of cells since day 4. The activation of β– galactosidase, a hallmark of senescence, was determined by using fluorescent probe on day 4 after treatment with $NaAsO_2$. The image analysis showed the increase of mean fluorescence intensity (MFI), which corresponds to the activation of β– galactosidase, in 1 µM $NaAsO_2$ treatment group compared to that observed in the control. Furthermore, the expression of genes related to pluripotency (*OCT4*, *SOX2* and *NANOG*), senescence–associated genes (*p16INK4A*, *p21CIP1*, and *GLB1*) and SASP (*CCL2* and *IL-8)* were determined by qRT–PCR. Although no alteration in the expression of studied genes was observed among treatment groups, a decreased expression of *SOX2* was observed in 1 µM $NaAsO_2$ treatment group compared to that found in the control. These results suggested that arsenic exposure induced premature cellular aging in human iPSCs without altering the expression of studied genes involved in cellular senescence. However, this premature cellular aging induced by arsenic exposure may decrease the pluripotency of human iPSCs.

2. Effect of $NaAsO_2$ treatment on the hematopoietic differentiation of human iPSCs

To investigate the impact of $NaAsO_2$ on the hematopoietic differentiation process, human iPSCs were pre–treated with different concentrations of $NaAsO_2$ for 4 days prior subjecting to the induction of hematopoietic differentiation. A decreased number of $CD34^+CD43^+$ $CD45^+$ cells were observed in cells treated with $NaAsO_2$ in a concentration–dependent compared to those observed in the untreated cells (control). Therefore, this data suggested that treatment with $NaAsO_2$ impaired hematopoietic differentiation of iPSCs.

Conclusion:

Collectively, these findings demonstrated that arsenic exposure induced premature cellular aging in human iPSCs and impaired the differentiation ability of iPSCs into HSCs. The impairment of HSCs generation would further compromise long– term immune system maintenance and function in the offspring.

References:

1. Tokar EJ, Person RJ, Sun Y, Perantoni AO, Waalkes MP. Chronic Exposure of Renal Stem Cells to Inorganic Arsenic Induces a Cancer Phenotype. Chemical Research in Toxicology. 2013;26(1):96-105.
2. Tokar EJ, Qu W, Waalkes MP. Arsenic, Stem Cells, and the Developmental Basis of Adult Cancer. Toxicological Sciences. 2010;120(suppl_1):S192-S203.
3. Cheng H, Qiu L, Zhang H, Cheng M, Li W, Zhao X, et al. Arsenic trioxide promotes senescence and regulates the balance of adipogenic and osteogenic differentiation in human mesenchymal stem cells. Acta Biochim Biophys Sin (Shanghai). 2011;43(3):204-9.
4. Dong Y, Lian X, Xu Y, Hu H, Chang C, Zhang H, et al. Hematopoietic stem/progenitor cell senescence is associated with altered expression profiles of cellular memory-involved gene. Bioscience Reports. 2018;38(1).
5. Rebuzzini P, Cebral E, Fassina L, Alberto Redi C, Zuccotti M, Garagna S. Arsenic trioxide alters the differentiation of mouse embryonic stem cell into cardiomyocytes. Scientific Reports. 2015;5(1):14993.

6. Kantisin S, Chaisatra K, Hunsonti P, Parnlob V, Navasumrit P, Ruchirawat M. In utero arsenic exposure increases DNA damage and gene expression changes in umbilical cord mesenchymal stem cells (UC-MSCs) from newborns as well as in UC-MSC differentiated hepatocytes. Toxicol Rep. 2022;9:1728-41.
7. Bain LJ, Liu J-T, League RE. Arsenic inhibits stem cell differentiation by altering the interplay between the Wnt3a and Notch signaling pathways. Toxicology Reports. 2016;3:405-13.
8. Perego MC, McMichael BD, McMurry NR, Ventrello SW, Bain LJ. Arsenic Impairs Differentiation of Human Induced Pluripotent Stem Cells into Cholinergic Motor Neurons. Toxics. 2023;11(8):644.

P-16

Effects of a novel estrogenic endocrine disruptor on breast cancer promotion and progression: the mechanistic insights from *in vitro* studies

Sornsawan Duangta[1], Phum Tachachartvanich[2], Panida Navasumrit[2,3], and Mathuros Ruchirawat[2,3]

[1]Environmental Toxicology Program, Chulabhorn Graduate Institute, Bangkok, Thailand, 10210
[2]Environmental Toxicology Laboratory, Chulabhorn Research Institute, Bangkok, Thailand, 10210
[3]Center of Excellence on Environmental Health and Toxicology (EHT) OPS, Thailand, 10210

Abstract:

Breast cancer is a malignant tumor and the second leading cause of cancer death among women globally. The estrogen receptor (ER) has been shown to regulate the promotion and development of ER+ breast cancer. Several lines of evidence indicated that exposure to estrogenic environmental chemicals is strongly associated with breast cancer incidence. Herein, we investigated the effects of an environmentally ubiquitous estrogenic flame- retardant 2-ethylhexyl diphenyl phosphate (EHDPP) on breast cancer promotion and development using two human breast cancer cell lines namely MCF-7 (ER+) and MDA-MB-231 (ER–). Cells were exposed to EHDPP at biologically relevant concentrations found in humans ranging from 0.1–10 µM. Interestingly, EHDPP significantly increased the cell viability and clonogenicity of MCF-7 (ER+) in a dose- and time-dependent manner, while a slight reduction in cell viability and clonogenicity was observed in the MDA-MB-231 (ER–) cells. Furthermore, a co-treatment with ICI 182, 780, a competitive ER inhibitor, significantly suppressed the EHDPP-induced breast cancer promotion, suggesting the effects of EHDPP were mediated through the activation of the ER signaling pathway. Additionally, the protein expression of ERs and anti-apoptotic protein (Bcl-2) were significantly increased. The mRNA expression of genes related to estrogenic activity (*ESR1*, *PGR*, *BRCA1*, and *pS2*) and proliferation (*KI67* and *MYC*) further supported that EHDPP is an estrogenic compound and promotes ER+ breast cancer development. Our result indicates that EHDPP may pose a significant human health risk associated with estrogenic endocrine disruption such as the development of ER+ breast cancer.

Keywords: Breast cancer, Estrogen receptor, Flame retardant, Endocrine disruptor

Introduction:

Breast cancer is one of the most malignant tumors that affects women worldwide. The increasing incidence and prevalence of breast cancer can be attributable to a wide array of disease risk factors, originating from both internal and external origins. The majority of breast cancer cases exhibit high expression of ERs which can be activated upon the binding by both endogenous and exogenous estrogenic chemicals.

EHDPP is an organophosphate flame retardant and is widely used as a plasticizer. EHDPP has been reported to alter sex hormones *in vivo* and is predicted to have a binding affinity towards ERs *in silico* (Rosenmai et al., 2021). However, the study on EHDPP-inducing breast cancer promotion and development has yet to be examined. Therefore, the ER-dependent action of EHDPP on breast cancer promotion and development was investigated using two breast cancer cell lines namely MCF-7 (ER+) and MDA-MB-231 (ER–).

Methodology:

Cell line and cell culture

Two breast cancer cell lines were used in the study: estrogen receptor-positive (MCF-7) and triple-negative (MDA-MB-231) breast cancer. Both were cultured following the manufacturer's instructions.

Cell viability assay

The viability of breast cancer cells was assessed using a colorimetric MTT assay. Cells were seeded in 96-well plates and treated with DMSO: vehicle control, 17β-estradiol (E2): positive control, ICI 182,780: an ER inhibitor, and EHDPP at concentrations ranging from 0.1 to 10 µM for 3, 6, and 9 days.

Colony formation assay

The capability of single cells forming large colonies induced by EHDPP was evaluated. In a 6-well plate, cells were seeded at low density, treated with EHDPP at various concentrations for 5–8 days, and fixed with 4% v/v formaldehyde.

Immunoblotting

The mechanism underlying breast cancer development induced by EHDPP was investigated through the expression of proteins. Protein samples obtained from EHDPP-treated MCF-7 (ER+) were subjected to gel electrophoresis, probed with specific primary and secondary antibodies, and visualized, respectively.

Gene expression assay

The total RNA of EHDPP-treated MCF-7 was extracted and converted into cDNA. The expression of genes relevant to ER and cell proliferation was assessed using RT-qPCR.

Result and discussion:

Estrogen receptor-dependent proliferative effect on human breast cancer cells

The result revealed that MDA-MB-231 as an ER– model showed a slight reduction in viability **(Figure 1A)**. On the other hand, EHDPP-treated MCF-7 at 3 different time points increased cell viability in a dose and time-dependent manner, corresponding to the responses exerted by E2 as an ER activator **(Figure 1B)**. Interstingly, cells co-treated between EHDPP and ICI 182, 780 exhibited a reduction in cell viability compared with EHDPP alone, indicating that EHDPP induces cell proliferation dependent on ER.

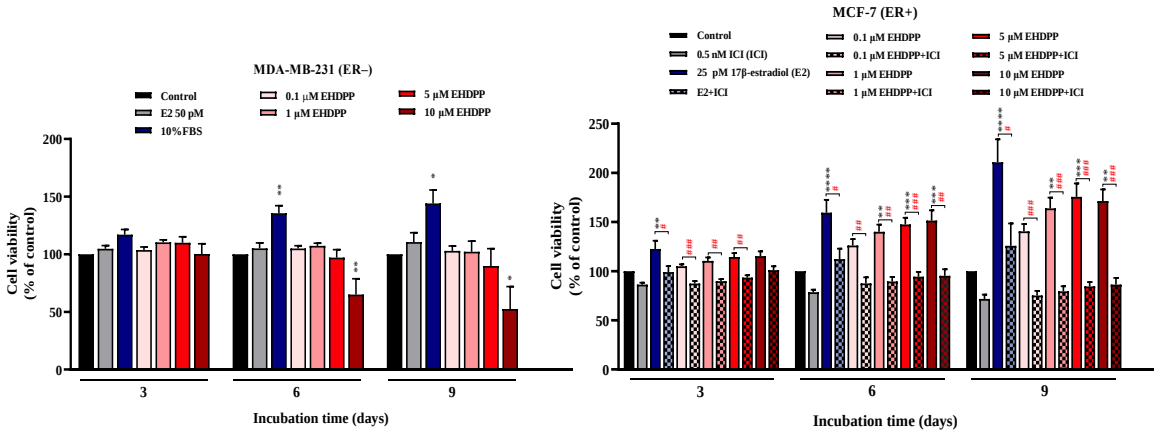

Figure 1 Cell viability of EHDPP-treated human breast cancer cell lines (A) MDA-MB-231 and (B) MCF-7 at various concentrations for 3, 6, and 9 days.

Induction of colony formation in human breast cancer cells

The result illustrated that EHDPP at 0.1, 1, 5 µM significantly induced clonal expansion of MCF-7 **(Figures 2A and 2B)**. However, ICI co-treatment exerted a significant decrease in clonogenic response. Similarly, EHDPP-treated MDA-MB-231 at 0.1 to 10 µM showed a reduction in clonogenicity **(Figures 2C and 2D)**.

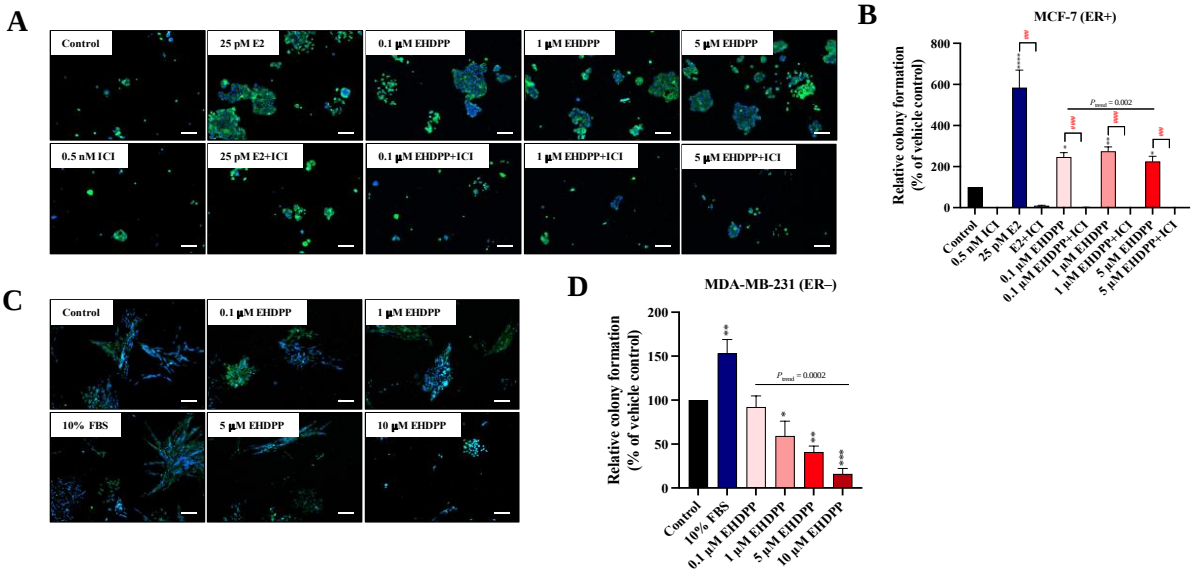

Figure 2 Clonogenic effect of EHDPP on (A–B) MCF-7 and (C–D) MDA-MB-231 cells. (A, C) Representative images of MCF-7 and MDA-MB-231 colonies stained with DAPI (nuclei) and Alexa Flour 488 phalloidin (actin) at 100×; scale bar: 200 µm. (B, D) Bar graphs show the percentage in the colony number of control and treatment groups compared to the control.

Expression of proteins associated with breast cancer development

While the expression of ERα significantly increased in EHDPP treatment and significantly inhibited when co-treated with ICI indicating the inducibility of EHDPP towards ERα, there were no significant changes in ERβ expression **(Figures 3A–3C)**. Moreover, EHDPP at 1 and 5 µM significantly increased the expression of Bcl-2, an anti-apoptotic protein **(Figures 3A and 3D)**.

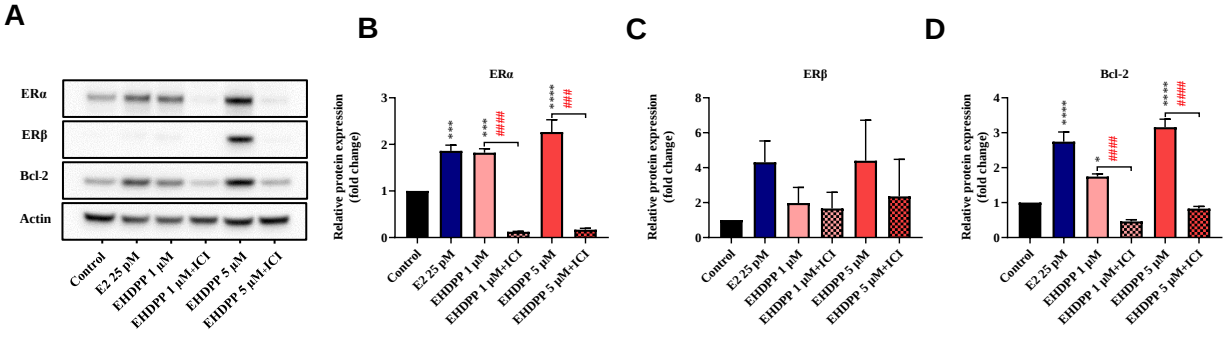

Figure 3 The effect of EHDPP on the expression of breast cancer-associated proteins as revealed in (A) the Western blot analysis. The bar graphs represent the fold change of (B) ERα, (C) ERβ, and (D) Bcl-2 protein expression in EHDPP-treated MCF-7 cells compared to the control.

Induction of breast cancer-mediated gene expression

At the transcription level, the ER+ breast cancer development relies primarily upon the ER signaling pathways, thereby, the genes associated with these pathways were investigated. As expected, EHDPP exposure increased the expression of ER responsive (*ESR1*, *pS2*, *PGR*, and *BRCA1*) **(Figures 4A–4D)** and proliferative genes (*MYC* and *KI67*) **(Figures 4E and 4F)** similar to the effect exhibited by the known ER activator, E2. ICI co-treatment showed a notable reduction in the gene expression, substantiating that EHDPP posed an estrogenic effect by upregulating ER-associated and proliferative genes promoting ER+ breast cancer development.

Among the investigated genes, the expression of gene-encoded for ERα namely *ESR1* in E2 treatment was relatively low. This can be explained by the strong potency of E2 towards ER which can eventually initiate the negative feedback regulation and reduce gene expression level, consistent with a study by Szmyd et al. (2024), that demonstrated the decrease in *ESR1* expression was observed upon E2 treatment in both ER+ breast cancer cells (T-47D and MCF-7).

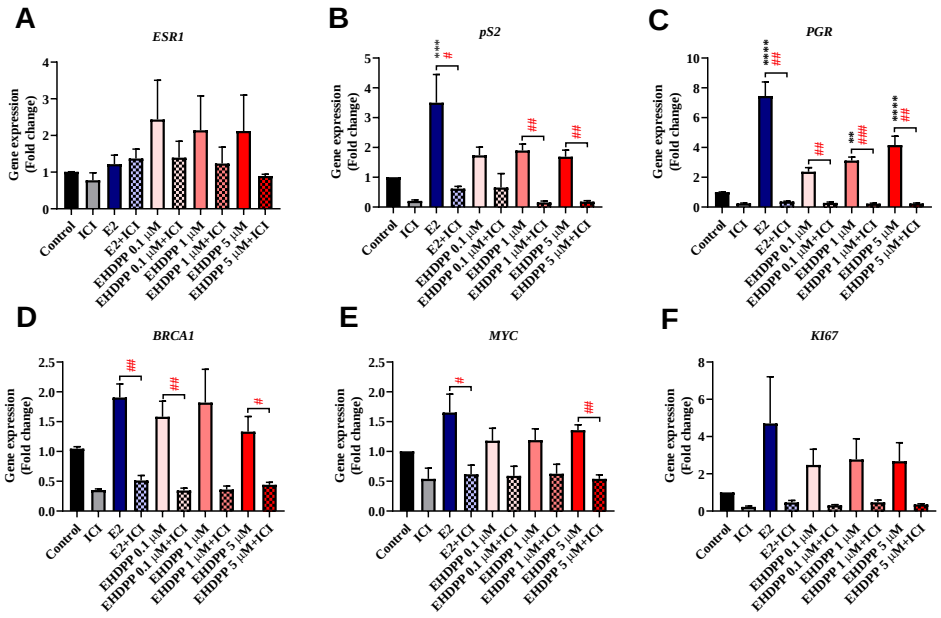

Figure 4 The expression of gene-associated (A–D) ER pathway and (E–F) proliferation.

Conclusion:

Collectively, EHDPP exerts the estrogenic effect on breast cancer dependently through the ER and ultimately induces breast cancer promotion and development.

References:

1. Rosenmai, A. K., Winge, S. B., Möller, M., Lundqvist, J., Wedebye, E. B., Nikolov, N. G., Lilith Johansson, H. K., and Vinggaard, A. M. (2021). Organophosphate ester flame retardants have antiandrogenic potential and affect other endocrine-related endpoints in vitro and in silico. Chemosphere, 263, 127703.
2. Szmyd, M., Zanib, A., Behlow, V., Hallman, E., Pfiffner, S., Yaldo, R., Prudhomme, N., Farrar, K., and Dinda, S. (2024). Modulation of Estrogen Receptor Alpha (ERα) and Tumor Suppressor Gene BRCA1 in Breast Cancer Cells by Bazedoxifene Acetate (BZA). Cancers, 16(4). Retrieved from

Food Safety and Food Contaminants

P-17

Food handlers' practices and coliform bacteria contamination in food stalls: a case study of flea markets in Prachuap Khiri Khan province, Thailand

Thapanapong Srirasitnanthiwat[1,2*], Chatchawal Singhakant[1,2], Supawadee Polprasert[1,2], Arthit Phosri[1,2], and Teerapong Lertassavakorn[1,2]

[1]Department of Environmental Health Sciences, Faculty of Public Health, Mahidol University 420/1 Rajvithi Rd., Rajchathawee, Bangkok, Thailand
[2]Center of Excellence on Environmental Health and Toxicology (EHT), OPS, MHESI, Thailand
* Corresponding author E-mail address: thapanapong.srr@student.mahidol.ac.th

Abstract:

This analytical survey study aimed to determine the association between the compliance with food sanitation principles of the food handle in food stalls and coliform bacteria contamination at flea markets in Prachuap Khiri Khan province area. The total sample of 265 food stalls from 8 flea markets were collected by randomized method. Each food stall, the food sanitation inspection forms were used to observe the food handlers' practices and the market hygiene and the SI-2 test kits were used to determine the coliform bacteria contamination in three samples of ready to eat food, kitchen utensil, and a hand of the food handler. The linear mixed model was used to investigate the association between the food handlers' practices and coliform bacteria contamination. The results showed that most of food handlers passed food sanitation practices in their food stalls (69.8%). The coliform bacteria contamination was found around half of food stalls' samples (50.2%), the majority of contamination was found on a hand of food handlers, following by contamination in ready to eat food and on kitchen utensil, respectively. There was no association between food sanitation practices and coliform bacteria contamination. However, there was an association between market hygiene and coliform bacteria contamination ($p<0.001$). Therefore, the flea market should be recommended strictly follow the laws and regulations related to market hygiene and promoted food sanitation practices in food handlers, which can help to minimize the risk from foodborne disease.

Keywords: Food handler, Flea market, Market hygiene, Food sanitation practices, Coliform bacteria

Introduction:

Food is an essential factor that can promote and contribute to good health and well-being for humans. However, if the food is unclean and contains contaminated substances, that can cause sickness and even death in people (1). Thus, people should select foods that are healthy for their health and free from hazardous substances contamination. To provide safe foods, the food seller should consider food sanitation practices that involve in management and control of several factors related to the food activities including 1) personal hygiene 2) food 3) kitchen utensils and equipment 4) food preparation, cooking, and establishment area and 5) disease-carrying pests (2). Nowadays, ready to eat food is sold in various locations, where customers can select a location and type of food as wanted. The place to buy ready to eat food could be a place with a permanent structure, such as a restaurant, structured market or it may be a place with no permanent structure, such as hawker stalls, flea markets, and night markets, where food handlers must have good food sanitation practices from food selection, storage, cooking and personal hygiene management. If the food handler is not careful or does not realize the importance of such a requirement, consumers may consume contaminated food and become ill or dead (3).

Therefore, the researcher has an interest in studying the association between food sanitation practices and the coliform bacteria contamination at food stalls in flea markets in Prachuap Khiri Khan province, Thailand. This study aims to improving and developing the regulation on the food selling in the flea market to ensure proper food sanitation surveillance encourages food handlers to pay attention and promoting awareness in food safety. Hence, consumers can purchase food with confidence and safe for their health, as well as reduce the rate of illness caused by foodborne disease.

Methodology:

This study was a cross sectional analytical survey research to study the food sanitation practices of food handlers and coliform bacteria contamination at food stalls from 8 flea markets in Prachuap Khiri Khan province, Thailand. The sample sizes of the food stall number in each market were calculated proportional and determined by Krejcie & Morgan method (4) and top up with 20% additional samples to be 249 samples in total to prevent loss and uncollectible data as shown in **Table 1.** The data were collected during June – August 2023. There were 3 tools used in this study including; 1) the inspection form for food sanitation practice in food stalls with 22 criteria that was modified from the criteria for food sanitation practice in food stalls developed by The Bureau of Food and Water Sanitation, Department of Health (5), 2) the inspection form for market hygiene practices with 12 criteria that was modified from the criteria for flea market sanitation developed by The Bureau of Food and Water Sanitation, Department of Health (6), and 3) the simple coliform bacteria contamination test kit (SI-2) to determine the contamination in 3 samples from each stall including ready to eat food, kitchen utensil, and a hand of the food handler. The association between the food handlers' food sanitation practices and coliform bacteria contamination at food stalls was determined by using generalized linear mixed model (GLMM) as the details in **Table 2**.

Table 1 Sample sizes of the food stalls from each flea market

Markets	Total population	Calculated samples	Sample sizes
Market A	15	6.9	8
Market B	21	9.7	12
Market C	38	17.5	21
Market D	25	11.5	14
Market E	56	25.8	31
Market F	54	24.8	30
Market G	187	86.0	103
Market H	55	25.3	30
Total	**451**	**207.5**	**249**

Table 2 The GLMM model for association testing among food sanitation practices, market hygiene, and coliform bacteria contamination

Model	Description
Generalized linear mixed model: C ~ P + MH + (1 | M)	C = Coliform bacteria contamination in the food stall P = Food sanitation practices in the food stall MH = Market hygiene practices M = Markets

Results and discussion:

Data were analyzed regarding food sanitation at food stalls in flea markets **(Table 3)**. The criteria for interpretation of food sanitation practices divided into 2 categories: pass (total score 80% and above) and fail (total score lower than 80 %). The result found that most food stalls with total of 185 stalls (69.8%) was assessed pass the food sanitation criteria. The criteria that can practices most correctly were the food stall was at least 60 cm. above the floor accounting for 264 stalls (99.6%) and food handlers wore clean clothes with sleeves accounting for 259 stalls (97.7%), respectively. While 80 stalls (30.2%) failed in some criteria such as the food stall do not have a solid waste container with a lid or coverings to prevent contamination into food (262 stalls, 98.9%), food handlers did not wear hair coverings and put on a suitable and clean apron (242 stalls, 91.3%) and ready to eat foods did not cover for preventing external contamination (185 stalls, 69.8%), respectively. Similar results were reported by Preongtook (2011) which found 39.4% of all the food stall samples in Ban Sang district, Prachinburi province failed the food sanitation criteria such as food must stored in clean and covered container with a total of 16 stalls (57.1%) (7) and Srisai and Yasaka (2016) studied situation of food sanitation in the area around Naresuan University found that most of food stalls failed in food sanitation criteria (87 stalls, 98.9%) including food handlers did not wear a clean apron and hair covering (71 stalls, 80.7%) and waste disposal did not follow sanitary practices (69 stalls, 78.4%), respectively (8).

Table 3 Result of the food sanitation survey at food stalls at flea markets

Markets	No. of sampling food stalls	Food sanitation practices criteria[1]		Coliform bacteria contamination (%)	Market hygiene survey[2]
		No. of Passed stall (%)	No. of Failed stall (%)		
Market A	8	3 (37.5%)	5 (62.5%)	3 (37.5%)	Failed
Market B	12	7 (58.3%)	5 (41.7%)	6 (50.0%)	Failed
Market C	21	14 (66.7%)	7 (33.3%)	12 (57.1%)	Failed
Market D	15	8 (53.3%)	7 (46.7%)	9 (60.0%)	Failed
Market E	33	17 (51.5%)	16 (48.5%)	18 (54.6%)	Failed
Market F	31	21 (67.7%)	10 (32.3%)	12 (38.7%)	Failed
Market G	112	82 (73.2%)	30 (26.8%)	66 (58.9%)	Failed
Market H	33	33 (100.0%)	0 (0.0%)	7 (21.2%)	Passed
Total	**265**	**185 (69.8%)**	**80 (30.2%)**	**133 (50.2%)**	

[1] Determination criteria: Pass (total score ≥ 80%) /Fail (total score < 80%)

[2] Determination criteria: Pass (passed all criteria)/ Fail (failed at least 1 criteria)

The results of coliform bacteria contamination in food stalls **(Table 3).** The coliform bacteria contamination was found in a total of 133 stalls (50.2%) which the contamination at food handlers' hand was the most contamination (80.5% of total failed stalls) following by contamination in ready to eat food (36.8% of total failed stalls) and kitchen utensils (9.0% of total failed stalls), respectively (as shown in **Table 4**), similar result with Suwannasri (2023) who studied food sanitation conditions of street food vendors in Nongbua Health Promoting Hospital, Udonthani municipality found that only 38% of the total number of food stalls that were not contaminated with coliform

bacteria and found the most contamination on hand of food handlers (15%), followed by on ready to eat food (14.7%) and kitchen utensil (14.4%), respectively (9). Another similar result, Phonthaworn (2011) who studied factors associated with food sanitation conditions of restaurants in Laksi District, Bangkok and found the most contamination on hands of food handlers (20.3%), followed by contamination on food (16.0%), and equipment or utensils (8.3%), respectively (10).

Table 4 The result of coliform bacteria contamination, classified by types of sample in contaminated stalls (n = 133)

Samples	Coliform bacteria contamination	
	Positive (+)	%
Ready to eat food	49	36.8
Kitchen utensil	12	9.0
Hand of food handler	107	80.5

The results of market hygiene survey **(Table 3)** found that most of flea markets except for market H did not pass the market hygiene criteria in terms of providing adequate restrooms and hand washing stations with clean water and soap, and use a trash can with a lid and no leaks. This was due to most flea markets still have no licenses for flea market establishment, the market operators were thus lack of knowledge and awareness in management of the market hygiene correctly.

There was no statistically significant association between food sanitation practices and coliform bacteria contamination in food stalls **(Table 5)**. This result was similar to Chongpiyawarang (2003) who studied the knowledge, attitude, and practices of food handlers and food sanitation conditions in the Bangkok Mass Transit Authority bus Zone 7 and found that sanitation practices of food handlers were not significant related to coliform bacteria contamination in food sample, food container, and hands of food handlers (11). However, it was found that market hygiene had a statistically significant negative effect on coliform contamination [95% confidence interval (CI): 0.0892 – 0.5327]. This means that flea markets that passed the hygienic criteria are less at risk of contamination than those that are not passed the hygienic criteria. Thus, effective market management and the availability of adequate sanitation facilities, such as proper waste containers with a lid, sufficient handwashing stations with soap and clean water, and clean and adequate restrooms, has directly contribute to the reduction of coliform bacteria contamination in food stalls.

Table 5. Analysis of the association between both food sanitation practices and market hygiene with the coliform bacteria contamination in food stalls.

	OR	95% CI Lower	95% CI Upper	Pr (>|z|)
(Intercept)	1.1053	0.7127	1.7142	0.6549
P - C	1.1176	0.6494	1.9234	0.6880
MH - C	0.2179	0.0892	0.5327	0.0008***

*** statistically significant at p-value < 0.001

Conclusion:

In summary, there was no association between food handlers' food sanitation practices and coliform bacteria contamination at food stalls in flea markets in Prachuap Khiri Khan province, Thailand. However, there was association between market hygiene and coliform bacteria contamination, it was found that markets that passed the hygiene criteria were found less contamination with coliform bacteria than markets that did not pass the criteria. Therefore, food handlers should be encouraged to attend food sanitation training to enhance correct practices including, proper washing their hand while on duties and using a trash can with a lid and no leaks to prevent contamination into food stalls. Additionally, market operators should be encouraged to obtain licenses for establish flea markets and following the market hygiene practices criteria. These advices can help to reduce the risk of coliform bacteria contamination at food stalls and then minimize the risk from foodborne disease.

References:

1. Intanasak, J. (2012). Relationship between Knowledge and Practice according to Criteria of Food Sanitation Standard of Food Selling Entrepreneurs in Chumphon Province. (Master of science). Phetchaburi: Phetchaburi Rajabhat University.
2. Ministry of Public Health, Department of Health. (2021). Food sanitation course guide for entrepreneurs and food handlers. Bangkok: Keawjawjom Printing & Publishing.
3. The Coverage. (2023). Check the list of 'communicable diseases' that must be reported for epidemiological surveillance. [Internet]. [cited 2023 Dec 1]. Available from: https://www.thecoverage.info/news/content/4535.
4. Krejcie, R. V., and Morgan, D. W. (1970). Determining Sample Size for Research Activities. Educational and Psychological Measurement, 30(3), 607-610.
5. Ministry of Public Health, Department of Health. (2013). Sanitary requirements for food stalls. Bangkok: Agricultural cooperatives association of Thailand printing.
6. Ministerial Regulations on Market Hygiene, B.E. 2008. (2008, January 17). Thai government gazette, 125 (13A), 5-17.
7. Preongtook, P. (2011). Microbial Contamination of Food Venders in Bansang District, Prachinburi Province. (Master of Public Health). Chonburi:Burapha University.
8. Srisai, Y., & Yasaka, S. (2016). Situation of food sanitation in the area around Naresuan University Phitsanulok Province Thailand. Disease Control Journal, 42(4), 327-36.
9. Suwannasri, K. (2023). Food sanitation conditions of street food vendors in Nongbua Health Promoting Hospital, Udonthani Municipality. Journal of Health and Environmental Studies, 8(1), 10-17.
10. Phonthaworn, O. (2011). Factors associated with food sanitation conditions of restaurants in Laksi District, Bangkok. (Master of Public Health).Bangkok: Thammasat University.
11. Chongpiyawarang, S. (2003). Knowledge Attitude and Practice of Food Handlers and Food Sanitation Condition in Bus Terminals At Bangkok Mass Transit Authority Bus Zone 7. (Master of Science). Bangkok: Mahidol University.

Developmental Origins of Human Disease

P-18

Huperzine a reduces amyloid-beta-induced neuroinflammation in human neuroblastoma cells

Anuttree Boontor[1], Phuttiphat Manarangtaweekul[1], Suwakon Wongjaikam[1], Chutikorn Nopparat[2], Parichart Boontem[1], Nopporn Thasana[3], and Piyarat Govitrapong[1,*]

[1]Chulabhorn Graduate Institute, Chulabhorn Royal Academy, Bangkok, Thailand,
[2]Innovative Learning Center, Srinakharinwirot University, Bangkok, Thailand,
[3]Program in Chemical Sciences, Chulabhorn Graduate Institute, Chulabhorn Royal Academy, Bangkok, Thailand,
Laboratory of Medicinal Chemistry, Chulabhorn Research Institute, Bangkok, Thailand.

E-mail: piyarat@cgi.ac.th

Abstract:

Alzheimer's disease (AD) is the most common neurodegenerative disease). The main hallmarks of AD are the presence of amyloid-beta (Aβ) plaques and the formation of abnormal tau tangles. Several studies have revealed that inflammation increased in people with AD. Huperzine A (Hup A) is a purified alkaloid compound extracted from *Huperzia Serrata*, has been established to exhibit anti-inflammatory and antioxidative properties. Our objective is to investigate the potential of Hup A in mitigating neuroinflammation in a model of Alzheimer's disease induced by amyloid beta. Human neuroblastoma SH-SY5Y cells were pretreated with Hup A (1 μM and 10 μM) for 1 h. Subsequently, the cells were treated with Aβ42 for 24 h before being collected. The cells were collected and different proteins (TNF-α, IL-1β, and NLRP3) were identified using western blot analysis. The result showed that 1 μM Aβ significantly enhanced the expressions of TNF-α, IL-1β, and NLRP3 while the induction of these proteins was significantly abolished by 10 μM Hup A. These results indicated that Hup A attenuated Aβ-induced NLRP3 pathway activation by inhibiting proteins associated with the NLRP3 pathway and thereby suppressing the expression of IL-1β and TNF-α. The current study aims to enhance understanding of the beneficial effects of Hup A, which has the potential to be a breakthrough therapy for preventing the onset or slowing the progression of AD in individuals at a high risk of developing the disease.

Keywords: Alzheimer's disease, Huperzine A, neuroinflammation, amyloid beta

Introduction:

Alzheimer's disease (AD) is a common neurological disease. The main hallmarks are the presence of amyloid-beta (Aβ) plaques and the formation of abnormal tau tangles (1). Multiple lines of evidence suggest that the pathogenesis of AD cannot be fully explained or accounted for by Apathways alone. Prior research has revealed a correlation between inflammation and Alzheimer's disease (AD), indicating that inflammation is heightened AD risk genes. All of these components are involved in innate immune functions and inflammation, which have a crucial impact on the pathology of AD (2). Neuroinflammation can lead to synaptic impairment, neuronal death, and numerous brain pathologies (3).

Huperzine A is (Hup A) a purified alkaloid compound extracted from *Huperzia Serrata*, a certain kind of club moss. Hup A is a reversible inhibitor of AChE causing acetylcholine (ACh) to be upregulated in the brain (4). Interestingly, Hup A also has an important role in non-cholinergic pathway (5). In addition, Hup A can reduce inflammation by decreasing the NLRP3 expression in microglia, and by inhibiting the expression of the NFkB p65 subunit in

astrocytes (6). However, few studies are performed on neuronal cells. The objective of this study is to investigate the potential of Hup A in inhibiting neuroinflammation in SH-SY5Y neuronal cells using the amyloid beta-induced Alzheimer's disease model.)

Materials and Methods:

SH-SY5Y cell cultures and treatments

SH-SY5Y cells were cultured in complete media containing Eagle's MEM and Nutrient Mixture F-12 with 10% FBS and 100 U/mL penicillin/streptomycin. Cells were maintained at 37°C, 5% CO_2 and 95% humidified air. Cells were pretreated with various concentrations of Hup A (1 µM and 10 µM) for 1 h, and then, cells were treated with $A\beta_{42}$ for 24 h before cell collection.

Western blot analysis

The cells were collected and lysed with RIPA buffer and sonicated for 30 seconds twice. Cell lysates were centrifuged at 12000 x g for 15 minutes at 4°C, and the supernatant was collected for Western blots analysis. Samples were then electrophoresed on SDS–PAGE gels and transferred onto PVDF membranes. The membranes were incubated with primary antibodies at 4°C overnight. After washing 3 times with TBS-T, the membranes were incubated with secondary antibodies for 90 minutes. After being washed three times with TBS-T, the signals on the membranes were detected using chemiluminescence ECL reagent. The immunoblots were quantified by measuring the density of each band using densitometry analysis with the Image J program.

Statistical analysis

The data were expressed as the mean and standard error of the mean (Mean ± SEM). Statistical analyses were performed by one-way analysis of variance (one-way ANOVA) and Tukey's post hoc test using Graph Pad Prism version 5. The p values < 0.05 were considered statistically significant.

Results:

Effect of Aβ on inflammatory cytokine expressions

SH-SY5Y cells were treated with 1 µM of Aβ. The results showed that 1 µM Aβ significantly enhanced the expression of TNF-α (Figure 1), IL-1β (Figure 2).

Effect of Hup A on Aβ-induced proinflammatory cytokine expressions

Various concentrations (1 and 10 µM) of Hup A were added and further incubated for 24 h. The results showed that the expression levels of TNF-α and IL-1β in cells that were pretreated with 10 µM Hup A followed by 1 µM Aβ were significantly ($p < 0.05$, Figure 1), ($p < 0.05$, Figure 2) respectively, decreased compared with those in cells treated with 1 µM Aβ alone.

Effect of Hup A on Aβ-induced inflammasome expression

SH-SY5Y cells were treated with 1 µM of Aβ. The results showed that 1 µM Aβ significantly enhanced the expression of NLRP ($p < 0.05$, Figure 3). After treatment with 1 µM Aβ, 1 and 10 µM Hup A were added and further incubated for 24 h. The results showed that the expression levels of NLRP3 in cells that were pretreated with 1 and 10 µM Hup A followed by 1 µM Aβ, were significantly ($p < 0.05$) decreased compared with those in cells treated with 1 µM Aβ alone (Figure 3). These results indicated that Hup A attenuated Aβ-induced NLRP3 pathway activation by inhibiting proteins related to the NLRP3 pathway and thereby suppressing the expression of IL-1β and TNF-α.

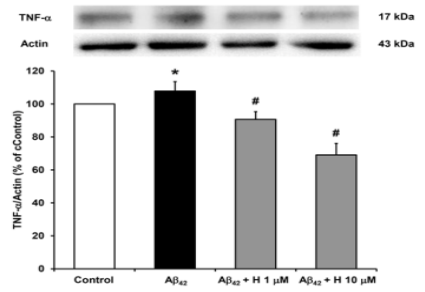

Figure 1 The effect of Hup A on Aβ-induced TNF-α cytokine expression in SH-SY5Y cells. Cells were pretreated with 1 μM or 10 μM Hup A for 1 h and followed by 1 μM Aβ treatment. Western blot analysis was used to determine the expression levels of cytokines TNF-α. The band densities were normalized to actin. The ratios were calculated as a percentage of the respective value in the control group. The data are expressed as the means ± S.E.M. N=3 (* denotes statistical significance at $p < 0.05$ compared to the control group, and # denotes statistical significance at $p < 0.05$ compared to the Aβ treatment group, respectively).

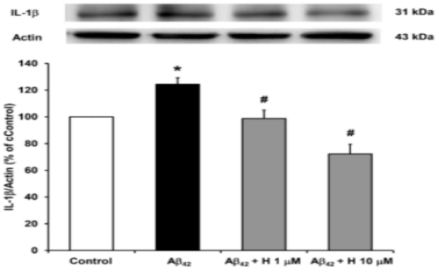

Figure 2 The effect of Hup A on Aβ-induced IL-1β cytokine expression in SH-SY5Y cells. Cells were pretreated with 1 μM or 10 μM Hup A for 1 h and followed by 1 μM Aβ treatment. Western blot analysis was used to determine the expression levels of cytokines IL-1β. The band densities were normalized to actin. The ratios were calculated as a percentage of the respective value in the control group. The data are expressed as the means ± S.E.M. N=3 (* denotes statistical significance at $p < 0.05$ compared to the control group, and # denotes statistical significance at $p < 0.05$ compared to the Aβ treatment group.

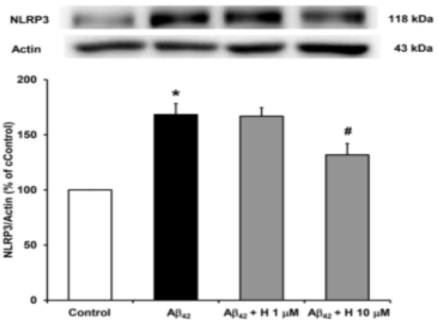

Figure 3. The effect of Hup A on Aβ-induced NLRP3 inflammasome proteins expression in SH-SY5Y cells. Cells were pretreated with 1 μM or 10 μM Hup A for 1 h followed by 1 μM Aβ treatment. Western blot analysis was used to determine the expression levels of NLRP3. The band densities were normalized to actin. The ratios were calculated as a percentage of the respective value in the control group. The data are expressed as the means ± S.E.M. N=3-4 (* denotes statistical significance at $p< 0.05$ compared to the control group, and # denotes statistical significance at $p < 0.05$ compared to the Aβ treatment group.

Discussion and conclusion:

A previous study indicated that inflammation was one of the genetic and environmental risk factors that induced AD progressions (7). Activation of NF-κB can induce downstream signaling cytokines such as IL-1β, IL-6, and TNF-α (8). The NF-κB pathway is essential for cytokine activation and AD pathology. Conversely, Aβ aggregation induces the NF-κB pathway and inflammasome activation (9), which can act as a vicious cycle to increase AD progression. The unnatural accumulation of Aβ in the brain is an early characteristic of AD that is typically accompanied by neuronal loss and inflammatory responses. Prior studies have demonstrated that Aβ has the ability to trigger NLRP3 inflammasome activation in microglia (9).

The present study in neuronal cell lines demonstrated that Aβ could upregulate NLRP3, the key component of the inflammasome. NLRP3 expression was induced by Aβ treatment. The present data are compatible with recent studies which showed that Aβ exposed to SH-SY5Y cells caused NLRP3 inflammasome activation (10). In addition, AD mice exhibited NLRP1 and NLRP3

upregulation and IL-1β and IL-18 production, which further contributed to the onset of AD (11). Inhibition of NLRP3 activation has been suggested as an emerging therapeutic approach in the management and treatment of AD. Thus, targeting the NLRP3 inflammasome is a promising therapeutic approach for treating AD. Our present data indicate that Hup A, a Chinese traditional drug can reduce inflammation by decreasing NLRP3 expression. This finding is consistent with previous research (6) showed that Hup A could reduce inflammation by decreasing the NLRP3 expression in microglia in vivo and inhibiting the expression of the NF-κB p65 subunit in astrocytes.

The present data indicate that Hup A can prevent neuroinflammation in the amyloid beta-induced neuronal cell. Moreover, this study has the potential to enhance our understanding of the advantageous impacts of Hup A, which could serve as a therapeutic breakthrough in preventing the development of AD or slowing its progression in individuals with a heightened susceptibility to the disease**.**

Acknowledgements:

This research project is supported by Thailand Science Research and Innovation (FRB660044/0240 Project code 180874) Chulabhorn Royal Academy.

References:

1. Braak H, Braak E. Neuropathological stageing of Alzheimer-related changes. Acta Neuropathol. 1991;82(4):239-259.
2. Calsolaro V, Edison P. Neuroinflammation in Alzheimer's disease: Current evidence and future directions. Alzheimers Dement. 2016;12(6):719-732.
3. Cunningham AJ, Murray CA, O'Neill LA, Lynch MA, O'Connor JJ. Interleukin-1 beta (IL-1 beta) and tumour necrosis factor (TNF) inhibit long-term potentiation in the rat dentate gyrus in vitro. Neurosci Lett. 1996;203(1):17-20.
4. Ratia M, Gimenez-Llort L, Camps P, Munoz-Torrero D, Perez B, Clos MV, Badia A. Huprine X and huperzine A improve cognition and regulate some neurochemical processes related with Alzheimer's disease in triple transgenic mice (3xTg-AD). Neurodegener Dis. 2013;11(3):129-140.
5. Qian ZM, Ke Y. Huperzine A: Is it an Effective Disease-Modifying Drug for Alzheimer's Disease? Front Aging Neurosci. 2014;6:216.
6. Mohseni-Moghaddam P, Sadr SS, Roghani M, Arabzadeh S, Khamse S, Zamani E, Hosseini M, Moradi F. Huperzine A ameliorates cognitive dysfunction and neuroinflammation in kainic acid-induced epileptic rats by antioxidant activity and NLRP3/caspase-1 pathway inhibition. Clin Exp Pharmacol Physiol. 2019;46(4):360-372.
7. Jones SV, Kounatidis I. Nuclear Factor-Kappa B and Alzheimer Disease, Unifying Genetic and Environmental Risk Factors from Cell to Humans. Front Immunol. 2017;8:1805.
8. Su F, Bai F, Zhang Z. Inflammatory Cytokines and Alzheimer's Disease: A Review from the Perspective of Genetic Polymorphisms. Neurosci Bull. 2016;32(5):469-480.
9. Schnaars M, Beckert H, Halle A. Assessing beta-amyloid-induced NLRP3 inflammasome activation in primary microglia. Methods Mol Biol. 2013;1040:1-8.
10. Zhong X, Liu M, Yao W, Du K, He M, Jin X, Jiao L, Ma G, Wei B, Wei M. Epigallocatechin-3-Gallate Attenuates Microglial Inflammation and Neurotoxicity by Suppressing the Activation of Canonical and Noncanonical Inflammasome via TLR4/NF-kappaB Pathway. Mol Nutr Food Res. 2019;63(21):e1801230.
11. Saresella M, La Rosa F, Piancone F, Zoppis M, Marventano I, Calabrese E, Rainone V, Nemni R, Mancuso R, Clerici M. The NLRP3 and NLRP1 inflammasomes are activated in Alzheimer's disease. Mol Neurodegener. 2016;11:23.

P-19

A model of Shwachman-Diamond Syndrome, the *SDO1* deletion mutant, exhibits phenotypic differences from mutations in *RPS19A* or *RPS19B* implicated in Diamond-Blackfan Anaemia

Vajira Shanil Kuruppu Nanayakkara[1] and Amornrat Naranuntarat Jensen[1,2*]

[1]Department of Pathobiology, Faculty of Science, Mahidol University, Bangkok 10400, Thailand
[2]Center of Excellence on Environmental Health and Toxicology (EHT), OPS, MHESI, Thailand
**Email: amornrat.nar@mahidol.edu*

Abstract:

Ribosomopathies are a group of diseases characterised by the presence of structural as well as functional abnormalities in the proteins that constitute the ribosome as well as defects in genes that participate in ribosome biogenesis. Due to the highly specific nature of protein assembly, ribosome integrity is maintained in a highly accurate and regulated manner in order to maintain error free protein synthesis. Mutations to genes involved in the production of mature ribosomes are implicated in several ribosome related diseases such as Shwachman-Diamond Syndrome (SDS) and Diamond-Blackfan Anaemia (DBA). In this study, we compare two yeast models of ribosomopathies, an *SDO1* knockout strain for SDS and the *RPS19A* and *RPS19B* knockout starins for DBA, in order to ascertain if phenotypic variances occur between mutations involved in these two ribosomopathies.

Keywords: Ribosomopathy, Shwachman-Diamond Syndrome, Diamond-Blackfan Anaemia, Yeast models of human disease.

Introduction:

Ribosomopathies are diseases characterised by the presence of congenital bone marrow failure syndrome in patients at birth followed by an elevated risk of cancer later in life. While the cause of the disease is rooted in the malfunction of human ribosomes, the poorly understood pathogenesis remains a key hurdle in the development of therapeutic solutions [**1,2**]. Ribosome assembly is a complex, highly regulated process that leads to the development of mature ribosomes from their precursor components. Aberrations in the assembly process of ribosomes has serious negative impacts on cellular function and leads to the production of abnormal translation products which could overall result in onset of ribosome related disease. Due to the complex array of enzymes, transcription factors, and proteins involved in ribosome biogenesis, ribosome related diseases have been found to be highly variable in both mechanisms as well as clinical presentation [**3**]. Ribosomal dysfunction has been shown in both humans and animal models to impact growth and survival of cells, however the exact nature of ribosome defects and their link to the manifestation of symptoms observed in the diseases remains unclear. One of the key knowledge gaps in our understanding is the variance of disease phenotypes that arise from mutations in genes related to ribosome biogenesis. Ribosomes are ubiquitous, essential players in protein synthesis and as such are found throughout human cells. Therefore, it could be expected that mutations to the genes that encode ribosomal proteins and subsequent ribosomal dysfunction should be observed in all cell types. Research and clinical data however points to more selective, tissue specific defects associated with ribosomopathies such as Diamond-Blackfan Anaemia (DBA) and Shwachman-Diamond Syndrome (SDS) [**2,3**]. SDS is an inherited bone marrow failure syndrome characterised by neutropenia while DBA is a congenital hypoplastic anaemia with clinical features of low red blood cell production. Both diseases share overlapping features including skeletal abnormalities and elevated risk of cancer [**3**].

However, the genes affected as well as the ribosomal pathway aberrations are markedly different; A mutation to the gene *SBDS* is heavily associated with the development of SDS while several gene mutations have been associated with DBA with *RPS19* being the most common, found in 20% of all cases [**4,5**]. A mutation of *SDO1*, the yeast ortholog of *SBDS*, shows disrupted iron homeostasis, growth rate decline, and stress intolerance [**6**]. To establish if a knockout model can be produced for DBA, here we aim to create a model of the disease with a knockout targeting the *RPS19* yeast ortholog. This comes with a unique set of challenges as yeast contains two paralogs of human *RPS19* named *RPS19A* and *RPS19B*. As such, the knocking out of a single *RPS19* gene may be insufficient to produce an accurate disease model as some paralogous genes have been reported to have the capacity to compensate for each other's function [**7**]. In this study, we attempt to test the viability of a disease model of DBA using yeast deletion strains for either *RPS19* genes in order to ascertain the feasibility of a single knockout model for paralogous genes.

Methodology:

RPS19A and *RPS19B* deletion mutants in BY4742 background were obtained from Open Biosystems, USA. Their growth rates were analysed by incubation in YPD media followed by measurement of optical density at 600nm every 4 hours using spectrophotometry. WT, *rps19a*Δ and *rps19b*Δ strain growth was also monitored by spotting 10^4, 10^3 and 10^2 cells onto solid plates containing YPD medium and cultured for 3 days at 30°C. The growth in respiration-requiring media was tested in media containing 2 percent glycerol and compared to wild type cells capable of respiration, and an established *SDO1* deletion strain which has shown impaired respiration [**6,8**]. Knockouts were tested under stress conditions including heat (37°C), oxidative stress (4mM H_20_2) and alcohol stress (10% ethanol). Por1 levels were quantified using western blotting followed by probing using anti-Por1 antibodies (Sigma). The intracellular iron content was measured using graphite furnace atomic absorption spectrophotometry (GFAAS) as previously published [**4**].

Results:

Cells lacking either *RPS19A* or *RPS19B* exhibit normal growth

Previous data indicates that yeast models of ribosomopathies tend to show slow growth phenotypes associated with ribosomal defects [**6**]. In order to establish if *RPS19A* or *RPS19B* deletion strains showed similar growth rate reductions, the growth of the mutants was monitored and compared to WT cells.

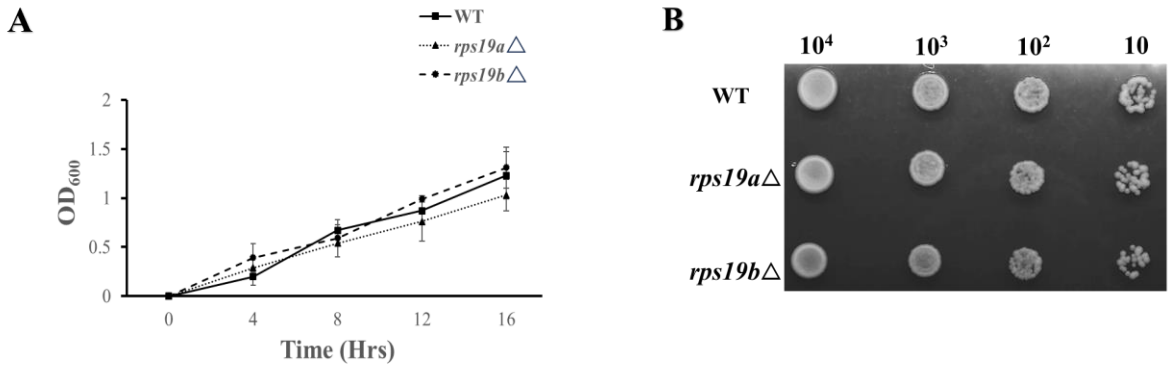

Figure 1 A) Normal growth rate was observed in r*ps19a*△ and *rps19b*△ mutants compared to WT cells. Wild type, *rps19a*Δ and *rps19b*△ strains were cultured in liquid YPD medium and incubated at 30°C. Growth of the cells was measured every 4 hours by measuring optical density at OD600. B) Spot test on solid YPD media, indicated cells were cultured at 30°C for 3 days.

As seen in figure 1, growth rates of *rps19a*Δ or *rps19b*Δ closely mirrored that of wild type yeast cells on both solid and liquid media indicating that mutation in either *RPS19A* or *RPS19B* knockout failed to show slow growth phenotypes associated with other ribosomopathy models.

Normal mitochondrial respiratory function was observed in *rps19a*△ *and rps19b*△

Previous results show that *sdo1*△ lacked the capacity to grow in non-fermentable carbon source due to mitochondrial dysfunction preventing respiration [**8**]. Here we observed that unlike *sdo1*△ mutants, *rps19a*△ and *rps19b*△ were capable of respiration in non-fermentable media (figure 2A and 2B) indicating a conservation of mitochondrial function.

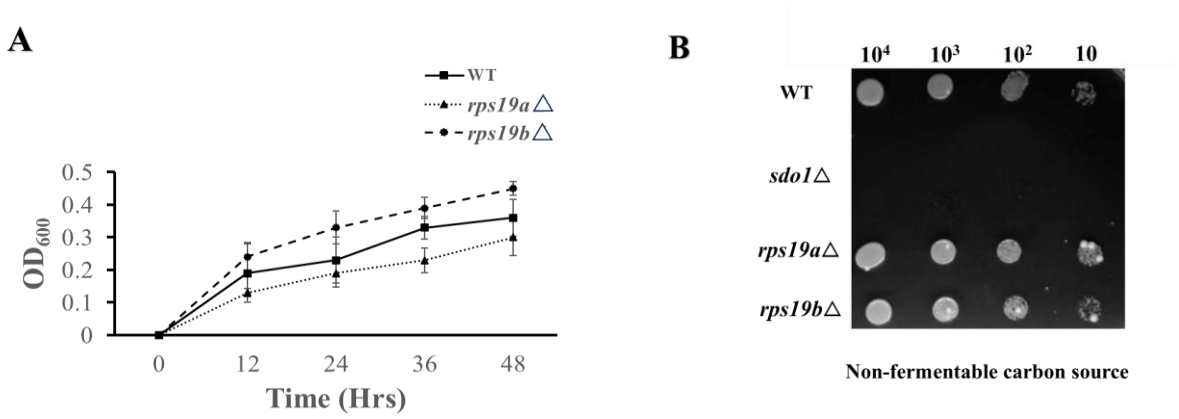

Figure 2 A) Normal mitochondrial respiratory function was observed in *RPS19⊿*. WT, *sdo1*Δ, *rps19a*Δ and *rps19b*Δ strains that were cultured in liquid media with 2% glycerol (YPG) and growth rate was monitored every 12 hours. B) Cells grown for 3 days on solid YPG media.

***rps19a*△ *and rps19b*△ strains have similar stress tolerance levels to WT cells**

Studies have shown that *sdo1*△ show diminished growth capacity when exposed to stress conditions [**6,8**]. Here we demonstrate that in line with previously reported data, *sdo1*△ were unable to grow when subjected to both heat and alcohol stress while showing partial growth in oxidative stress conditions [**6**]. However, *rps19a*△ and *rps19b*△ showed stress tolerance levels comparable to WT cells which may suggest a partial or full conservation of ribosomal function in *rps19a*△ *and rps19b*△ strains.

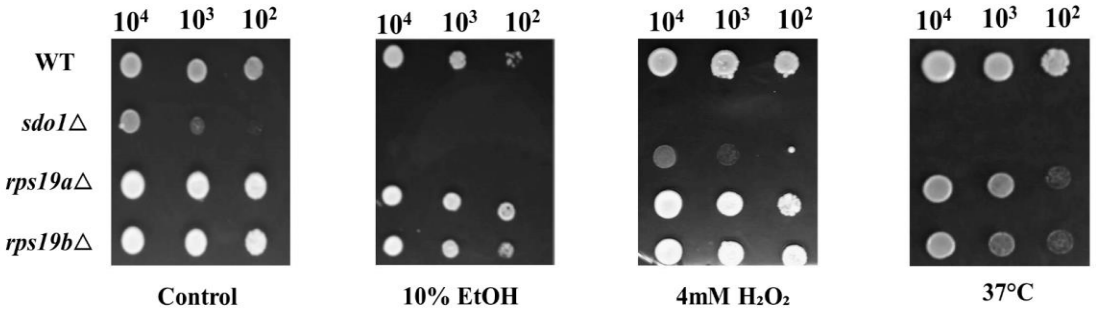

Figure 3 *RPS19A or RPS19B* deletion strains show normal growth rate as well as tolerance to various stress compared to WT cells. Cells were grown on YPD plates for 3 days with various stress conditions introduced.

Cells lacking *RPS19A* or *RPS19B* show normal levels of Por1 and intracellular iron

In this experiment we observe if the level of mitochondrial porin Por1, a protein channel found on the mitochondrial membrane, and the fidelity of intracellular iron regulation was maintained in *rps19a*△ and *rps19b*△ mutants. The disruption in iron homeostasis as well as elevating levels of Por1 associated with increased susceptibility of cells to environmental stress conditions as well as increasing cellular ROS levels were reported previously in *sdo1*△ mutants [**6,8**].

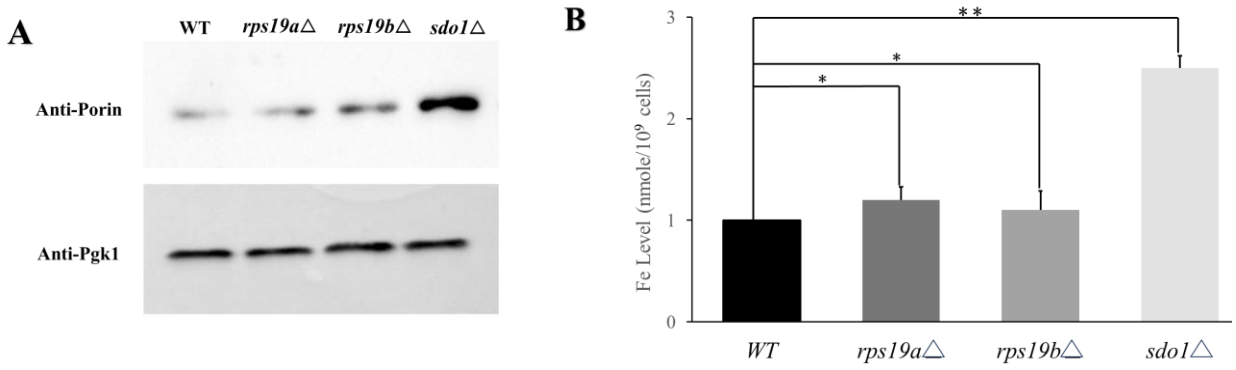

Figure 4 A) Total cell lysates of WT, *SDO1* and *RPS19A*, and *RPS19B* knockouts were separated using western blotting (14 percent SDS-PAGE gel) followed by probing with anti-Porin antibody in order to detect Por1 expression levels. Anti-Pgk1 was used as a loading control. Results show a high level of Por1p expression in *sdo1*∆ while *RPS19A* and *RPS19B* deletion strains showed no significant increase in expression levels. B) The intracellular iron levels of *rps19a*∆ and *rps19b*∆ mutants were similar to that of wild-type cells. WT, *sdo1*∆, and *rps19a*∆ and *rps19b*∆ strains were cultured in liquid YPD medium for 15 hours and intracellular iron levels were measured using graphite furnace atomic absorption spectrometry (GFAAS). Values (from 3 independent experiments) are mean + SD, **P <0.01 and *P < 0.05 determined by using Student's T-test compared between the means of indicated groups.

Our data revealed that while *sdo1*△ showed both an increase in intracellular iron accumulation (figure 4B) and elevated Por1 expression (figure 4A), both *rps19a*△ and *rps19b*△ mutants showed Por1 expression and iron levels similar to those of WT cells indicating a maintenance of iron homeostasis.

Discussion:

The lack of cures for ribosomopathies along with the diminished expectancy and quality of life of patients suffering these conditions necessitates better understanding of ribosomal genes and pathways in order to devise viable therapeutic strategies. *SDO1* knockout models for Shwachman-Diamond Syndrome have already yielded valuable data and in this study, we aimed to establish if a viable yeast model could be produced for the Diamond-Blackfan Anaemia using yeast deletion strain for *RPS19*, the most commonly mutated gene in DBA. The presence of two paralogs of the *RPS19* gene however, may have contributed to the inability to observe any disease associated phenotypes as previously reported in other yeast models for ribosomopathies [**6,8**]. Cells that were missing either one of the paralogs showed no major growth defects or any of the cellular aberrations previously observed in the *SDO1* deletion strain. This phenomenon can be attributed to the compensatory or overlapping functions of the paralogs. Previous research has shown a double knockout *RPS19* model is unviable due to lethality; therefore, in order to better understand and develop a viable disease model for DBA, other techniques such as gene knockdowns should be explored.

References:

1. Nakhoul H, Ke J, Zhou X, Liao W, Zeng SX, Lu H. Ribosomopathies: mechanisms of disease. Clin Med Insights Blood Disord. 2014;7:7-16.
2. Farley-Barnes KI, Ogawa LM, Baserga SJ. Ribosomopathies: Old Concepts, New Controversies. Trends Genet. 2019;35(10):754-67.
3. Hashmi SK, Allen C, Klaassen R, Fernandez CV, Yanofsky R, Shereck E, et al. Comparative analysis of Shwachman-Diamond syndrome to other inherited bone marrow failure syndromes and genotype-phenotype correlation. Clin Genet. 2011;79(5):448-58.
4. Campagnoli MF, Ramenghi U, Armiraglio M, Quarello P, Garelli E, Carando A, et al. RPS19 mutations in patients with Diamond-Blackfan anemia. Hum Mutat. 2008;29(7):911-20.
5. Kawashima N, Oyarbide U, Cipolli M, Bezzerri V, Corey SJ. Shwachman-Diamond syndromes: clinical, genetic, and biochemical insights from the rare variants. Haematologica. 2023;108(10):2594-605.
6. Jain A, Nilatawong P, Mamak N, Jensen LT, Jensen AN. Disruption in iron homeostasis and impaired activity of iron-sulfur cluster containing proteins in the yeast model of Shwachman-Diamond syndrome. Cell Biosci. 2020;10:105.
7. Diss G, Ascencio D, DeLuna A, Landry CR. Molecular mechanisms of paralogous compensation and the robustness of cellular networks. J Exp Zool B Mol Dev Evol. 2014;322(7):488-99.
8. Kanprasoet W, Jensen LT, Sriprach S, Thitiananpakorn K, Rattanapornsompong K, Jensen AN. Deletion of Mitochondrial Porin Alleviates Stress Sensitivity in the Yeast Model of Shwachman-Diamond Syndrome. J Genet Genomics. 2015;42(12):671-84.

P-20

Tetracycline induces minocycline resistance in *Stenotrophomonas maltophilia*

Amita Mekarunothai[1], Nuchjaree Boonyong[1], Ratiboot Sallabhan[2], Skorn Mongkolsuk[1,2,3], Nisanart Charoenlap[2,3], and Paiboon Vattanaviboon[1,2,3].

[1]Program in Applied Biological Sciences: Environmental Health, Chulabhorn Graduate Institute, Bangkok, Thailand
[2]Laboratory of Biotechnology, Chulabhorn Research Institute, Bangkok, Thailand
[3]Center of Excellence on Environmental Health and Toxicology (EHT), OPS, MHESI, Thailand

Abstract:

The misuses and overuses of tetracycline antibiotic in veterinary and agriculture purpose rises the concerns of emergence and spreading of antimicrobial resistance (AMR) microorganisms in environment. *Stenotrophomonas maltophilia*, a gram-negative obligate aerobe bacterium, is one of the most important opportunistic pathogens worldwide. In this study we focused on the effect of tetracycline on induction of minocycline resistance in *S. maltophilia* SMBT strain, isolated from clinical sample.Tetracycline resistance strains of *S. maltophilia* SMBT strain were isolated using sequential passage method in the presence of increasing concentrations of tetracycline ranging from 2 to 32 µg/mL. Thirty-five colonies that grew on medium containing 32 µg/ mL were purified and tested for antimicrobial susceptibility against minocycline, a drug of choice for *S. maltophilia* treatment.The five candidate clones with different levels of minocycline resistance were further analysis of the mutated genes using whole genome sequencing. All of the tested clones showed mutations on *smlt*4073 *(smeT)* gene encoding transcriptional repressor of the RND efflux pump SmeDEF. To our knowledge, the contribution of *smeT* gene mutation to minocycline resistance of *S. maltophilia* has never been reported. Further analysis is required to elucidate the role of *smeT* on minocycline resistance of *S. maltophilia*.

Keywords: *Stenotrophomonas maltophilia*, Antimicrobial resistance (AMR), Tetracycline resistance, Minocycline resistance

Introduction:

Antimicrobial Resistance (AMR) has become a significant global health concern over time as pathogenic bacteria develop mechanisms to evade antibiotics. *Stenotrophomonas maltophilia*, considered as a "newly emerging pathogen of concern, "is among the bacteria showing increasing resistance (1). According to British microbiologists, it ranked as the ninth most significant pathogen and remains a challenging topic within the infectious disease community and research studies (2). It spreads within and outside healthcare settings (2, 3), *S. maltophilia* infections can occur in both nosocomial (hospital- acquired) and community-acquired including pneumonia, acute exacerbations of chronic obstructive pulmonary disease[COPD], bloodstream infections, and others, particularly in immunocompromised individuals (2, 4). Human activities, including the inappropriate use of antimicrobials, contribute to the emergence and spread of antimicrobial-resistant microorganisms. Tetracycline is an antibiotic in tetracycline family, it normally utilized in veterinary and agricultural practices for both prophylactic and therapeutic purposes. Tetracycline inhibit bacterial growth and replication (5). It is commonly administered to animals through feed. However, after administration, animals excrete tetracycline into the environment via urine and feces, leading to contamination of soil, surface, and ground waters through leaching off (5-7). This increases the likelihood of the development of antibacterial resistance in *S. maltophilia* through increased mutation rates, posing challenges in infection control and treatment. Current therapeutic options using minocycline remains effective in treating *S.maltophilia* infections, its classification as a second-

generation antibiotic in the tetracycline family. However, minocycline resistance in S. maltophilia remains a concern, with reported low prevalence. This study aims to fill this gap by investigating the effect of tetracycline on induction of minocycline resistance in *S. maltophilia*.

Methodology:

Bacterial strains and growths conditions

Bacterial strains that will be used in this study is *S. maltophilia* SMBT strain isolated from hospital. *S. maltophilia* was aerobically cultured in Luria-Bertani (LB) medium and incubated at 35°C for 20-24 hours with constant shaking at 180 rpm.

Isolation antimicrobial resistance (AMR) strains

To generate tetracycline resistance strains, *S. maltophilia* SMBT (wild-type strain) was used in this experiment. Sequential passage technique was performed, the exponential-phase cell was cultured in LB medium supplemented with 2 µg/ mL of tetracycline (sub-minimum inhibitory concentration; the minimum inhibitory concentration of tetracycline is 4 µg/ mL) and incubated overnight. The overnight cells were continued sequential sub-culturing, treated with increasing concentrations of tetracycline at 4, 8, and 16 µg/mL until reaching a final concentration of 32 µg/ mL. At the final concentration of 32 µg/ mL, cells were streaked onto LB agar plates containing 32 µg/mL of tetracycline to select single colonies of tetracycline-resistance strains.

Antimicrobial susceptibility testing

The susceptibility profiles of *S. maltophilia* SMBT strain to minocycline were determined using the Kirby Bauer disk diffusion method (8). A single colony on LB agar was resuspended in sterile normal saline, and the turbidity was adjusted to 0.5 McFarland standard (OD_{600} = 0.132). The suspension was then evenly spread using a swab over the entire dried Mueller Hinton Agar (MHA) surface plate. Minocycline antibiotic disk was placed onto the MHA surface, and the plates were incubated at 35°C overnight. Subsequently, the inhibition zone of minocycline was measured and reported in millimeters (mm.). Finally, the results were interpreted into three phenotypic groups: resistance, intermediate, and susceptibility, according to the criteria described in the CLSI guideline (9).

Determination of mutated genes

The selected candidate clone from phenotypic data of minocycline resistance strain were determined the mutated genes in the genome by comparing them with the SMBT (wild-type strain) through whole-genome sequencing. This process involved aligning or mapping the reads to the reference genome sequence, which, in this case, was *S. maltophilia* SMBT (wild-type strain). The analysis was particularly focused on identifying mutations at single nucleotide polymorphism (SNP) sites and detecting insertion or deletion events.

Results:

Isolation of antimicrobial resistance strains

The sequential passage technique was used to generate *S. maltophilia* SMBT tetracycline resistance strains by cultivating bacteria in LB medium supplemented with tetracycline. The presence of tetracycline-resistance strains was isolated after treatment with 32 µg/ mL tetracycline.

Antimicrobial susceptibility testing

The phenotypic pattern data which included it parental tetracycline sensitive strain (SMBT; wild type) and tetracycline resistance strains. 35 colonies of tetracycline-resistance strains were tested for antibiotic susceptibility to minocycline using the disk diffusion method. The inhibition

zone of minocycline was measured and interpreted the results into three phenotypic groups: resistance (≥ 14 mm), intermediate (15-18 mm), and sensitivity (≤ 19 mm), following the criteria described in the CLSI guideline (9). The results of the phenotypic data, the inhibition zone (mm.) of minocycline of tetracycline resistance strains were shown in Figure 1.

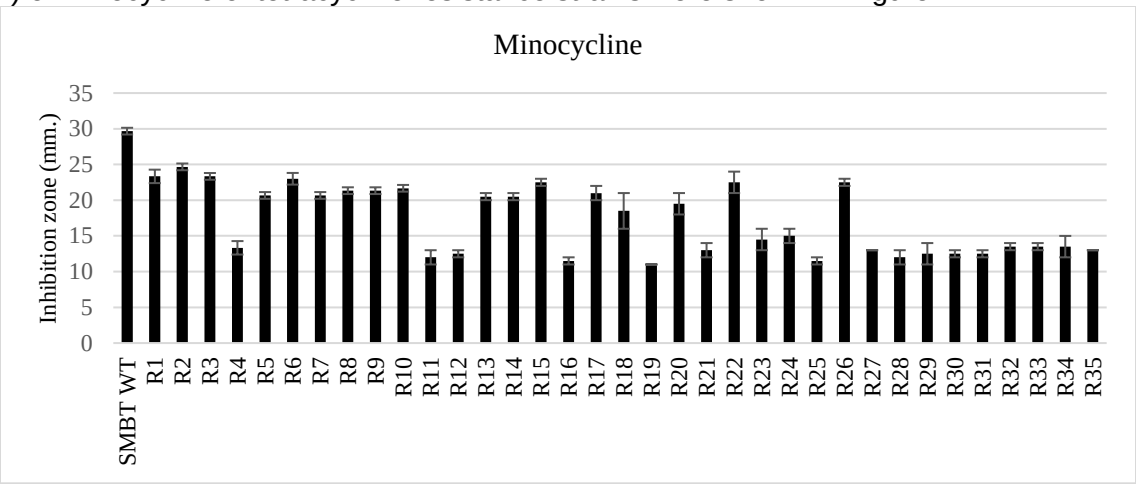

Figure 1 Inhibition zone (mm.) of minocycline of the selected tetracycline resistance strains

Among the 35 clones of tetracycline resistance strains, 18 clones exhibited resistance to minocycline. These included R4, R11, R12, R16, R19, R21, R23, R24, R25, R27, R28, R29, R30, R31, R32, R33, R34, and R35.

Determination of mutated genes

5 candidate clones showing a phenotypic pattern indicating minocycline resistance were randomly chosen by the different size of inhibition zone and determined the mutated gene using whole genome sequencing. These consisted of R16, R24, R28, R29, and R34

Table 1 The annotated results of mutations in clones R16, R24, R28, R29, and R34 genome

Strains	Mutation			
	Gene name	**Type**	**Protein name**	**Amino acid change**
R16	*smlt*4073 (*smeT)*	Frameshift insertion _ > T	Putative TetR family regulatory protein	I16fs
R24		Nonsynonymous SNV G>A		A19T
R28		Frameshift insertion _ > A		H25fs
R29		Frameshift insertion _ > T		I16fs
R34		Frameshift insertion _ > T		I16fs

SMBT tetracycline resistance strain clone R16, R28, R29, and R34 exhibited frame shift insertions at different positions, while a nonsynonymous single nucleotide variant (SNV) was detected in clone R24. Notably, all five strains showed mutations in the *smlt*4073 (*smeT*) gene. This gene encodes SmeT, a transcriptional repressor that regulates the expression of *smeDEF*, encoding SmeDEF efflux pump that involves in antibiotic resistance mechanisms (4).

Conclusion:

Tetracycline might trigger the development of minocycline resistance in *S. maltophilia*. The mutation on *smeT* gene may contributed to minocycline resistance of *S. maltophilia*. However, it is still low prevalence of minocycline resistance among *S. maltophilia* worldwide and there is no study reporting the association of *smeT* in minocycline resistance in *S. maltophilia*. The role of *smeT* in minocycline resistance of *S. maltophilia* is being investigated.

References:

1. World Health Organization. Antimicrobial resistance [Internet]. 2023 [13 Feb, 2024]. Available from: https://www.who.int/news-room/fact-sheets/detail/antimicrobial-resistance.
2. Said MS TE, Lesho E. Stenotrophomonas maltophilia [Internet]. StatPearls; 2023 [10 Mar, 2024]. Available from: https://www.ncbi.nlm.nih.gov/books/NBK572123/.
3. Dadashi M, Hajikhani B, Nazarinejad N, Noorisepehr N, Yazdani S, Hashemi A, et al. Global prevalence and distribution of antibiotic resistance among clinical isolates of Stenotrophomonas maltophilia: A systematic review and meta-analysis. Journal of Global Antimicrobial Resistance. 2023;34:253-67.
4. Brooke Joanna S. Advances in the microbiology of Stenotrophomonas maltophilia. Clinical Microbiology Reviews. 2021;34(3):10.1128/cmr.00030-19.
5. Mollie C. Shutter HA. Tetracycline [Internet]. 2024 [cited 20 Feb, 2024. Available from: https://www.ncbi.nlm.nih.gov/books/NBK549905/.
6. National Library of Medicine. Tetracycline [Internet]. 2017 [20 Feb, 2024]. Available from: https://medlineplus.gov/druginfo/meds/a682098.html.
7. Coculescu BI. Antimicrobial resistance induced by genetic changes. J Med Life. 2009;2(2):114-23.
8. Hudzicki J. Kirby-Bauer disk diffusion susceptibility test protocol [Internet]. 2009 [10 Feb, 2024]. Available from: https://asm.org/getattachment/2594ce26-bd44-47f6-8287-0657aa9185ad/Kirby-Bauer-Disk-Diffusion-Susceptibility-Test-Protocol-pdf.pdf.
9. CLSI. Performance standards for antimicrobial susceptibility testing. 34th ed: Wayne, PA: Clinical and Laboratory Standards Institute; 2024.

Science and Technology for the Treatment and Management of Environmental Pollutants

P-21

Economic benefits of nutrients removal and recovery processes from slaughterhouse wastewater treatment using AnA^2/O^2 SBR incorporation with ASD and P precipitation

S. Buayoungyuen[a,c*], B. Panyapinyopol[a,c], P. Fongsatitkul[a,c], W. Patthanaissaranukool[b,c], and C. Warodomrungsimun[b,c]

[a]Department of Sanitary Engineering, Faculty of Public Health, Mahidol University
[b]Department of Environmental Health Sciences, Faculty of Public Health, Mahidol University
420/1 Rajvithi Rd., Rajchathawee, Bangkok 10400, Thailand
[c]Center of Excellence on Environmental Health and Toxicology (EHT), OPS, MHESI, Thailand
**Corresponding author: surusnut@gmail.com*

Abstract:

This study aimed to evaluated the economic benefits of nutrients removal and recovery processes from slaughterhouse wastewater treatment using AnA^2/O^2 SBR, ASD, and MAP process. The previous studies have been shown that each process could reduce pollutant contamination and prevent environmental harm while also contributing to resource conservation, thus demonstrating the environmental friendliness of these processes. In the economic analysis, the results indicated that each process had the potential to reduce operating costs and reduce electricity consumption. Also, it could generate revenue during operations. Therefore, all three processes were appropriate and had the possibility of being applied further.

Keywords: Economic benefits, Nutrients removal, Nutrients recovery, P precipitation

Introduction:

Slaughterhouse wastewater contains high concentrations of organic matters, nutrients, colloidal, and suspended solids [1,2]. When it is discharged directly into water bodies, it can cause eutrophication and algal blooms and lead to a decrease of dissolved oxygen (DO) until insufficiency for aquatic organisms in streams. Therefore, effective slaughterhouse wastewater treatment technologies are required for pollution control.

AnA^2/O^2 SBR is one technology in biological nutrient removal (BNR) process that consists of a series in anaerobic-anoxic-oxic-anoxic-oxic condition. The previous studies indicated that it is a well-promoted and proven alternative with advantages over the conventional activated sludge (CAS) process [3,4]. This process can achieve a high efficiency of organic oxidation, nitrogen reduction, and phosphorus removal simultaneously. With the removal efficiencies of organic matter and nutrients were highly effective capability (over 90% for COD, TKN, and TP) [5-7]. In addition, it can be preserved a high nutrients concentration in excess sludge. With the phosphorus concentration in the excess sludge from the small and large reactors was 18.30 - 22.80 mg P/g sludge and 15.67 - 23.16 mg P/g sludge, respectively. Therefore, this process not only improves the quality of the effluent but can also be used to recover nutrients that can be applied to the land as soil conditioner or used as fertilizer in agriculture [8,9].

Anaerobic sludge digestion (ASD) process is a simple technique and low operating costs for sludge stabilization technology. This process not only reduces the volume of sludge that needs to be disposed of and produces biogas as an alternative energy source. But it also releases high concentrations of nutrients from the waste sludge into the digested effluent, providing a good opportunity for the removal and recovery of these compounds [10,11].

The technique has proven to be a successful method of removing and recovering nutrients from anaerobic digested effluent is the phosphorus precipitation process, especially the

precipitation process of the magnesium ammonium phosphate (MAP, also known as struvite). Since it is highly effective for removing and recovering both nitrogen and phosphorus nutrients from waste and wastewater [12,13]. Also, it can be used as a slow nutrient-releasing mineral and as raw material for industrial applications [14,15]. The process not only removes nutrients from effluent but also recovers valuable resources for agricultural and industrial use. This is related to increasing concerns about limited natural resources and the importance given to sustainable treatment technologies.

However, previous studies have not considered the economic feasibility of each process, resulting in increased risks for use on a larger scale. Therefore, this study aims to investigate the economic benefits of all procedures in the process design to pave the way for future applications.

Materials and methods:

- ***Reactor setup and operation***

AnA^2/O^2 SBR process was operated continuously with a cycle time of 12 h at SRT 25 d. AnA^2/O^2 SBR operating time series consist of static fill under anaerobic conditions and the reaction under alternating anoxic and oxic conditions (Ax/Ox/Ax/Ox = 1.5/2.5/2.5/1.5 h). After treatment, the process continued to the settle phase to separate the mixture before the treated wastewater was drained from the reactor and entered the idle phase.

AnA^2/O^2 SBR process

ASD process was performed continuously with a 24 h cycle time at SRT 10 d and an anaerobic SBR operating time series, consisting of static fill and intermittent mixing reactions (mixing 2 h, alternating without mixing 2.5 h) throughout the 18 h working period. Subsequently, the process continued with the settling, decanting, and idling phases, respectively.

ASD process

MAP process was proceeded through 4 steps per cycle, starting with the pumping of the supernatant from the ASD process into the reaction tank and then adjusting the supernatant condition to have a Mg: P ratio of 1.2: 1 and a pH of 9.5. The process then continued with a mixing step for 45 min, divided into rapid mixing (150 rpm) for 15 min and slow mixing (50 rpm) for 30 min, before leaving it for 60 min to allow the crystals to precipitate. After that, the supernatant was slowly poured out and the crystals formed were collected. The crystals were then evaporated and dried at 103 - 105°C for about 1 - 2 h.

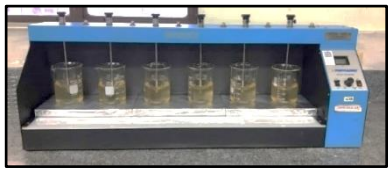

MAP process

Figure 1 Three processes for removing and recovering nutrients in waste and

- ***Analytical methods***

The economic benefits were determined by the cost of operating to removal and recover nutrients. The operating costs were calculated based on chemical additions and electricity consumption in each process, as calculated in Equation (1) and (2), respectively. In addition, the evaluation also considered the profit margin of the products obtained, which calculated from the cost used in the P precipitation process compared to the market price of P-containing fertilizers, as calculated in Equation (3) [13,16].

$$\text{Chemical costs (Baht/m}^3\text{)} = \frac{\text{Chemicals used (ton) x Chemical Prices (baht/ton)}}{\text{Volume of solution (m}^3\text{)}} \quad \text{… (Eq.1)}$$

$$\text{Electricity costs (Baht/m}^3\text{)} = \text{Electricity used (kWh/m}^3\text{) x 3.9086 (baht/kWh)} \quad \text{… (Eq.2)}$$

$$\text{Product's market price (Baht/m}^3\text{)} = \text{P-containing solid (ton/m}^3\text{) x P in } P_2O_5 \text{ (\%) x Fertilizer Prices (baht/ton)} \quad \text{… (Eq.3)}$$

Results and discussion:

The process of removing nutrients from slaughterhouse wastewater using AnA^2/O^2 SBR process, it was found that this process had high potential in generating electricity and cost savings over CAS process, as shown in Table 1. It showed the electrical power requirement for the equipment used in the AnA^2/O^2 SBR process was approximately 42.65 kWh/m^3 of wastewater, corresponding to 0.039 kWh/g of COD, which was equivalent to the wastewater treatment cost of about 0.167 THB/L (or about 0.005 USD/L) of wastewater flowing in the process. These results identified that the electrical power required in this process was around 50% lower than that required by the CAS process, resulting from the reduction of the aeration system during operation. Since the process is carried out through the operation of an automatic timer switch, the process could maintain the efficiency of oxygen transfer and avoid excessive aeration for mixing and biological activities. In addition, it did not need pipelines and pumps to return the sludge, which reduced the amount of energy consumption during the operation. Also, the process combined all treatment steps in a single reactor without adding chemicals to the system, which led to reducing electricity and operating costs [17,18].

Table 1 Comparison of electricity consumption in WWTP using AnA^2/O^2 SBR and CAS process

AnA^2/O^2 SBR process			
Process	**Power (W)**	**Working times (h/d)**	**Electricity (kWh/d)**
Fill phase			
Pump $_{feed}$	22	1.0	0.022
Timer $_{feed}$	3	1.0	0.003
React phase			
Stirrer	34	16.0	0.544
Air pump	10	8.0	0.080
Air pump	10	8.0	0.080
Timer $_{stirrer}$	3	16.0	0.048
Timer $_{air}$	3	8.0	0.024
Timer $_{air}$	3	8.0	0.024
Settle phase			
-			0.000
Decant phase			
Pump $_{decant}$	22	0.5	0.011
Timer $_{decant}$	3	0.5	0.002
Idle phase			
Pump $_{excess}$	22	0.25	0.006
Stirrer	34	0.25	0.009
Timer $_{excess}$	3	0.25	0.001
Timer $_{stirrer}$	3	0.25	0.001
Total electricity consumption (kWh/d)			**0.853**
Total cost (Baht)			**3.334**
Electricity cost (Baht/L)			**0.167**

CAS process			
Process	**Power (W)**	**Working times (h/d)**	**Electricity (kWh/d)**
Influent tank			
Pump $_{feed}$	22	24.0	0.528
Timer $_{feed}$	3	24.0	0.072
Aeration tank			
Air pump	10	24.0	0.240
Air pump	10	24.0	0.240
Timer $_{air}$	3	24.0	0.072
Timer $_{air}$	3	24.0	0.072
Settling tank			
-			0.000
Effluent tank			
-			0.000
Return sludge			
Pump $_{decant}$	22	24.0	0.528
Timer $_{decant}$	3	24.0	0.072
Sludge storage			
Pump $_{excess}$	22	0.25	0.006
Timer $_{excess}$	3	0.25	0.001
Total electricity consumption (kWh/d)			**1.830**
Total cost (Baht)			**7.154**
Electricity cost (Baht/L)			**0.358**

Remark: Exchange rate = 33.432 Thai Baht (THB) to 1 US Dollar (USD)

For the nutrients recovery process from waste activated sludge using ASD and MAP processes, both methods have the potential to improve waste sludge removal in wastewater treatment plants and lower sludge management technique operating costs. Since anaerobic digestion process was simple, requires minimal equipment, and operating under anaerobic conditions, resulting in installation, operation, and maintenance costs and the electrical power requirements of the process were relatively low. It also caused a reduction in the amount of sludge after treatment, which decreased the expense of sludge transportation and disposal costs, including saving space and extending the lifespan of the landfills. In addition, the large amount of nutrients accumulated in the digested effluent leaded to nutrients recovery by chemical precipitation, especially the precipitation in the form of struvite. Its unique properties caused the quantity and demand for agricultural fertilizers to decrease [19,20].

Although the economic feasibility analysis of nutrients recovery process in this study (Table 2) revealed that the MAP process lacks profitability. Due to the cost of materials and electrical power used in the process was higher than the revenue from the sale of phosphate crystals. Especially regarding the cost of chemicals used to control the pH and Mg content in the solution to be suitable for operations. In addition, the presence of foreign ions in the effluent resulted in a decrease in struvite crystal purity, which reduced commercial sales profits. However, the ability to recover nutrients in the effluent indicated that the process reduces environmental impact and preserves resources. Consequently, this process is highly beneficial and should be extended on a large scale to demonstrate its efficiency. These benefits are expected to create financial burdens associated with chemical costs.

Table 2 Economic analysis of waste and wastewater treatment process

Parameters	Units	AnA^2/O^2 SBR	ASD process	MAP process
Electricity consumption:				
Daily electricity consumption	kWh/d	0.853	0.111	0.020
Daily inlet flow	m^3/d	0.020	0.005	0.001
Electricity consumption	kWh/m^3	42.65	24.67	20.00
Chemical additions:				
- $MgCl_2 \cdot 6H_2O$	kg Mg/m^3	-	-	0.023
- NaOH	kg $NaOH/m^3$	-	-	0.051
Products produced:				
Precipitating solids	kg/m^3	-	-	0.169
P content in solids	%	-	-	20.537
P-containing solid	kg P/m^3	-	-	0.035
Cost-Benefit analysis:				
(1) Energy cost[a]	$Baht/m^3$	166.70	96.41	78.17
(2) Chemical cost[b]				
- $MgCl_2 \cdot 6H_2O$	$Baht/m^3$	-	-	234.66
- NaOH	$Baht/m^3$	-	-	29.37
(3) Product's market price[c]	$Baht/m^3$	-	-	4.09 - 14.67
(4) Expenses; (1)+(2)	$Baht/m^3$	166.70	96.41	342.20
Profit margin[d]; (3)-(4)	$Baht/m^3$	-	-	-338.11 to -327.53

Note: The calculations in each process were performed under optimal conditions.

a Thailand's electricity cost from Metropolitan Electricity Authority (www.mea.or.th)

b Prices were derived from commercial webpages.

c OAE.go.th. (Lowest price for N-P-K formula 18-46-0 and highest price for formula 13-13-21; P as P_2O_5)

d Profit margin; (+) indicates profit gain from fertilizer selling, and (-) indicates financial loss

Conclusions:

All three processes not only had a positive impact on the environment because it could remove contaminated organic matter and nutrients from wastewater, treat excess sludge, and could recover nutrients, but there also had economic advantages over alternative processes. Each process had the potential to lower operating costs and reduce electricity consumption. Also, it could generate revenue during operations. Therefore, all three processes were appropriate and had the possibility of being applied further.

Acknowledgements:

This research work is supported in part by the grant from Center of Excellence on Environmental Health and Toxicology (EHT), OPS, Ministry of Higher Education, Science, Research, and Innovation. The authors also express their gratitude to the laboratory personnel of the Department of Sanitary Engineering, Faculty of Public Health, Mahidol University, for all of their support and assistance during the experimental study.

References:

1. Liu, Y.Y. & Haynes, R.J. (2011). Origin nature and treatment of effluents from dairy and meat processing factories and the effects of their irrigation on the quality of agricultural soils. *Critical Reviews in Environmental Science and Technology*, 41(17), 1531-1599.
2. Jia, Y., Gao, C., Zhang, L., Jiang, G. (2012). Effects of pre-fermentation and influent temperature on the removal efficiency of COD, NH_3-N and PO_3-P in slaughterhouse wastewater by using SBR. *Energy Procedia*, 16, 1964-1971.
3. Warodomrungsimun, C. & Fongsatitkul, P. (2009). Kinetic rate and mass balance of COD TKN and TP using SBR treating domestic and industrial wastewater. *Journal of Medical Association of Thailand*, 92, 134-141.
4. Kundu, P., Debsarkar, A., Mukherjee, S. (2013). Treatment of slaughterhouse wastewater in a sequencing batch reactor: performance evaluation and biodegradation kinetics. *BioMed Research International*, 134872. https://doi.org/10.1155/2013/134872.
5. Warodomrungsimun, C. (2011). *Development of a biological nutrient removal model for AnA^2/O^2 SBR process.* Ph.D. Thesis in Environmental Technology, Mahidol University, Thailand.
6. Saikomon, S. (2013). *Denitrification improvement and phosphorus removal efficiency of slaughterhouse wastewater using the short-cycle operation of AnA^2/O^2 SBR*. M.S. Thesis in Environmental Technology, Mahidol University, Thailand.
7. Pinvattanachai, S., Patthanaissaranukoo, W., Warodomrungsimun, C. (2019). The Effect of the solid retention time on simultaneous COD, TKN, and TP removal from slaughterhouse wastewater using sequencing batch reactor. *Proceedings of the 5th Environment Asia International Conference*; 2019 June 13-15; Convention Center, The Empress Hotel, Chiang Mai, Thailand, III1-10.

8. Mtshali1, J.S., Ababu, T.T., Amos, O.F. (2014). Characterization of Sewage Sludge Generated from Wastewater Treatment Plants in Swaziland in Relation to Agricultural Uses. *Resources and Environment,* 4(4), 190-199.
9. Gordon, M.I. (2015). *Nutrient recovery by anaerobic co-digestion of lipid-extracted Chlorella vulgaris and waste activated sludge*. B.S. Thesis in Bioresource Research with an option in Bioenergy, Oregon State University, Oregon.
10. Vanwonterghem, I., Jensen, P.D., Rabaey, K., Tyson, G.W. (2015). Temperature and solids retention time control microbial population dynamics and volatile fatty acid production in replicated anaerobic digesters. *Scientific Reports*, 5, 8496. https://doi.10.1038 /srep08496.
11. Liu, X., Xu, Z., Peng, J., Song, Y., Meng, X. (2016). Phosphate recovery from anaerobic digester effluents using $CaMg(OH)_4$. *Journal of Environmental Sciences-China*, 44, 260-268.
12. Yilmazel, Y.D. & Demirer, G.N. (2011). Removal and recovery of nutrients as struvite from anaerobic digestion residues of poultry manure. *Environmental Technology*, 32(7), 783-794.
13. Yetilmezsoy, K., Ilhan, F., Kocak, E., Akbin, H.M. (2017). Feasibility of struvite recovery process for fertilizer industry: A study of financial and economic analysis. *Journal of Cleaner Production*, 152, 88-102.
14. Rahman, M.M., Salleh, M.A.M., Rashid, U., Ahsan, A., Hossain, M.M., Ra, C.S. (2014). Production of slow release crystal fertilizer from wastewaters through struvite crystallization – A review. *Arabian Journal of Chemistry*,7(1), 139-155.
15. Wang, F., Fu, R., Lv, H., Zhu, G., Lu, B., Zhou, Z., Wu, X., Chen, H. (2019). Phosphate recovery from swine wastewater by a Struvite precipitation electrolyzer. *Scientific Reports*, 9, 8893. https://doi.org /10.1038/s41598-019-45085-3.
16. Pinatha, Y., Polprasert, C., Englande, A.J.Jr. (2020). Product and cost perspectives of phosphorus recovery from human urine using solid waste ash and sea salt addition - A case of Thailand. *Science of the Total Environment*, 713, 136514. https://doi.org /10.1016/j.scitotenv.2020.136514.
17. Alagha, O., Allazem, A., Bukhari, A.A., Anil, I., Mu'azu, N.D. (2020). Suitability of SBR for wastewater treatment and reuse: Pilot-scale reactor operated in different anoxic conditions. *International Journal of Environmental Research and Public Health*, 17, 1617. https://doi:10.3390/ijerph17051617.
18. Capodaglio, A.G. & Olsson, G. (2020). Energy issues in sustainable urban wastewater management: use, demand reduction and recovery in the urban water cycle. *Sustainability*, 12, 266. https://doi:10.3390 /su12010266.
19. Shrestha, B., Hernandez, R., Fortela, D.L.B., Sharp, W., Chistoserdov, A., Gang, D., Revellame, E., Holmes, W., Zappi, M.E. (2020). A review of pretreatment methods to enhance solids reduction during anaerobic digestion of municipal wastewater sludges and the resulting digester performance: implications to future urban biorefineries. *Applied Sciences*, 10, 9141. https://doi:10.3390/app 10249141.
20. Domini, M., Abbà, A., Bertanza, G. (2022). Analysis of the variation of costs for sewage sludge transport, recovery and disposal in Northern Italy: a recent survey (2015-2021). *Water Science & Technology*, 85(4), 1167-1175.

P-22

Exploration of reactivities of 4-haloisocoumarins as buildindg blocks in preparing other heterocycles

Kooljira Koekon[1], Charnsak Thongsornkleeb,[1,3,*] and Somsak Ruchirawat[1,2]

[1] Program on Chemical Sciences, Chulabhorn Graduate Institute, Center of Excellence on Environmental Health and Toxicology (EHT), OPS, MHESI, 54 Kamphaeng Phet 6, Laksi, Bangkok, 10210, Thailand
[2] Laboratory of Medicinal Chemistry, Chulabhorn Research Institute, 54 Kamphaeng Phet 6, Laksi, Bangkok, 10210, Thailand
[3]Laboratory of Organic Synthesis, Chulabhorn Research Institute, 54 Kamphaeng Phet 6, Laksi, Bangkok 10210 Thailand
*E-mail: charnsak@cri.or.th

Abstract:

3-Benzoyl-2-phenylisoindolin-1-one (isoindolinones) could be synthesized from 4-chloroisocoumarin via sequential nucleophilic addition and intramolecular cyclization. In this work, the reaction optimization studies of the reactivity of the nucleophilic addition were examined and investigated using an aniline and 2-aminopyridine as the nucleophiles. It was proposed that aniline could add to 4-chloroisocoumarin that then opened the isocoumarin ring which re-cyclized to provide the desired isoindolinones. The protocol is being developed with the emphasis on the ability to produce the desired isoindolinones products under mild, environmentally friendly and sustainable conditions.

Keywords: 4-Chloroisocoumarin, Isoindolinones, Cascade reactions, Nucleophilic addition

Introduction:

Isoindolinones, a class of nitrogen-containing heterocycles, are crucial in organic chemistry and widely present in nature. Due to their significance across various fields such as agrochemicals, polymers, pharmaceuticals, and medicine, synthesizing these compounds is a focal point of research. With few reported methods for their production, we aim to develop a novel synthesis route utilizing readily available chemical feedstocks. Here, we present a new method involving sequential addition, ring-opening, and re-cyclization reactions of 4-chloroisocoumarins and anilines, offering a mild and convenient protocol.

Mechanistically, 4-chloroisocoumarin (**I**) has an active C=O bond that is prone to nucleophilic attack to easily open the ester ring. Thus, a nucleophile could attack the C=O bond to open the ring to form an enolate species (**II**). The enolate species could be trapped with an electrophile to provide compound (**III**) while if it accepts a proton, compound (**IV**) with electrophile C-Cl bond is resulted. For a nucleophile with doublye nucleophilic activity, upon addition to form compound (**IV**), the other nucleophilic site could react intramolecularly with the C-Cl bond in a substitution reaction to form a 5-membered product (**V**). It could also be envisioned that if a molecule with extended nucleophilic sites is employed, it could react to form compound **VI**, with a ring larger than five-membered or a more complicated ring system.

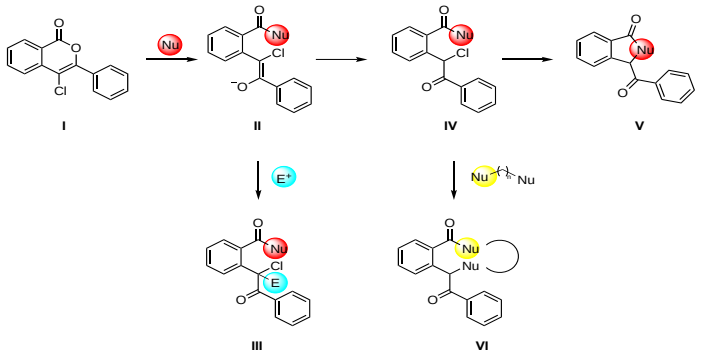

Results and Discussion:

In our preliminary investigations, we selected aniline (**2**) as the reacting nucleophile to react with 4-chloroisocoumarin (**1**) to construct 3-benzoyl-2-phenylisoindolin-1-one (**3**). The results were summarized in Table 1.

Table 1 Optimization studies of the conversion of **1** to **3**.

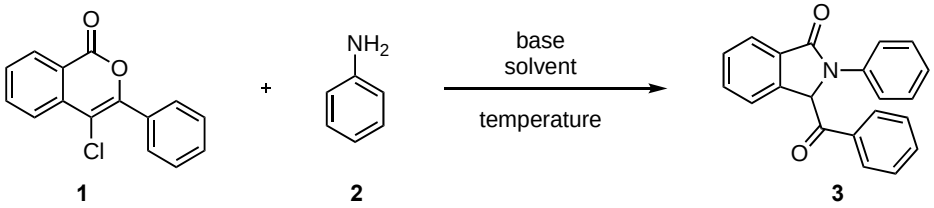

1 **2** **3**

entry	aniline (equiv)	base (equiv)	solvent	temp (°C)	time (h)	yield (%)[a]
1	1.5	KOH (1.1)	MeOH	60	24	NR
2	1.5	KOH (2.5)	MeOH	60	24	NR
3	1.5	KOH (5.0)	MeOH	60	24	Complex mixture
4	1.5	NaOH (5.0)	THF/H_2O	60	24	NR
5	1.5	DMAP (5.0)	THF	60	24	NR
6	1.5	NaH (5.0)	THF[b]	60	3	21
7	3.0	NaH (5.0)	THF[b]	60	3	37
8	6.0	NaH (5.0)	THF[b]	60	15 min	61
9	6.0	NaH (5.0)	THF[b]	rt	2 days	NR
10	6.0	NaH (5.0)	THF[b]	40	3	43
11	6.0	NaH (5.0)	THF[b]	80	10 min	34
12	6.0	NaH (5.0)	THF[b]	100	5 min	25
13	6.0	NaH (5.0)	dioxane[b]	60	3	34
14	6.0	NaH (5.0)	toluene[b]	60	3	28
15	6.0	NaH (5.0)	MeCN[b]	60	1	Complex mixture
16	6.0	NaH (5.0)	DMF[b]	60	3	Complex mixture
17	6.0	NaH (5.0)	DCM[b]	60	2 days	NR

[a]Yield was determined by ^{1}H-NMR. [b]Dry solvent. NR = no reaction.

As shown in entry 1, when the reaction was conducted using 1.5 equiv of **2** and 1.1 equiv of KOH as the base in methanol at 60 °C for 24 h, no reaction was observed. Identical result was observed when KOH was increased to 2.5 equiv (entry 2) whereas when 5.0 equiv of KOH was used, a complex reaction mixture was resulted (entry 3). When 5.0 equiv of NaOH in THF/H_2O (entry 4) and 5.0 equiv DMAP in THF (entry 5) were examined, both at 60 °C, no conversion was observed in both cases. The base was next changed to 5.0 equiv of NaH to react with 1.5 equiv of **2** in dry THF under thermal conditions (60 °C). The reaction provided the desired product **3** in 21% yield after 3 h (entry 6). Next, the equiv of aniline (**2**) were increased to 3.0 (entry 7) and 6.0 equiv (entry 8) while everything else remained the same. Under these conditions, yields of the desired product (**3**) could be increased to 37% and 61% (entries 7-8). Particularly of note, the reaction time could be reduced to a complete conversion within 15 min as shown in entry 8. Different reaction temperatures were also studied as shown in entries 9-12. While the reaction yielded 61% of product **3** in entry 8, either lower temperatures (entries 9-10) or higher temperatures (entries 11-12) resulted in inferior results, compared to entry 8. Furthermore, we studied the effect of different solvents (entries 13-17) while conducting the reaction at 60 °C. Different solvents included dioxane, toluene, MeCN, DMF, and DCM; none of which provided a better result than THF. Therefore, the reaction was most optimal in THF with the conditions shown in entry 8.

Conclusion:

In summary, we have identified efficient and mild reaction conditions for the synthesis of 3-benzoyl-2-phenylisoindolin-1-one (**3**) in moderate yield from aniline (**2**) and 4-chloroisocoumarin **1**. Further studies for the expansion of reaction scope, including employment of other nucleophiles, as well as utilizing this protocol in synthetic applications are underway in our laboratory.

References:

1. Norseeda K, Chaisan N, Thongsornkleeb C. Metal-Free Synthesis of 4-Chloroisocoumarins by TMSCl-Catalyzed NCS-Induced Chlorinative Annulation of 2-Alkynylaryloate Esters. J. Org. Chem. 2019;84:16222-16236.
2. Yanai H, Ishii N, Matsumoto T. Synthesis of 1,2,3,4-tetrasubstituted naphthalenes through a cascade reaction triggered by silyl acetal activation. Chem. Eur. J. 2023;29:e20230173.
3. Sreedharn R, Gandhi T. Brønsted Base Prompted *sp*3 C−H Latent Nucleophiles to Access *α*-Branched Amines Bearing *β*-Carbonyl by Cleaving Amide and Ester Bonds. J. Org. Chem. 2023;88:8480-8492.
4. Kerru N, Gummidi L, Maddila S, Gangu KK, Jonnalagadda SB. A Review on Recent Advances in Nitrogen-Containing Molecules and Their Biological Applications. molecules. 2020;29:1909.

P-23

Geospatial analysis of total coliform bacteria distribution: a case study at Bang Pakong river mouth area

Supansa Suriya[1,2], Norawit Wongsawat[1,2] and Suwisa Mahasandana[1,2*]

[1] *Department of Sanitary Engineering, Faculty of Public Health, Mahidol University 420/1 Rajvithi Rd., Rajchathawee, Bangkok, Thailand*
[2]*Center of Excellence on Environmental Health and Toxicology (EHT), OPS, MHESI, Thailand*

** Corresponding author. E-mail address: suwisa.mah@mahidol.ac.th*

Abstract:

Biological parameters should be considered when monitoring water quality to ensure compliance with standards. Therefore, this study investigated the presence of total coliform bacteria (TCB) and searched for a suitable spatial interpolation method to create TCB spatial distribution mapping in the Bang Pakong river mouth area using a Geographic Information System (GIS). The research processed TCB data and applied GIS with four spatial interpolated method approaches, including inverse distance weighted (IDW), Spline with Barrier (SB), Ordinary Kriging (OK), and Universal Kriging (UK). Data showed that sampling during the dry season yields TCB concentrations within the range of 1.80 to 70.00 MPN/100 mL, with an average of 9.46 MPN/100 mL, demonstrating compliance with established standards. The spatial distribution of TCB is mapped utilizing GIS techniques, and the accuracy of these maps is validated by comparing the sampling values with the estimated values. The study identifies the IDW GIS as a suitable method for this river mouth area, with the coefficient of determination (R^2) of linear regression correlation at 0.8916.

Keywords: Total coliform bacteria, River mouth, Water quality monitoring, Distribution mapping analysis

Introduction:

The quality of the water is controlled to keep it within acceptable standards, not only physico-chemical parameters are considered, but biological parameters are also taken into consideration. Thus, the TCB are part of the parameters that will be used in the indexing of surface and marine water quality. (Pollution Control Department, 2020a, 2020b).

The presence of coliform bacteria in a water sample indicates the possibility of the existence of harmful pathogenic bacteria (Pepper & Gerba, 2015).

The Bang Pakong estuary is in the northeastern part of the Gulf of Thailand have run off from the major rivers that flows into the sea is the Bang Pakong river. This river is regarded as a place where waste can be discharged from residences, agriculture, farm and industrial factory (Pollution Control Department, 2020c). Therefore, it is possible that the mouth of the Bang Pakong river may be contaminated with coliform bacteria. So, it's crucial to figure out how much contamination there is and how it spreads once it reaches the sea.

In GIS, a technique called spatial interpolation is used to estimate values at unknown points using known values. In order to produce a continuous map (Sutton, Dassau, Marcelle, Nsibande, & Mthombeni, 2024). In this study we used four spatial interpolated methods, including IDW, SB, OK, and UK. IDW is a method where the value of a point on a map is determined by nearby sampled locations. It assumes that closer points have more influence

(ESRI). SB is a tool that smooths maps. It starts with a coarse grid, then gradually refines this grid from coarse to finer grids until it achieves a smooth surface (ESRI). Kriging is a method that relies on statistical models. It works on the assumption that the distance or direction between sampled points shows a spatial correlation, which helps to understand the variation in the surface being studied (ESRI).

This study focused on the presence of TCB at the Bang Pakong river mouth area using GIS to show the spatial distribution of TCB. The aims of our study were to study the concentration of TCB and to select the suitable spatial interpolated GIS method to create TCB spatial distribution mapping in Bang Pakong river mouth areas.

Materials and Methods:

Study area

The Bang Pakong river mouth is in the inner Gulf of Thailand. The inner Gulf of Thailand is an area of utilization in six categories, including type 1 for natural resource conservation, type 2 for coral reef conservation, type 3 for aquaculture, type 4 for recreation, type 5 for industry and port and type 6 for community areas (Pollution Control Department, 2020c).

Data collection

The water sample were collected in dry season on December 19th, 2020, from the Bang Pakong river mouth out to the Gulf of Thailand and returned to the starting point. The total amount of sea water samples was from 35 sampling stations.

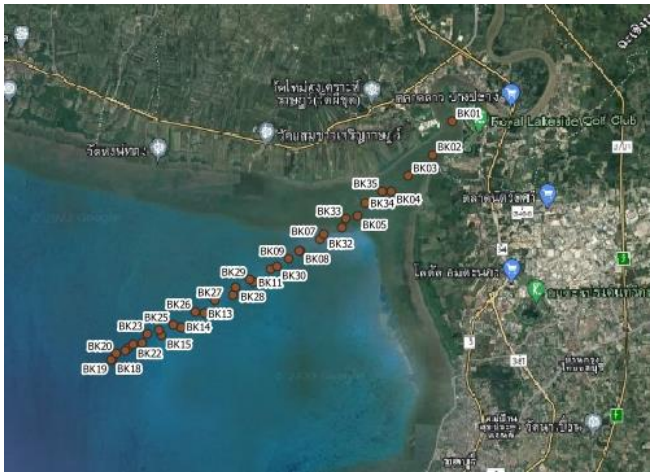

Figure 1 Sampling stations at the Bang Pakong river mouth area, where BKx was the station number.

Statistical analysis and Distribution mapping

Descriptive statistics were applied to describe characteristics of total coliform bacteria (TCB). The TCB distribution map in Bang Pakong river mouth was performed by the concentration of TCB data and location information. Make an interpolation map based on concentrations by processing from ArcMap 10.4.1 using 4 methods including IDW, SB, OK, and UK. The linear regression correlation was assessed between the estimated data and sampling data for each method, and the method with the highest coefficient of determination (R^2) was chosen as the most suitable method.

Results and Discussion:

Statistical analysis

The average concentration of total coliform bacteria from 35 sampling stations was found 9.46 MPN/100mL and maximum was found 70 MPN/100mL which were both still within the established standards for all types of uses of 1,000 MPN/100mL (Pollution Control Department, 2020b).

Distribution mapping using GIS

The distribution mapping results for TCB are illustrated in Figure 2. When estimated values were tested with sampling TCB values, the average percentage error were 29.09, 42.84, 36.26, and 89.80 percent for IDW, SB, OK, and UK respectively.

The linear regression correlation between sampling and estimated TCB found that the R^2 were 0.8916, 0.8812, 0.8861, and 0.8062 for IDW, SB, OK, and UK respectively.

The IDW method gave the lowest average percentage error and highest R^2 value. The distribution map showed concentration of TCB were higher in areas closer to the river mouth area than in areas further away. The distance from the river mouth area demonstrated a negative correlation with total coliform bacteria. The results may be explained by areas close to the river mouth, which is close to the source of total coliform bacteria. Consequently, the river mouth area displays higher concentrations of coliform bacteria in contrast to more remote areas. The findings of this study are consistent with several previous study, which noted that coliform bacteria higher residential, industrial, agricultural, animal livestock area, than remote areas (Hong, Qiu, & Liang, 2010; Sinaga, Robson, Gasong, Halel, & Pertiwi, 2016).

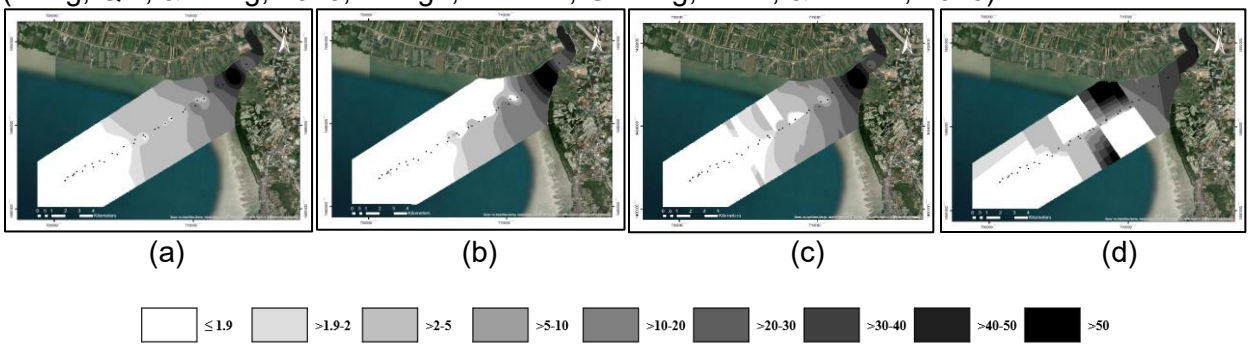

Figure 2 Distribution mapping of TCB by IDW (a), SB (b), OK (c), and UK (d) respectively.

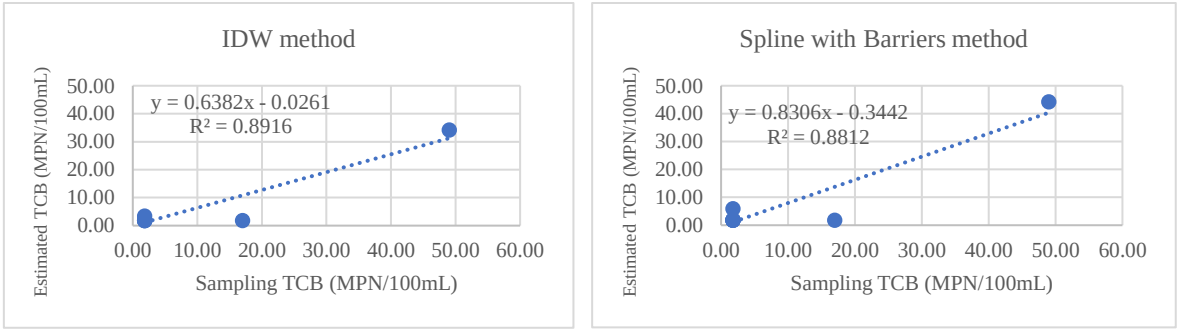

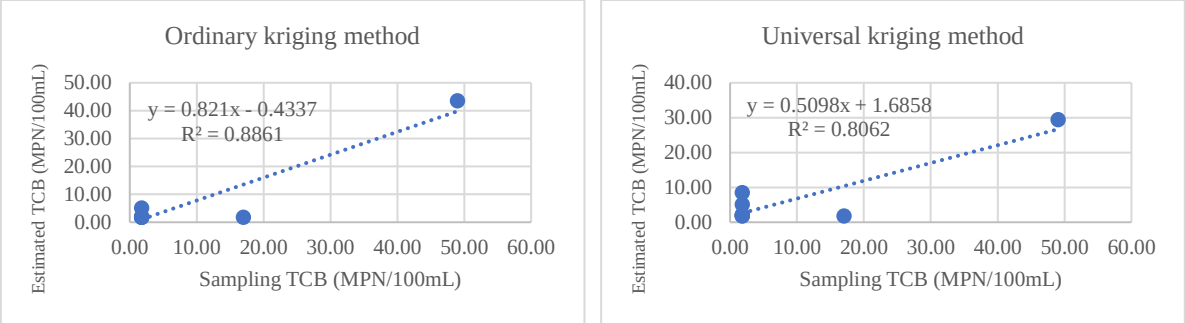

Figure 3 The correlation between sampling TCB concentrations from the study area and estimated TCB from ArcGIS

Conclusion:

1.The concentration of TCB at the Bang Pakong river mouth area in this dry season complied with regulatory standards.

2. Distribution mapping showed locations nearer the river mouth area had greater levels of total coliform bacteria than locations farther away.

3. The most suitable interpolation method for this study was the IDW method because this method gave the highest R^2 value. The use of the Spatial Interpolation toolset in GIS software offered an effective alternative to convey data continuity through value estimation, leading to a more comprehensive representation of coverage data in the study area.

Acknowledgement:

This project is funded by National Research Council of Thailand.

References:

1. ESRI. How IDW works. Retrieved from https://pro.arcgis.com/en/pro-app/latest/tool-reference/3d-analyst/how-idw-works.htm
2. ESRI. How Kriging works. Retrieved from https://pro.arcgis.com/en/pro-app/latest/tool-reference/3d-analyst/how-kriging-works.htm
3. ESRI. How Spline with Barriers works. Retrieved from https://pro.arcgis.com/en/pro-app/latest/tool-reference/3d-analyst/how-spline-with-barriers-works.htm
4. Hong, H., Qiu, J., & Liang, Y. (2010). Environmental factors influencing the distribution of total and fecal coliform bacteria in six water storage reservoirs in the Pearl River Delta Region, China. *Journal of Environmental Sciences, 22*(5), 663-668. doi:https://doi.org/10.1016/S1001-0742(09)60160-1
5. Pepper, I. L., & Gerba, C. P. (2015). Chapter 10 - Cultural Methods. In I. L. Pepper, C. P. Gerba, & T. J. Gentry (Eds.), *Environmental Microbiology (Third Edition)* (pp. 195-212). San Diego: Academic Press.
6. Pollution Control Department. (2020a). Announcement of the National Environment Board No. 8 (B.E. 2537) on the determination of water quality standards in surface water sources. Retrieved from https://www.pcd.go.th/laws/4168
7. Pollution Control Department. (2020b). Announcement of the National Environment Board on the determination of marine water quality standards. Retrieved from https://www.pcd.go.th/laws/4147
8. Pollution Control Department. (2020c). Annual Report of Water Quality Management Division 2019. Retrieved from https://www.pcd.go.th/wp-content/uploads/2020/05/pcdnew-2020-05-17_14-50-30_573382.pdf

9. Sinaga, D. M., Robson, M., Gasong, B., Halel, A., & Pertiwi, D. (2016). Fecal coliform bacteria and factors related to its growth at the Sekotong shallow wells (West Nusa Tenggara, Indonesia). *Public Health of Indonesia, 2*, 47-54. doi:10.36685/phi.v2i2.62
10. Sutton, T., Dassau, O., Marcelle, S., Nsibande, L., & Mthombeni, S. (2024). 11. Spatial Analysis (Interpolation). Retrieved from https://docs.qgis.org/3.34/en/docs/gentle_gis_introduction/spatial_analysis_interpolation.html

P-24

The efficacy of *Canna indica* in textile wastewater treatment

Danuphon Radomthong[1], Toemthip Poolpak[1,2], Prayad Pokethitiyook[1,2], and Patompong Johns Saengwilai[1]

[1]Department of Biology, Faculty of Science, Mahidol University, Bangkok, Thailand
[2]Center of Excellence on Environmental Health and Toxicology, OPS, MHESI, Thailand

Abstract:

The textile industry remains a significant source of environmental problems due to the discharge of textile wastewater, which is harmful to ecosystems and human health. Textile manufacturing processes had high levels of toxic, mutagenic, and carcinogenic substances in the textile wastewater. Among all dyes used in manufacturing processes, Methylene Blue (MB) is one of the most concerning. Currently, wetland plant species are studied to determine the efficacy of textile wastewater treatment in the vertical flow constructed wetland. In this study, *Canna indica* was examined for it efficacy in hydroponic conditions with synthetic wastewater concentrations of 0, 5, 10, and 20 mg/L of MB. We found that *C. indica* showed the highest decolorization at 97.66% after 14 days. Additionally, water treatment ability at different concentrations showed great removal percentages of COD, nitrogen, and phosphate, as well as a higher final BOD and pH than the initial period. Also, the response to MB toxicity was determined by plant growth indicators, including shoot height, root length, tiller number, and plant biomass. The results of plant morphology showed a difference in growth rates at different concentrations. Therefore, these results exhibited the potential of *C. indica* for further promoting the vertical flow constructed wetland, which could be used as a biological technology for increasing efficiency in textile wastewater treatment.

Keywords: *Canna indica*, Textile Wastewater, Methylene Blue, Decolorization

Introduction:

The textile industry plays an important role in Thai economy because we are an exporter of various textile products, including fibers, yarns, fabrics, and clothing, with a total export value of 4,717.6 million US dollars in 2021 [1]. However, textile wastewater contains many textiles manufacturing processes, including bleaching, printing, dyeing, etc. It relates to source of environmental problems such as harmful aquatic ecosystems and human health due to its toxicity [2].

The dyeing process is mainly a source of textile wastewater due to using a higher volume of water than other production processes, which account for approximately 30–40% of the whole process [3]. Methylene Blue (MB) is a synthetic dye that is widely used in the dyeing process for dyeing woods, cotton, leather, silk, fabrics, plastics, and clothing. Although MB is very useful in the textile industry, it is toxic, mutagenic, and carcinogenic, which can lead to contamination of the food chain and the environment in directly or indirectly negative ways to humans and aquatic animals [4].

Currently, the vertical flow constructed wetland is biological technology and interesting for removing pollutants and dye from textile wastewater due to their low cost, fewer construction operations, lower energy demand. In addition, its higher effectiveness, environmental friendliness, and sustainable wastewater management also the advantage of this technology [5]. Wetland plant species can contribute to effective dye removal in the vertical flow constructed wetland. However, only a few have reported for their different effects on the decolorization of MB. *Canna indica*, *Phragmites australis*, and *Typha angustifolia* are common wetland plant species in

Thailand that could serve this purpose [6]. Therefore, the aim of this study was to assess the ability of *C. indica* for textile wastewater treatment.

Methodology:

Wetland plant species

The wetland plant species in this experiment was Indian shot (*C. indica*). This wetland plant is common in Thailand and could promote potential phytoremediation in constructed wetland systems that were selected in many research studies [5,7]. Wetland plant was purchased from Thap Ma, Mueang Rayong district, Rayong province, Thailand. The roots of the wetland plant were removed from the soil, and they were washed carefully first with tap water then by deionized water to remove the apoplastic soil. Wetland plant was propagated in half strength of Hoagland's solution for 14 days for root formation. Then, uniformly healthy plants with a 15 cm shoot height and a 5 cm root length were selected for further experiments.

The efficiency of *C. indica* in textile wastewater treatment

To study the ability of *C. indica* for textile wastewater treatment, the laboratory scale hydroponic system was performed. The root mass of each wetland plant was transplanted in 400 mL half strength of Hoagland's solution in 1000 ml flask volume. The plant samples were grown at 25 ± 2 °C and performed with fluorescent light for a photoperiod of 12/12 h light dark for two weeks in plant room (B413/2) at Mahidol University, Bangkok, Thailand. The flasks were covered by aluminum foil to maintain a dark condition and prevent light sensitivity to root growth. All samples were performed in five replicates in a hydroponic system. After two weeks, the experiments were replaced with synthetic wastewater solutions containing 0, 5, 10, and 20 mg/L of MB respectively, for another two weeks. Then, plant samples were measured for plant growth, including plant biomass (root and shoot), root length, shoot height, and tiller number. Finally, water sample was measured for decolorization, nitrogen and phosphate removal, pH, BOD, and COD.

Data and statistical analysis

The experimental data was analyzed using R program version 3.5. The results were analyzed using statistical One-way ANOVA, followed by Tukey's Honestly Significant Difference (HSD), and were considered significant at $P < 0.05$.

Results and Discussion:

Effect of *C. indica* on decolorization

The ability of the synthetic wastewater containing MB decolorization was determined at OD_{660nm}. Figure 1 showed the different dye removal percentages at different MB concentrations by *C. indica*. The synthetic wastewater concentration of 5 mg MB/L showed the highest decolorization at 97.66% dye removal on 14 days when compared to the other MB concentrations. Wetland plant species have the capability to degrade azo dyes (e.g., MB) because they produce enzymes such as lignin, peroxidases, and manganese. The roots in the rhizosphere create both aerobic and anaerobic conditions necessary for dye degradation. Additionally, plants can accumulate dyes from wastewater through phytoremediation mechanisms, aiding in wastewater decolorization [8]. In addition, the other study investigated the use of *C. indica* for dye removal in a constructed wetland containing iron scraps and found that this approach significantly enhanced decolorization, especially with higher concentrations of dye in the wastewater [9].

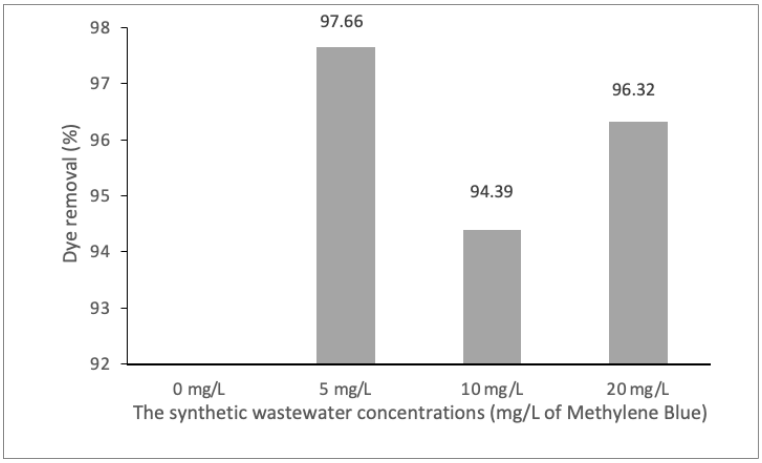

Figure 1 The efficacy of *C. indica* for dye removal percentages

Effect of *C. indica* on textile wastewater treatment

Water quality at the difference MB concentrations was analyzed after treated with *C. indica*. Figure 2A showed the different COD removal percentages at different MB concentrations by *C. indica*. The synthetic wastewater concentrations of 10 and 20 mg MB/L both showed the highest COD removal percentages at 100% after 14 days. Figure 2B showed a higher final BOD than the initial of all the synthetic wastewater concentrations, while the highest BOD was the set of concentration of 5 mg MB/L at the value of 54.01 BOD_5 mg/L. Nitrogen removal percentages illustrated in all the concentrations, while the highest was the synthetic wastewater of 5 mg MB/L at 54.65% on 14 days, as shown in Figure 2C. Conversely, phosphate removal percentages showed only the concentration of 20 mg MB/L at 61.43%, as shown in Figure 2D. Figure 2E showed the final pH after 14 days, which was lower than the initial pH at 6 to 5 in pH water. Pollutants are uptake directly into the plant biomass and a process known as phytodegradation may be involved in dye removal. Moreover, the roots of plants offer a substantial surface area for bacterial attachment, facilitating the uptake and release of oxygen into the rhizosphere, which promotes aerobic pollutant degradation. Furthermore, microorganisms are key contributors to reducing COD, BOD, organic pollutants, and inorganic nitrogen in textile wastewater [6]. In another study using *C. indica* for the removal of MB, they found that it achieved a 93% removal rate for MB at a concentration of 50 mg/L, as well as a 93% removal rate for COD in a vertical flow constructed wetland model with zeolite over a period of 1 month [10].

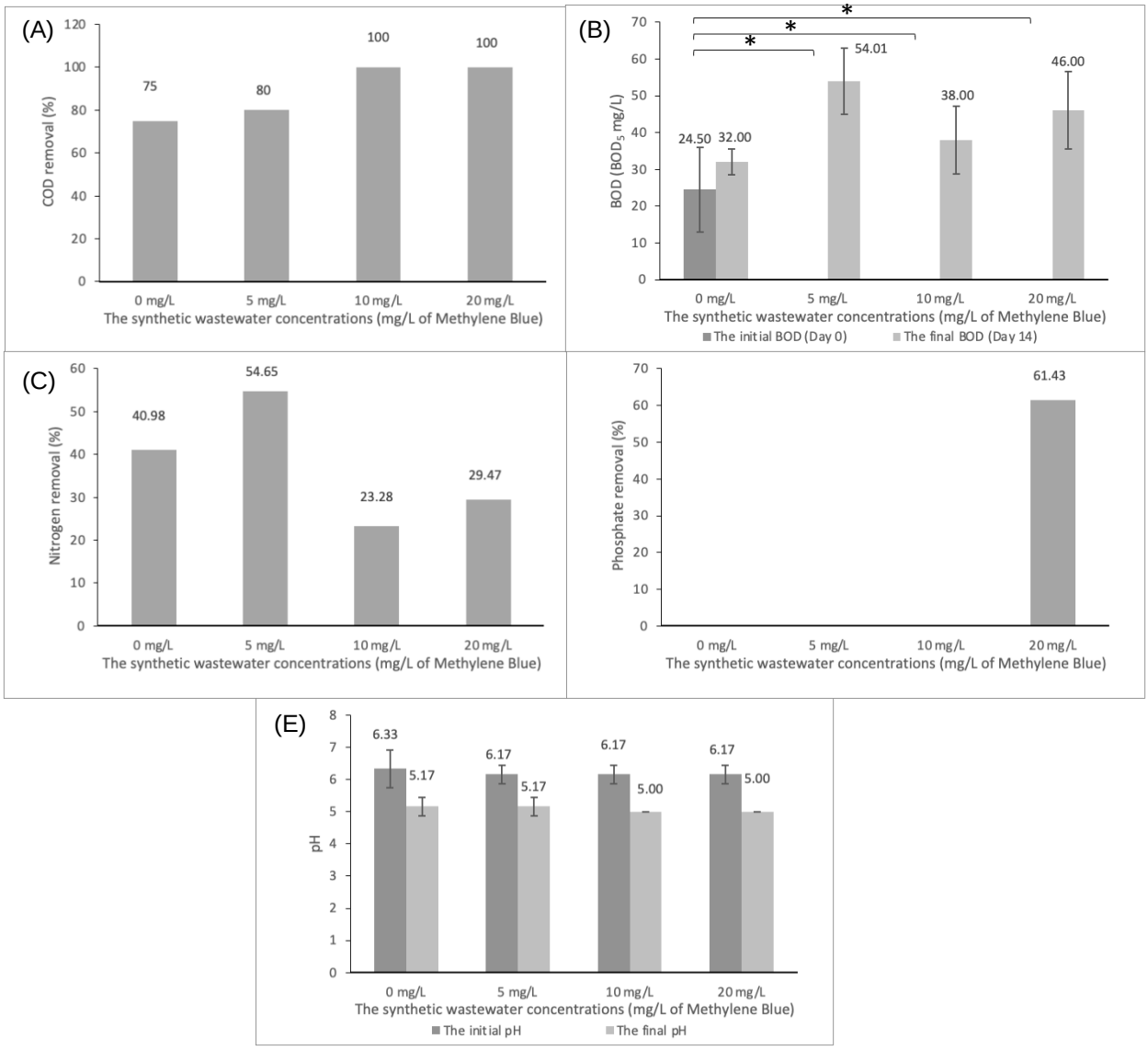

Figure 2 The efficacy of *C. indica* for textile wastewater treatment (A) COD removal percentages, (B) The initial and final of BOD on 14 days, (C) Nitrogen removal percentages, (D) Phosphate removal percentages, (E) The initial and final of pH on 14 days

Plant growth of *C. indica* in the hydroponic condition

Plant growth of *C. indica* was determined after 14 days in the hydroponic condition at different synthetic wastewater concentrations (mg/L of MB). Figures 3A and 3B showed shoot height and root length at the synthetic wastewater concentrations of 10 and 20 mg MB/L higher than 0 and 5 mg MB/L after 14 days. Conversely, the number of tillers at the synthetic wastewater concentrations of 0 and 5 mg MB/L was higher than 10 and 20 mg MB/L after 14 days, as shown in Figure 3C. Figure 3D showed decreasing plant biomass percentages as a slight difference according to higher synthetic wastewater concentrations. Azo dye (including MB) effects to reduce plant growth, metabolism, and photosynthetic activity. The toxicity of azo dye product the

oxidative stress that it damages a high abundance in DNA of some plants. The variability of damage is dependent on the gene tolerance of plant species to the oxidative stress induced by dye toxicity, which in turn affects plant morphology [11].

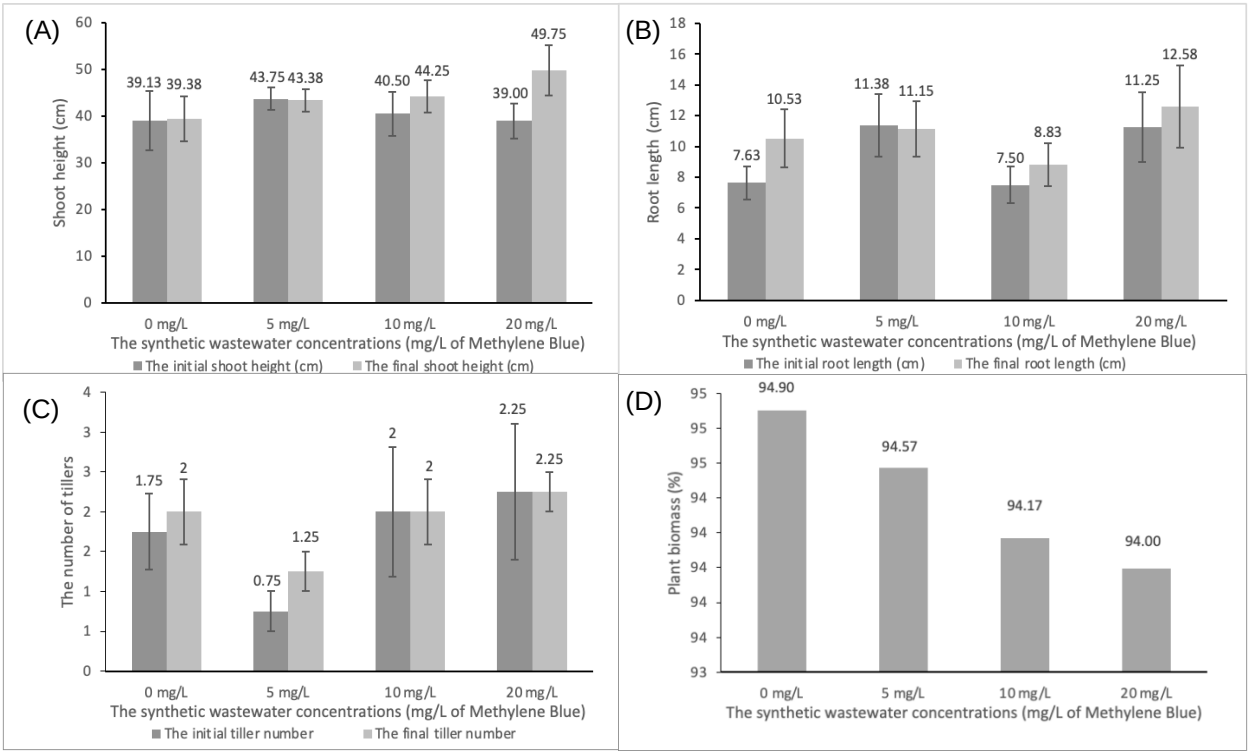

Figure 3 Plant growth of *C. indica* (A) Shoot height, (B) Root length, (C) The number of tillers, (D) Plant biomass percentages

Conclusion:

C. indica had great potential for the efficiency of MB decolorization and textile wastewater treatment at different synthetic wastewater concentrations due to its promotion of phytoremediation, biodegradation, and plant adsorption. The results showed the greatest decolorization at 97.66% dye removal after 14 days at a concentration of 5 mg MB/L. Also, it can help treat textile wastewater by showing 100% COD removal at both 10 mg MB/L and 20 mg MB/L concentrations after 14 days. Additionally, it had great other water quality indicators, including BOD, nitrogen, phosphate, and pH. Furthermore, it had great potential to tolerate MB toxicity, and it still shows great plant growth at different concentrations after the harvest period, including shoot height, root length, tiller number, and plant biomass. Therefore, this study can contribute to the highly effective selection of wetland plant species by promoting decolorization and textile wastewater remediation for the vertical flow constructed wetland.

Acknowledgements:

This research received funding support from the Center of Excellence on Environmental Health and Toxicology (EHT), OPS, MHESI, and Mahidol University, Bangkok, Thailand.

References:

1. Thailand Textile Institute, (2022). Thai Textile Statistics 2021/2022, pp. 36. From www.thaitextile.org.
2. Wang, X., Jiang, J., & Gao, W. (2022). Reviewing textile wastewater produced by industries: characteristics, environmental impacts, and treatment strategies. Water Science and Technology, 85(7), 2076–2096. https://doi.org/10.2166/WST.2022.088
3. Yaseen, D. A., & Scholz, M. (2019). Textile dye wastewater characteristics and constituents of synthetic effluents: a critical review. International Journal of Environmental Science and Technology, 16(2), 1193–1226. https://doi.org/10.1007/S13762-018-2130-Z/TABLES/7
4. Oladoye, P. O., Ajiboye, T. O., Omotola, E. O., & Oyewola, O. J. (2022). Methylene blue dye: Toxicity and potential elimination technology from wastewater. Results in Engineering, 16, 100678. https://doi.org/10.1016/j.rineng.2022.100678
5. Dogdu, G., & Yalcuk, A. (2016). Evaluation of the treatment performance of lab- scaled vertical flow constructed wetlands in removal of organic compounds, color and nutrients in azo dye-containing wastewater. International Journal of Phytoremediation, 18(2), 171–183. https://doi.org/10.1080/15226514.2015.1073672
6. Sharma, R., & Malaviya, P. (2022). Constructed wetlands for textile wastewater remediation: A review on concept, pollutant removal mechanisms, and integrated technologies for efficiency enhancement. Chemosphere, 290, 133358. https://doi.org/10.1016/j.chemosphere.2021.133358
7. Hassan, M. M., & Carr, C. M. (2018). A critical review on recent advancements of the removal of reactive dyes from dyehouse effluent by ion-exchange adsorbents. Chemosphere, 209, 201–219. https://doi.org/10.1016/j.chemosphere.2018.06.043
8. Goud, B.S., Cha, H.L., Koyyada, G., Kim, J.H., (2020). Augmented biodegradation of textile azo dye effluents by plant endophytes: a sustainable, eco-friendly alternative. https://doi.org/ Curr. Microbiol. 77 (11), 3240-3255.
9. Yadav, A.K., Jena, S., Acharya, B.C., Mishra, B.K., (2012). Removal of azo dye in innovative constructed wetlands: influence of iron scrap and sulfate reducing bacterial enrichment. https://doi.org/ Ecol. Eng. 49, 53-58.
10. Jayalakshmi, R., Soundaranayaki, K., & Subhash Kannan, M. (2023). Removal of Methylene Blue dye from textile wastewater using vertical flow constructed wetland. Materials Today: Proceedings, 77, 365–370. https://doi.org/10.1016/j.matpr.2022.12.030
11. Xu, X.R., Li, X.Z., (2010). Degradation of azo dye Orange G in aqueous solutions by persulfate with ferrous ion. https://doi.org/Purif. Technol. 72 (1), 105-111.

Center of Excellence on
Environmental Health and Toxicology (EHT)
Faculty of Science, Mahidol University
K Building, 5th Floor, K 514, Rama VI Road
Bangkok 10400, Thailand
Tel: 0-2201-5913-14
Website - eht.sc.mahidol.ac.th